Cheng Yang

Distributed Piezoelectric Transducers and Their Applications in Structural Health Monitoring

Distributed Piezoelectric Transducers and Their Applications in Structural Health Monitoring

genehmigte

DISSERTATION

zur Erlangung des Grades eines Doktors

der Ingenieurwissenschaften

vorgelegt von

M. Sc. Cheng Yang

aus China

eingereicht der Naturwissenschaftlichen-Technischen Fakultät

der Universität Siegen

Siegen 2017

Referent: Prof. Dr.-Ing. Claus-Peter Fritzen

Korreferent: Prof. Dr. rer. nat. habil. Xin Jiang

Tag der mündlichen Prüfung

3. Juni 2016

Acknowledgement

This Ph.D work could not be finished without the generous help from different individuals. To begin with, I greatly appreciated Professor Loffeld from Center of Sensor Systems to accept me into the International Postgraduate Program, and my supervisor Professor Fritzen, whom I have known since my Master's study in Siegen, and lead me to the field of Structural Health Monitoring and guided me through the way, and Professor Jiang, who is willing to take the responsibility as my second examiner.

Followed with all my colleagues, who have been creating such a friendly and warm working atmosphere. Our two "handy men": Mr. Richter and Mr. Dietrich, who have been keeping the lab running in order and helped me through all my experiments and trivia things, from repairing a device to gluing a sensor, from constructing an experimental setup to ordering a component, without their help I could only achieve nothing, my gratitude is out of what the words could express. And Ms. Thomas, Mrs. Niet-Wunram and Dr. Nies who helped me to prepare all kinds of paperwork efficiently. Many thanks to my officemates Martin and Erion, who were always there to help, started from my first day in that office, and Yan, Miguel, Peter, Maksim, Philip, Inka and Henning, for their fruitful discussion as well as friendship.

Lots of scientists outside our institute whom I will always remember for their unconditional help. Mr. Henkel and Mr. Butters from Chemistry of Building Materials; Professor Fukada from Kobayashi Institute in Japan; Dr. Hillenbrand from Darmstadt University; Professor Butt and Dr. Koynov from Max Planck; Dr. Mutke from Münster University; Marian from Complutense University of Madrid and Carlos from Technical University of Madrid. Without their generous help I could not finish this Ph.d work. I just wish I could help other people the way I was helped in the future.

The last but not the least, my parents, my husband Hao and my little boy Alex, who supported me at my highs and lows, who encouraged me when the journey was tough.

Table of contents

Table of Symbols

The following listed the symbols appear in this dissertation. Those which are not listed in this table are explained in the text.

Greek symbol	Explanation for symbol
α	Attenuation constant
β	Decay constant
γ	Complex part of the wave propagation constant
ε_0	Electric permittivity of vacuum
ε_{ij}	Dielectric tensor
χ	Dielectric susceptibility
ρ	Density
$\rho_{polymer}$	Density of polymer in piezoelectric paint
ρ_{Piezo}	Density of piezoelectric ceramic powder
σ_1, σ_2	In-plane stress
ϕ	Model shape
δ_{nm}	Kronecker delta
δ_e	Geometric error
τ	Wavenumber

Symbol	Explanation for symbol
A_e	Effective piezoelectric paint area
A_b	Cross section
B	Magnetic flux density
b_b	Beam width

c_{ijkl}	Elastic stiffness tensor
C_p	Capacitance
D	Dielectric displacement
d_{kij}	Piezoelectric charge constant
e_{kij}	Piezoelectric tensor
E	Electric field
$\mathbf{E}$	Electric field vector
E_b	Young's modulus of cantilever beam
$F(x, y)$	Surface electrode pattern
h_b	½ thickness of a beam
I_b	Cross sectional moment of inertia
i, j, k, l	Indices of Einstein notation
k	Wave number
K^2	Electromechanical coupling coefficient
l_b	Beam length
m	Mass
m_p	Mass of piezoelectric ceramic powder
M_b	Bending moment
P	Electric polarization
p	Period of structure
$P_0(x, y)$	Polarization profile
q	Electrical charge
S	Strain
$\mathbf{S}$	Strain vector
s_{ijkl}	Compliance tensor

S_{kl}	Strain tensor
T	Stress
$\mathbf{T}$	Stress vector
T_{ij}	Stress tensor
$vol\%$	Volume percentage
vol	Volume
v	Phase velocity
v_r	Phase velocity at open circuit
v_m	Phase velocity at short circuit
w	Transverse displacement of the cantilever beam
$wt\%$	Weight percentage before sintering
$wt'\%$	Weight percentage after sintering
x, y, z	Cartesian coordinates
u_1, u_2, u_3	Displacement in x, y, z direction

Abbrivations and acronyms

AlN	Aluminum Nitride
γ-TiAl	Gamma Titanium Aluminide
NDT	Non-Destructive Testing
SHM	Structural Health Monitoring
SAW	Surface Acoustic Waves
PZT	Lead Zirconate Titanate
EMCC	Electromechanical Coupling Coefficient
TGA	Thermal gravimetric analysis

Abstract

Structural Health Monitoring (SHM) is an upcoming technology, which combines disciplines of smart materials, structural dynamics, structural engineering, Non-Destructive Testing (NDT), sensor and actuator development, signal processing and more. It deals with the development and implementation of techniques where monitoring, inspection and damage detection becomes an integral part of a structure. Piezoelectric materials have been explored and applied in many fields since its first discovery. Recently, with the rapid growth of piezoelectric transducers, they have become an essential part of an SHM system due to many of their prior advantages, for instance, light weight, low cost, ability to be integrated into a structure, easy to apply and so forth. Generally, the conventional piezoelectric transducers used in SHM are discrete piezoelectric ceramic sensors. They are widely accepted in many SHM applications due to the above-mentioned features. However, they are also known for their brittleness, hardness, unable to be applied on a single or multi-curved structural surface, difficult to cover a large area, as well as error performance due to bonding layer failure. These drawbacks compromise the reliability of a SHM system.

The research presented here focuses on the investigation and development of a new type of smart material - the distributed piezoelectric transducer, with a target application in SHM fields where the traditional piezoelectric ceramics are not suitable anymore. One of the main focuses is the development of a piezoelectric ceramic and polymer based flexible piezoelectric composite: the piezoelectric paint. The production of a high quality piezoelectric paint is investigated and its material properties are characterized. To enhance the low piezoelectricity, which is the main drawback of a piezoelectric paint, its improvement is studied. The enhanced piezoelectric paint is compared with traditional strain gauges and ceramic sensors. Afterwards, its applications in SHM as strain sensors for strain measurement, modal sensors for modal filtering, vibration sensors for modal analysis are demonstrated. Besides, its thermal properties are studied as well. Since the piezoelectric paint contains a polymer phase, its applications are limited for ambient temperature applications, therefore, another group of piezoelectric material for high temperature SHM applications – Aluminum Nitride (AlN), is explored. This part focuses on a three-layer structure, AlN, Diamond, gamma Titanium Aluminide (γ-TiAl). AlN is deposited on the substrate as

distributed Surface Acoustic Wave (SAW) transducer. Numerical calculation of the structure is performed to study the dispersion features of SAW on the three-layer structure. With the help of the Finite Element Method (FEM), the propagation of SAW is demonstrated by modeling and simulation. Structural flaws are simulated to illustrate that with the combination of Interdigital Transducers (IDT), AlN can be used as distributed SAW sensors in high temperature SHM applications.

Kurzfassung

Structural Health Monitoring (SHM) ist eine vielversprechende Technologie zu Überwachung von Struktur, in der die Disziplinen von smarten Materialien, Strukturdynamik, Bautechnik, zerstörungsfreien Prüfungen, Sensor- und Aktor-Entwicklung, Signalverarbeitung und mehr kombiniert werden. Ein SHM-System befasst sich mit der Entwicklung und Umsetzung von Verfahren, bei denen die Überwachung, Kontrolle und Schadenserkennung ein integraler Bestandteil einer Struktur wird.

Seit ihren Entdeckung wurden Piezoelektrische Materialien in vielen Bereiche erforscht und angewendet. Dank ihrer umfangreichen Vorteile, z.B. geringes Gewicht, niedrige Kosten, Fähigkeit zur Strukturintegration, leicht zu verarbeiten, sind sie in letzter Zeit ein wesentlicher Bestandteil eines SHM-Systems geworden. Im allgemeinen werden herkömmliche piezoeletrische Wandler – diskrete Piezokeramiksensoren für SHM-Systeme verwendet. Aufgrund der oben genannten Vorteile sind sie in vielen SHM Anwendungen weit verbreitet. Jedoch sind Piezoelektrische Wandler sehr spröde und hart. Dies verhindert ihre Applikation auf ein- oder mehrfach gekrümmten Oberflächen. Außerdem sind sie nicht für die groß flächige Applikation geeignet. Fehler in der Klebschicht, die den piezoelektrischen Wandler mit der Struktur verbindet, führen zu ungewollten Effekten in der Nutzung der Wandler. Diese Nachteile schränken die Zuverlässigkeit eines SHM-Systems ein.

Die vorliegende Arbeit konzentriert sich auf die Erforschung und Entwicklung eines neuartigen smarten Materials ─ der flächige piezoelektrische Sensor. Zielanwendungen sind SHM-Systeme, für die die traditionellen piezoelektrischen Keramiken nicht mehr geeignet sind. Einer der Schwerpunkte ist die Entwicklung eines piezoelektrischen Verbundmaterials: Piezoelectric-Paint, die auf piezoelektrischer Keramik und Polymeren basiert. Die Herstellung einer hochwertigen Piezoelectric-Paint und die Eigenschaften werden untersucht. Um ihre niedrige Piezoelektrizität zu verbessern, was der Hauptnachteil der Piezoelectric-Paint ist, wird deren Verbesserung untersucht. Die verbesserte Piezoelectric-Paint wird mit traditionellen Dehnungsmessstreifen und Keramiksensoren verglichen. Danach werden verschiedene Anwendungen für SHM-Systeme getestet: als Dehnungssensoren, als modale Sensoren für Filterung, und als Vibrationssensoren für Modalanalyse. Außerdem sind ihre thermischen Eigenschaften untersucht. Da die

Piezoelectric-Paint eine Polymerphase enthält, sind ihre Anwendungen für die Umgebungstemperatur beschränkt, daher wird eine weitere Gruppe von Sensoren aus piezoelektrischem Material für Hochtemperatur-Anwendungen untersucht. Dieser Teil der Arbeit konzentriert sich auf einen Dreischichtstruktur, Aluminiumnitrid (AlN), Diamant und γ-Titanaluminid (γ-TiAl). Der flächige Sensor aus AlN wird hierbei auf die Struktur aus Diamant und γ-TiAl aufgebracht. Verteilte Elektroden sind als Interdigital Tranducer (IDT) ausgeführt und ermöglichen die Anregung von Oberflächenwellen, sog. Surface Acoustic Wave (SAW). Die numerische Berechnung der Struktur wird ausgeführt, um die Dispersionseigenschaften von SAW, die sich auf der Dreischichtstruktur ausbreitet, zu studieren. Mit Hilfe der Finite Elemente Methode (FEM), wird die Ausbreitung der SAW durch Modellierung und Simulation demonstriert. Um die Fehlererkennungsfunktion des Sensors im Rahmen einer SHM-Anwendung zu demonstrieren, wird ein struktureller Fehler simuliert.

1 Introduction

1.1 Review of Structural Health Monitoring

All engineering structures, such as bridges, buildings, railways and aircrafts, all of them are built to function safely; especially for facilities which concern the public safety [BOLLER *et al.* 2009]. However, unexpected accidents happened, either due to natural disasters or unforeseen problems. A well-known example is the NASA Columbia disaster: the leading edge of the wing was impacted by a large piece of insulating foam dislodged from the external fuel tank, which was detected only later after the analyzing of video and pictures [DUNN 2003] after collapsing. Figure 1.1 is a damaged model of the space shuttle leading edge made with carbon fiber-reinforced carbon. Later reports pointed out that due to the cost and schedule considerations, the shuttle only relied on a time-based inspection plan, which meant engineers only have had limited access to the structural condition during launch and on the ground after a mission [PEAIRS 2006]. Dramatic lessons are also learned in the past from many aircraft accidents, such as the Aloha airline Flight 243 accident caused by a failed maintenance program [BOARD 1988], the Japan airline Flight 123 accident caused by an insufficient repair [HARUTA and HALLAHAN 2003], the China airline Flight 611 accident caused by delayed maintenance [LI, W.-C. and HARRIS 2005], etc. Disasters like these pointed out that an in-situ or on-line monitoring system is desired to monitor the condition of a structural system continuously on a regular base, thus not only preventing extreme conditions, such as severe impact, strong wind, but also taking care of unnoticed flaws such as small fatigue, crack, or delamination, which may grow into major problems with time.

A traditional way to maintain structural systems functioning safely involves checking at regular intervals during the lifetime of a structural system, usually it is done by a visual inspection with experienced personal, more advanced Non-Destructive Testing (NDT) techniques including ultrasonic testing, eddy current are also adopted frequently. These methods are time consuming and labor intensive, furthermore, they share a big part of the operational cost of a structure. In addition, the cost due to downtime of structures also has to be counted in. In the commercial aircraft industry, the maintenance and repair cost is approximately a quarter of the operational costs [GIURGIUTIU 2008]. Nowadays, with the increasing amount of aging infrastructures, the question of how to maintain them function safely and cost-effectively has been becoming an on-going concern.
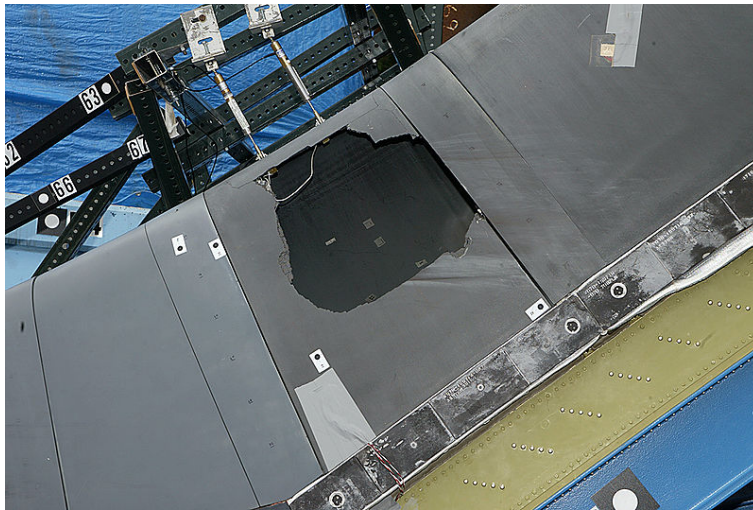
Figure 1.1 Simulation of known and possible conditions of the foam impact on Columbia (Courtesy of NASA, 2003)

Under these circumstances, the concept of Structural Health Monitoring (SHM) arose from the field of structural engineering in the late 1980s [BOLLER *et al.* 2009]. Unlike NDT, which interrogates a structure only as planed from time to time, SHM is an in-service monitoring system which is integrated with the host structure as a part of it [BOLLER *et al.* 2009]. It may alleviate the great burden of maintaining a scheduled structural system with as-needed maintenance, thus saving the cost of unnecessary maintenance and preventing unscheduled maintenance [GIURGIUTIU 2008]. With appropriate data acquisition, processing and interpretation, it can help to evaluate the healthy status of an aging structure and predict the remaining lifetime of it. Nowadays, for a newly constructed structural system, all the sensors and part of the interrogation

systems for SHM can be integrated into the structure as a part of it in the design stage, this can reduce the maintenance cost considerably [NI *et al.* 2011; NI *et al.* 2008; NI and ZHOU 2010].

1.2 Methods for Structural Health Monitoring

Generally, Structural Health Monitoring is comprised of four steps, they are to be performed sequentially in order to solve a complete SHM problem. These are: a.) determination of the existence of a damage, b.) damage localization, if a damage exists, c.) quantification of the damage severity level, d.) prediction of the remaining life time [BALAGEAS *et al.* 2006; RYTTER 1993]. Besides, there are two further steps: self diagnose and self healing [BALAGEAS *et al.* 2006], since these two steps involve very complicated methods and require advanced material science technologies, at the moment, most of the SHM research works mainly focus on the first four steps.

Giurgiutiu categorized Structural Health Monitoring as two species: passive SHM and active SHM [GIURGIUTIU 2008]. For the passive SHM, usually various operational parameters are measured and the health status of a structure is determined from the measured data. Contrarily, an active SHM tries to use integrated damage detection sensors and monitoring methods to obtain the structural health on demand [GIURGIUTIU 2008]. Another popular way to categorize the SHM methods is to specify them as model-based method, such as vibration-based SHM, which intends to have a global information of a structure [FRITZEN 2005], and data-based methods, such as ultrasonic wave based damage detection, electromechanical impedance method, which aim to obtain a local information of a structure [FRITZEN 2005].

1.3 Piezoelectric transducers in Structural Health Monitoring

In an SHM system, no matter what kind of method is used, the sensors always play crucial roles to the whole structural system. Sensors and their signal communication pathways for an SHM system are like the nerve systems for the human being, while neurons react to the stimuli and change of the outside world and report information back to the brain through nerves, sensors monitor the dynamic change of the host structure, collect information and send signals to the central controller, usually a computer or microcontroller, through cables or radio frequencies (wireless) for decision making. After processing the information collected by the sensors, the question about whether this structure is healthy or not can be answered. Without a nerve system,

the human being is subjected to all kinds of dangers from the outside world, such as burning, hitting, cutting illness, etc. Likewise, a SHM system cannot exist without sensors, which provide information for different SHM methods.

Since the piezoelectricity makes the transformation of electrical energy to mechanical energy possible and vice versa, they are widely used in many fields such as electromechanical frequency filter, ultrasonic transducer, motor, resonators, delay lines, microphones, and many other piezoelectric devices. In 1920 Born published his studies which provided the first lattice-theoretical calculation of a piezoelectric coefficient of β-ZnS. In 1921 Cady invented the first circuit to control frequencies based on quartz crystal resonators [CADY, W. G. 1921] and received two fundamental patents on resonators and their applications to radio in 1923 [CADY, W. G. 1923a; CADY, W. G. 1923b]. Bechmann began his work on piezoelectric crystals in 1933 and was one of the four independent inventors of zero-temperature-coefficent AT-, BT-cuts of quartz. The first serious application work of piezoelectricity was performed by Langevin during World War I. Langevin and coworkers developed a piezoelectric transducer to generate ultrasonic waves for submarine detection through echo location [CARTZ 1995]. Since then the development of sonar transducers has been continuing, until now the Langevin type piezoelectric transducer is still widely used in under water communication applications.

Traditional transducers for NDT are very bulky and expensive, they are not suitable for a permanent installation because of their cost and weight. Recently emerged sensors and actuators made from piezoelectric materials are small, light weighted, inexpensive, robust and low energy consuming, they are quite ideal for many SHM applications and have been adopted in different occasions. Piezoelectric wafer active sensors, which are made from piezoelectric ceramic and often seen in square or round shape, are the most widely used piezoelectric transducers in SHM. They can be bonded on a structural surface, embedded in between structural layers or mounted inside built-up structures [GIURGIUTIU 2008] as acoustic emission sensors [MARTIN, T. *et al.* 2001; YANG, CHENG *et al.* 2011], lamb wave transducers [BAO 2003; GIURGIUTIU 2002; THOMAS *et al.* 2004; YU, L. and GIURGIUTIU 2012], electromechanical impedance transducers [GIURGIUTIU and ZAGRAI 2005; ZAGRAI and GIURGIUTIU 2002], ultrasonic transducers [GIURGIUTIU 2003; MICHAELS and MICHAELS 2004] and more.

In addition to piezoelectric wafer active sensors, other piezoelectric transducers, such as Polyvinylidene fluoride (PVDF) [BÄCKER *et al.* 2011; GU, H. and WANG 2009; GU, H. *et al.*

2005; SIZOV *et al.* 2008], piezoelectric smart patches [WANG, J. and ZENG 2011; WANG, Q. and QUEK 2004] have also been used in the health monitoring field. However, as every coins has two sides, although these piezoelectric transducers mentioned above have been proved to be useful and essential in many NDT and SHM applications, there are still many application requirements which cannot be covered by them, such as distributed sensing, high temperature sensing, which require sensors other than discrete piezoelectric ceramic, PVDF or piezoelectric patches.

The research work described in this dissertation focuses on the investigation of spatially distributed piezoelectric sensors, which aim to fill in the application-gap left by the traditional piezoelectric transducers. In the next section, the organization of the thesis will be presented.

1.4 Organization of the dissertation

This dissertation explores piezoelectric materials as spatially distributed transducers for SHM applications. It focuses on two groups of piezoelectric materials, the piezoelectric paint and the Aluminum Nitride (AlN). An introduction of the contents in each chapter is as follows:

Chapter 2: Theoretical background

This chapter introduces necessary theoretical backgrounds of the work. It starts with an introduction of the piezoelectricity history, polarization and hysteresis of piezoelectric materials. The constitutive equation of piezoelectricity, which is one of the most important basics of this work, is also introduced. Three types of piezoelectric materials: piezoelectric crystal, ceramic and polymer are introduced, especially their piezoelectric principles. The last section brings out the distributed piezoelectric transducers and introduces their basics for the followed chapters.

Chapter 3: Investigation on development and characterization of piezoelectric paint

The main focus of this chapter is to develop a new type of flexible and distributable smart sensors, the piezoelectric paint. To start with, the state-of-the-art of the piezoelectric paint, including lab fabrication methods and applications, are presented and compared. Since the piezoelectric paint is still a new smart material whose production is only limited in research labs, its fabrication is investigated in the followed section, to produce a high quality piezoelectric paint. Before using it in further applications, the fabricated piezoelectric paint is characterized through different tests. From the characterization process material properties are calculated. In order to solve the low piezoelectricity problem of the paint, which may limit its potential application and acceptability,

a refinement method is explored to enhance the piezoelectricity, these enhanced samples are characterized as well.

Chapter 4: Application of piezoelectric paint as spatially distributed sensors

In this chapter, two typical applications of piezoelectric paint have been performed. First, the piezoelectric paint is applied as spatially distributed sensors, which is a very promising application of it. Because this application requires a piezoelectric transducer which is distributable, flexible and easy to be shaped, they are the features the piezoelectric paint can offer. In this application, analytical calculations of modal sensors for a one-dimensional beam are considered, and the shape of modal sensors is deduced from the calculation. Experiments are performed to verify the theory and the results are discussed, followed by an optimization. At the beginning of the second application, the performance of piezoelectric paint is compared with two traditional sensors: the strain gauge and the piezoelectric ceramic. Afterwards the piezoelectric paint is applied as an integrated vibration sensor in an impact modal analysis.

Chapter 5: Aluminum Nitride as distributed transducers in high temperature application

The thermal testing of the piezoelectric paint indicates that the piezoelectric paint is not suitable for applications involving high temperature, as the temperature goes high, its performance is severely compromised. Therefore, in Chapter five, another group of piezoelectric material, Aluminum Nitride, is considered to be used in high temperature SHM applications.

In this chapter, Aluminum Nitride is applied as a distributed piezoelectric transducer in a three layered structure for Surface Acoustic Wave (SAW) generation and receiving, which is used for high temperature corrosion protection and damage detection. Theoretical backgrounds of SAW and SAW device is presented, including constitutive equations and SAW device principles. An analysis of elastic waves propagation in unbounded and bounded media is presented, as well as the dispersion behavior. Finally, Finite Element simulations are performed to simulate a surface damage which can be detected by the SAW.

Chapter 6: Conclusion and outlook

Chapter six concludes the achieved works and results, followed with an outlook of future works.

2 Theoretical background

2.1 History of piezoelectricity

Piezoelectricity refers to the phenomenon existing in certain materials, which generates an electric field when the material is subjected to a mechanical stress, and conversely, induces a mechanical strain in response to an applied electric field. The former is called direct piezoelectric effect and the later is the converse piezoelectric effect [TRAINER 2003]. Started from 1880 of its undoubted discovery, the piezoelectricity has grown to be a significant commercial importance until today. This part is going to review the milestones in the piezoelectricity development history.

Coulomb was reported as the first to conjecture that the stress applied on solid object would produce electrical charges [GILLMOR 1971]. From 1781 to 1806 he submitted important discoveries to the French Academie des Sciences about electricity and magnetism [GILLMOR 1971]. This led to experiments by Haüy and Becquerel with inconclusive results [GRAF 1981]. In 1817, Haüy observed that certain crystals showed electrical effects when compressed, and Becquerel confirmed these same electrical effects in 1820 [GRAF 1981].

The actual discovery of direct piezoelectric effect was performed through two young physicists -- the brothers Pierre Curie and Jacques Curie, in 1880. They firstly discovered the direct piezoelectricity in tourmaline, and found out as a results of pressure applied along a particular direction, electrical charges proportional to the pressure and of opposite polarities were generated on crystal surfaces [TICHÝ et al. 2010]. Later, they discovered the similar effect in quartz,

Rochelle salt and other crystals, all of which have no center of symmetry [TICHÝ *et al.* 2010]. They announced that "We have found a new method for the development of polar electricity in these same crystals, consisting of subjecting them to variations in pressure along their hemihedral axis" [BALLATO 1996]. In 1881 W. G. Hankel proposed the name "piezoelectricity" in a report, and it was widely accepted by all the researchers at that time [TICHÝ *et al.* 2010]. At the same year, the converse piezoelectric effect was mathematically deduced from fundamental thermodynamic principles by Lippmann [LIPPMANN 1881], it was immediately confirmed via an experiment by the Curies in the following year of 1882 [CURIE and CURIE 1882]. In 1893, Kelvin made a significant contribution to piezoelectricity by presenting analogy models and laying down some of the basic framework that led to the modern theory of piezoelectricity [TRAINER 2003]. In 1894 Voigt developed tensor equations to describe the linear behavior of piezoelectric crystals in a paper " Beiträge zur molecularen Theorie der Piezoelectricität" [TICHÝ *et al.* 2010].

In the following years, many works have been reported to expand the core of piezoelectricity, which grew into a versatile and complete framework, however, the problem of piezoelectricity was still remained as a laboratory curiosity, until Voigt published the first rigorous formulation of piezoelectricity [VOIGT 1890]. Continued in 1910, Voigt published "Lehrbuch der Kristallphysik" [VOIGT 1910], the formulations used in the physics of crystals today still owns much to this monumental book. With the work of Voigt, the theory of piezoelectricity reached maturity.

2.2 Polarization

When applying a mechanical stress on a piezoelectric material, the change of polarization or the polarization itself is the most basic parameter, on which all the magnitudes of intrinsic dielectric, pyroelectric, ferroelectric and piezoelectric properties depend [SAFARI and AKDOGAN 2008]. In dielectrics, a phenomenon called polarization is observed on the application of an external electric field. It indicates the separation of positive and negative electric charges at different ends of the dielectric material, which is usually caused by reorientation of dipole moments of polar molecules in the material. The electric polarization P can be expressed as a linear function of the field

$$P = \chi E \tag{2-1}$$

where P describes the surface charge, which is the charge separation, χ is the dielectric susceptibility, it represents the polarization per unit of the existing electric field in the dielectric, E represents the electric field. The total surface-charge density in the material is represented by the dielectric displacement D, which is the sum of charges associated with polarization of the material P and the charges generated by the polarization of free space, therefore, the electric displacement D can be related to the polarization density P and electric field E by [GIURGIUTIU 2008]

$$D = \varepsilon_0 E + P \tag{2-2}$$

where D represents charge per unit area and ε_0 is the electric permittivity of vacuum. For a dielectric capacitor, P represents the additional charges stored in it as compared with a vacuum capacitor. Therefore polarization is the explanation of the fact that the dielectric capacitor can hold much more charges than the vacuum capacitor [GIURGIUTIU 2008]. Besides induced polarization, some substances have permanent polarization which is caused by asymmetry of the molecules [SCHADOWITZ 1988]. In certain crystals, whose centers of positive and negative charges do not coincide, a phenomenon called spontaneous polarization is observed, which is often seen in perovskite crystal structures. It indicates that the polarization appears without the application of an external electric field. Change of the spontaneous polarization generated by the temperature increase or decrease is called pyroelectric effect [TICHÝ et al. 2010], which means the materials display electric charges on material surfaces due to change of temperature. Every pyroelectric material is necessarily piezoelectric [TICHÝ et al. 2010].

Generally, the polarization depends on the electric field intensity, thus it disappears with the absence of the electric field. However, for a special group of pyroelectric materials, permanent polarization exists, which means the polarization is "frozen" in the material with the absence of an external electric field, this is the so called ferroelectric effect. Pyroelectric properties are necessary, but not sufficient conditions for ferroelectricity [TICHÝ et al. 2010], in other words, all ferroelectric crystals belong to one or another pyroelectric class, and an external electric field can reverse its polarization [GONZALO and JIMENEZ 2005].

Piezoelectricity is related to the permanent polarization since it indicates the property of displaying electric charge on the material surface under the application of an external mechanical stress. As the material undergoes mechanical deformation due to applied stress, the permanent

polarization is changed. With proper signal conditioning devices, this variation can be measured and it could trace the magnitude of the applied stress. Figure 2.1 shows the relationship between piezoelectricity, pyroelectricity, ferroelectricity, and strong dielectrics.
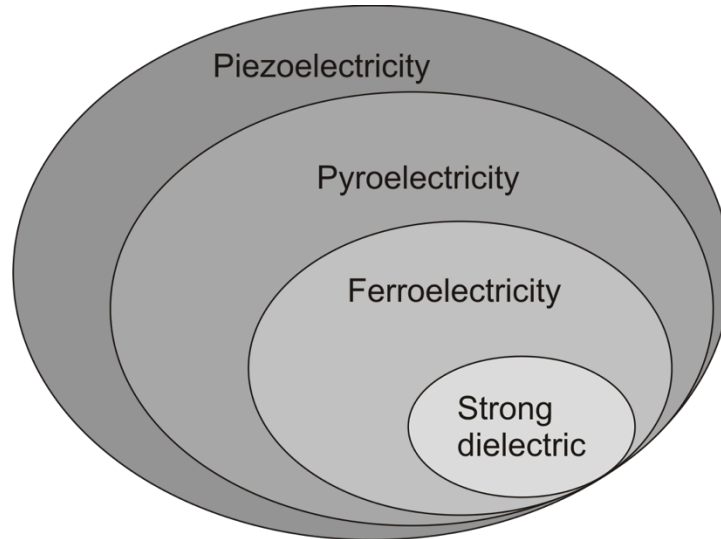

Figure 2.1 The relationship between piezoelectric, pyroelectric, ferroelectric and strong dielectric [HEYWANG *et al.* 2008]

2.3 Hysteresis

For most of the dielectrics or paraelectric material, they polarize linearly with the external electric field, of which the polarization decreases to zero after cancellation, this is demonstrated in Figure 2.2(a). On the contrary, a distinguishing feature of ferroelectrics is that they remain a net polarization when the electric field is removed, this is explained in terms of the residual alignment of permanent dipoles [ASHBY 2009], furthermore, their spontaneous polarization direction can be reversed by the external electric field, thus yielding a hysteresis loop. This is illustrated in Figure 2.2(b). As the positive electric field reaches the coercive field E_c, the polarization jumps to a high value immediately, with further increasing of the electric field the dipoles reach a saturation polarization, they are aligned with respect to the field direction. If we decrease the electric field to zero, this high value of polarization is roughly held until a point called permanent spontaneous polarization P_s is retained, this is due to a coupled interaction between dipoles. Further decrease of the electric field to a negative coercive field $-E_c$ will remove the polarization, beyond $-E_c$ the polarization is reversed to a large negative value, and the permanent spontaneous polarization is obtained at zero field. The trace of polarization constructs a hysteresis loop.

However, it should be noticed that not all materials which have permanent dipoles possess ferroelectric behavior, since their dipoles are back to random arrangement after the external electric field is removed, no net polarization remains afterwards [ASHBY 2009].
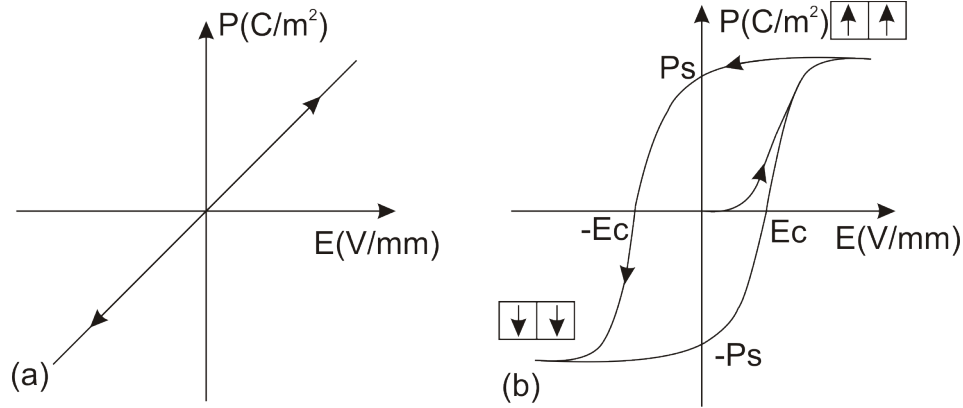

Figure 2.2 Comparison between (a) normal dielectric polarization and (b) ferroelectric polarization [GIURGIUTIU 2008]

2.4 Piezoelectric constitutive equations

The ANSI/IEEE Standard 176-1987 describes the linear relationship between the electrical and mechanical variables of piezoelectric materials. The linear constitutive equations are presented in the following tensor form [GHODSSI and LIN 2011],

$$T_{ij} = c_{ijkl}^{E} S_{kl} - e_{kij} E_k \qquad (2\text{-}3)$$

$$D_i = e_{ikl} S_{kl} + \varepsilon_{ij}^{S} E_k \qquad (2\text{-}4)$$

i, j, k, l are equal to 1, 2, 3, they are indices of the Einstein notation. c_{ijkl}^{E}, e_{kij} and ε_{ij}^{S} are the elastic, piezoelectric, and dielectric tensors, respectively. T_{ij} and S_{kl} are the stress and strain tensors. D_i is the electric displacement, which is a vector and E_k is the electric field vector. (2-3) and (2-4) are the stress-charge form of the piezoelectric constitutive equations. (2-3) represents the inverse piezoelectric effect, and (2-4) represents the direct piezoelectric effect. These two equations combine the mechanical and electrical properties together. In (2-3), the first term on the right hand side is the generalized form of Hooke's law, the second term represents the additional mechanical stress induced by electric field, which happens in a piezoelectric material. In (2-4), the second term on the right hand side indicates how the electric field influences the organization of electrical charges in a given medium, including charge migration and electric dipole

reorientation, the first term represents how a strain change in a piezoelectric material induces electrical charges. (2-3) and (2-4) can also be written with T_{kl} and E_j as independent variables:

$$S_{ij} = s_{ijkl}^E T_{kl} + d_{kij} E_k \tag{2-5}$$

$$D_i = d_{ikl} T_{kl} + \varepsilon_{ik}^T E_k \tag{2-6}$$

where s_{ijkl}^E is the tensor of compliance constants, d_{kij} is the tensor of piezoelectric charge constant. (2-5) and (2-6) are the strain-charge form of the piezoelectric constitutive equations. The superscript E, S, and T appears in these equations indicating that the quantities are measured under zero electric field, zero strain or zero stress. In order to write the elastic and piezoelectric tensors in matrix form, a compressed matrix notation is introduced to replace the tensor notation. This is by replacing ij or kl with p or q, where $i, j, k, l = 1, 2, 3$ and $p, q = 1, 2, 3, 4, 5, 6$. Table 2.1 shows the reduced subscripts.

p, q	ij, kl
1	11
2	22
3	33
4	23, 32
5	13, 31
6	12, 21

Table 2.1 Reduction of subscripts

Therefore, the 6×6 stress and strain tensors T_{ij} and S_{kl} are replaced by 6 components vectors T_p and S_q,

$$\begin{Bmatrix} S_{11} \\ S_{22} \\ S_{33} \\ S_{23} \\ S_{31} \\ S_{12} \end{Bmatrix} \rightarrow \begin{Bmatrix} S_1 \\ S_2 \\ S_3 \\ S_4 \\ S_5 \\ S_6 \end{Bmatrix}, \quad \begin{Bmatrix} T_{11} \\ T_{22} \\ T_{33} \\ T_{23} \\ T_{31} \\ T_{12} \end{Bmatrix} \rightarrow \begin{Bmatrix} T_1 \\ T_2 \\ T_3 \\ T_4 \\ T_5 \\ T_6 \end{Bmatrix} \tag{2-7}$$

Thus the constitutive equations (2-5) and (2-6) can take the matrix form,

$$
\begin{Bmatrix} S_1 \\ S_2 \\ S_3 \\ S_4 \\ S_5 \\ S_6 \end{Bmatrix} = \begin{bmatrix} s_{11} & s_{12} & s_{13} & 0 & 0 & 0 \\ s_{21} & s_{22} & s_{23} & 0 & 0 & 0 \\ s_{31} & s_{32} & s_{33} & 0 & 0 & 0 \\ 0 & 0 & 0 & s_{44} & 0 & 0 \\ 0 & 0 & 0 & 0 & s_{55} & 0 \\ 0 & 0 & 0 & 0 & 0 & s_{66} \end{bmatrix} \begin{Bmatrix} T_1 \\ T_2 \\ T_3 \\ T_4 \\ T_5 \\ T_6 \end{Bmatrix} + \begin{bmatrix} d_{11} & d_{21} & d_{31} \\ d_{12} & d_{22} & d_{32} \\ d_{13} & d_{23} & d_{33} \\ d_{14} & d_{24} & d_{34} \\ d_{15} & d_{25} & d_{35} \\ d_{16} & d_{26} & d_{36} \end{bmatrix} \begin{Bmatrix} E_1 \\ E_2 \\ E_3 \end{Bmatrix} \qquad (2\text{-}8)
$$

$$
\begin{Bmatrix} D_1 \\ D_2 \\ D_3 \end{Bmatrix} = \begin{bmatrix} d_{11} & d_{12} & d_{13} & d_{14} & d_{15} & d_{16} \\ d_{21} & d_{22} & d_{23} & d_{24} & d_{25} & d_{26} \\ d_{31} & d_{32} & d_{33} & d_{34} & d_{35} & d_{36} \end{bmatrix} \begin{Bmatrix} T_1 \\ T_2 \\ T_3 \\ T_4 \\ T_5 \\ T_6 \end{Bmatrix} + \begin{bmatrix} \varepsilon_{11} & \varepsilon_{12} & \varepsilon_{13} \\ \varepsilon_{21} & \varepsilon_{22} & \varepsilon_{23} \\ \varepsilon_{31} & \varepsilon_{32} & \varepsilon_{33} \end{bmatrix} \begin{Bmatrix} E_1 \\ E_2 \\ E_3 \end{Bmatrix} \qquad (2\text{-}9)
$$

or in a compact matrix form,

$$
\{S\} = [s]\{T\} + [d]^{t}\{E\} \qquad (2\text{-}10)
$$

$$
\{D\} = [d]\{T\} + [\varepsilon]\{E\} \qquad (2\text{-}11)
$$

In practical applications, many components of the d_{ij} matrix have negligible values since the piezoelectric materials respond preferentially along certain directions depending on their intrinsic polarization [GIURGIUTIU 2008].

2.5 Piezoelectric materials

The piezoelectric material can be classified as three types: natural piezoelectric crystals or man-made crystals; synthetic piezoelectric ceramic and piezoelectric polymer [SINGH and JOSHI 2006]. Although they are all piezoelectric active, their mechanical and electrical properties, as well as their piezoelectric principles are way different from each other. Since the investigation of them is the main focus of this work, in this section, these three types of piezoelectric material are reviewed, to give an overview of how their piezoelectric properties are related to specific applications.

2.5.1 Piezoelectric crystal

There exist crystals, which have piezoelectricity in nature, such as, quartz, tourmaline and topaz, they are also the earliest piezoelectric materials that have been found [MASON 1950]. Besides the

naturally exists piezoelectric crystalline minerals, there are also man-made crystals, such as Gallium orthophosphate ($GaPO_4$), Langasite ($La_3Ga_5SiO_{14}$) and Aluminum Nitride (AlN) [MASON 1950]. They have crystal structures but producing much more piezoelectric current than the natural crystals, and are widely employed as sensors and actuators.

The Curies have observed that when compressing certain crystals in different directions, positive and negative charges appeared on the crystal surfaces. As being explained in section 2.2, the piezoelectric crystals have an asymmetrical charge distribution, so that the relative displacement of the positive and negative charges within the lattice is effected by the lattice deformation, and the displacement of internal charges produces equal amount of external charges of opposite polarity on the opposite sides of the crystal [BHATTACHARYA 1995].

The principle of piezoelectric crystals can be graphically illustrated in Figure 2.3. Figure 2.3(a) is a molecular model of quartz, whose main component is SiO_2. One silicon and two oxygen atoms interlace with each other and occupy the vertices alternatively, forming a hexagonal shape. Before subjecting to any external stress, the positive charges of silicon and negative charges of oxygen compensate each other, the sum of all the charges in the material is null, the crystal is in a neutral state (Figure 2.3(a)). When exerting a mechanical stress on the material, its internal reticular molecular structure is deformed, which breaks the balance and causes separation of the positive and negative charges on the crystal surfaces, thus an external electric field is produced.
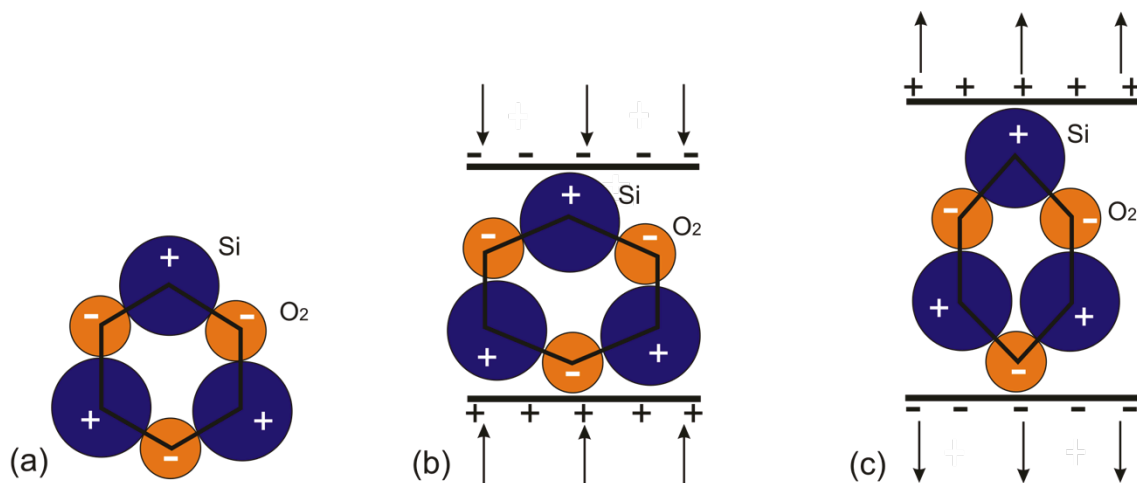

Figure 2.3 Molecular model to explain the piezoelectric effect of quartz crystal (a) neutral state (b) subjected under compression force (c) subjected under tension force [BHATTACHARYA 1995]

In Figure 2.3(b), a compression force is exerted on the molecular model, causing a deformation of the crystal to an extent of being polarized, because the neutral balance is broken, positive and negative charges are generated on the two faces. In the contrary, a tension force exerted on the crystal will generate opposite sign of charges on the crystal surface, as indicated in Figure 2.3(c). This is the phenomenon that could transform the mechanical energy used in the material's deformation into electric energy.

Nowadays, artificially piezoelectric crystals, such as AlN, Zink Oxide (ZnO), play an indispensable role in MEMS [GHODSSI and LIN 2011; HSU 2008], ultrasonic transducers [ARNAU 2008; COLBERT and DALE 1968; MARTIN, P. M. *et al.* 2000; TOLE and OSTENSEN 2005], electrical resonators [PIERCE 1923], filters [ABDOLVAND 2008] and delay lines [ARNAU 2008]. There are not many works investigating deploying of piezoelectric crystals in SHM for damage detection. The work discussed in this dissertation will study the application of AlN as spatially distributed actuator and sensor for surface damage detection, which is one of the main topics of the research work. The theories and details will be presented in Chapter five.

2.5.2 Piezoelectric ceramic

For many years after the discovery of the piezoelectricity, the natural crystals were the exclusive source of piezoelectric capabilities, and many types of products were developed with these materials. In the mid 1960s, a new piezoelectric material, the man-made piezoelectric ceramic, was developed from metallic oxides, it has replaced the natural piezoelectric materials in many fields and have enabled designers to employ the piezoelectric effect and the inverse piezoelectric effect in applications for which natural pyroelectric materials are unsuitable [APC_INTERNATIONAL_LTD 2002]. Besides, this piezoelectric ceramics can have higher sensitivity than natural crystals, and the geometrical dimension, as well as physical properties can be tailored to meet a specific requirement. Therefore, piezoelectric ceramics are of particular importance for the fabrication of piezoelectric transducers.

The synthetic piezoelectric ceramic does not have an asymmetrical charge distribution, therefore, they have to be polarized artificially under strong electric field, by which the asymmetric lattice is produced. Traditionally, the piezoelectric ceramics are perovskite varieties in which the linear piezoelectric behavior dominates [GIURGIUTIU 2008]. Before sintering, finely mixed piezoelectric powder is shaped into a required form. The piezoelectric ceramics consists of a large number of

ferroelectric grains, before polarization, it shows no piezoelectricity, because the electric dipoles in each domain are randomly oriented, as indicated in Figure 2.4(a). If a high electric field is applied on the ceramic through which the spontaneous polarization is partially aligned, the dipoles will be aligned in the field direction (Figure 2.4(b)), after poling most of the dipoles are "frozen" in the alignment direction, they show remnant polarization (Figure 2.4(c)). The polarized ceramics show high piezoelectric coupling and electric permittivity.
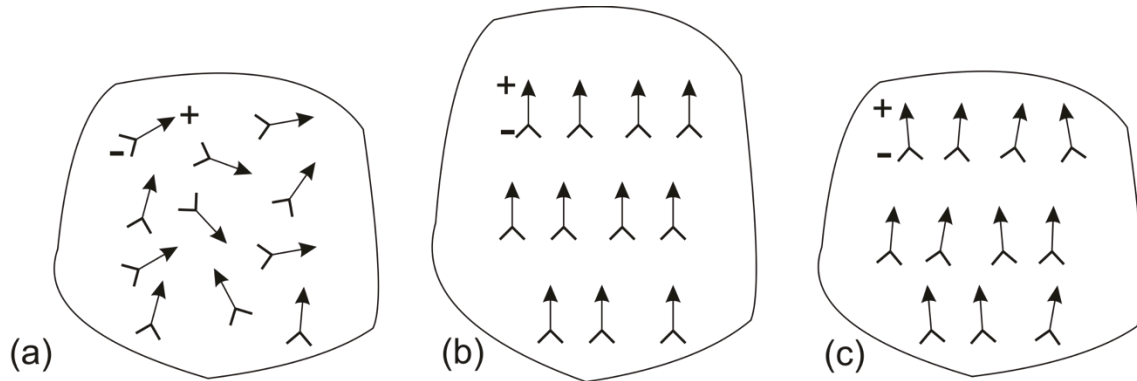

Figure 2.4 Polarization of piezoelectric ceramics (a) unpoled (b) during polarization (c) remnant polarization [APC_INTERNATIONAL_LTD 2002]

A poled piezoelectric ceramic possesses piezoelectricity, and therefore a physical compression or tension will generate a voltage. Figure 2.5(a) shows a piezoelectric ceramic at its original status after polarization. It is informed from Figure 2.5(b) that a compression of the piezoelectric ceramic parallel to the direction of polarization will generate a voltage potential which has the same polarity of the poling voltage. Contrarily, a tension in the same direction will generate a voltage potential which has the reverse polarity of the poling voltage (Figure 2.5(c)). Figure 2.5(d) shows that if the piezoelectric ceramic is placed under an electric field which has the same polarity as the poling voltage, the element will be elongated and its diameter becomes smaller. Similarly, an electric field having a reverse polarity as the poling voltage will cause the element to be shortened (Figure 2.5(e)). In general, Figure 2.5(b) and (c) represents the actuator function of the piezoelectric ceramic, and Figure 2.5(d) and (e) represents the sensor function.

Figure 2.6 shows some commercial piezoelectric transducers of different types. They can be produced in square, rectangular or slender shape with various thicknesses, in addition, they also can be used to produce other advanced sensors, for instance, acoustic emission sensors (VS900-M in Figure 2.6).
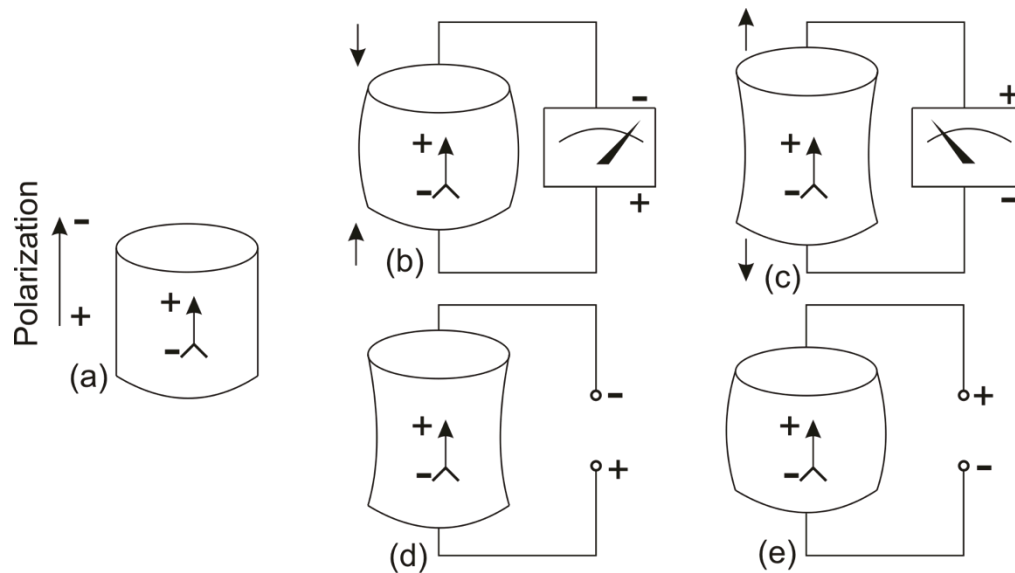
Figure 2.5 Sensor and actuator behaviors of piezoelectric ceramics (a) polarized piezoelectric ceramic at original status (b) piezoelectric ceramic under compression (c) piezoelectric ceramic under tension (d) voltage having same polarity as polarization voltage applied on piezoelectric ceramic (d) voltage having opposite polarity as polarization voltage applied on piezoelectric ceramic [APC_INTERNATIONAL_LTD 2002]

Figure 2.6 Piezoelectric ceramic transducers of different types

The traditional piezoelectric material which has been used in a wide range of applications as sensors and actuators is the piezoelectric ceramic. It is very popular and favorable in non-destructive testing, structural health monitoring and vibration control due to the following advantages [WEBSTER 1999]:

- High piezoelectricity

- High robustness to harsh environment
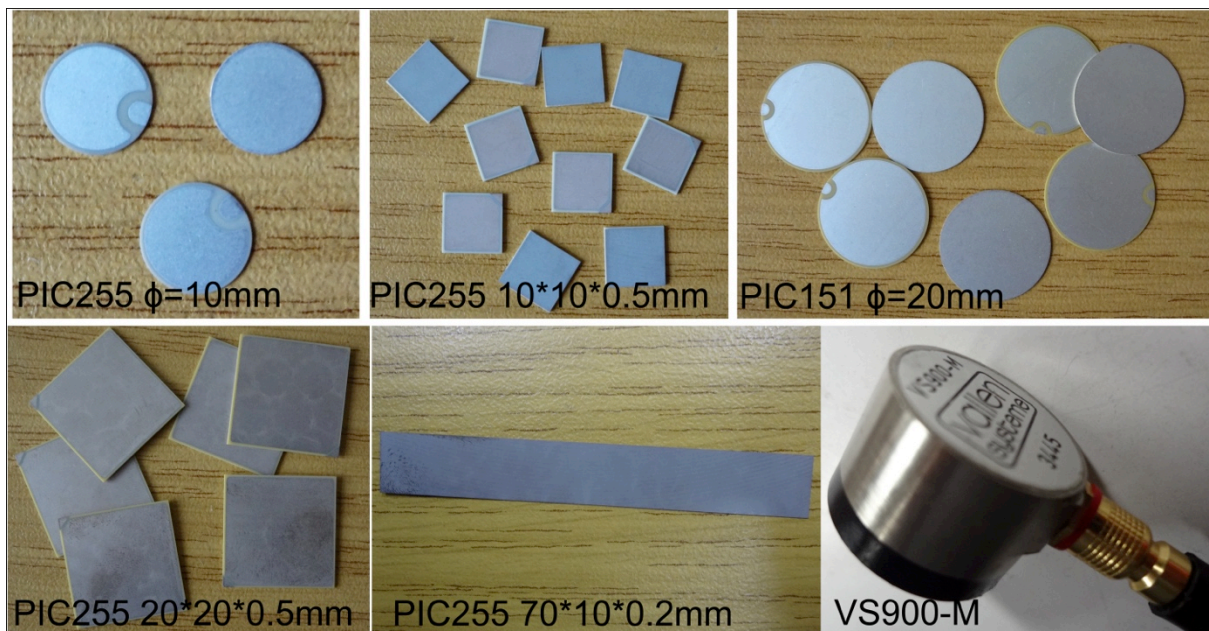
- High Curie point

- Physical, chemical and piezoelectric properties can be optimized to suit particular applications by adjusting the ratio of PZT

- High power applications suitability

- High signal-to-noise ratio

However, these advantages also come along with some serious drawbacks. One of the most serious issue is the high brittleness, meaning it can only withstand very small bending moments, thus the host structural surface must be flat and smooth, in order to ensure a robust and seamless adhesion for a confident measuring result. The problem is more severe for thin ceramic sensors with thickness less than 0.5mm, they should be handled with great care to avoid partial damage. For all the piezoelectric ceramic sensors, once they are adhered on a structural surface, it takes a great effort to peel them off from the host structure.

On the other side, curved structural surfaces are very usual in many applications, these are often seen in water pipelines, welding joints, in these occasions, if no extra treatment was applied, the conformability between the ceramic sensor and the host structure would be very poor. Figure 2.7 shows a piezoelectric ceramic sensor adhered on a steel tube. To ensure a strong conformability between the ceramic and the tube, a flat contacting area was prepared beforehand, consequently the tube is prone to damage [YANG, C. and FRITZEN 2011; YANG, C. and FRITZEN 2012].

Figure 2.7 A piezoelectric ceramic sensor adhered on a steel tube

The second issue associated with the piezoelectric ceramic transducers is that they cannot be shaped easily due to the high hardness, e.g. the hardness of a bulk PZT is approximately 9GPa [BAHR et al. 1999]. All the piezoelectric ceramics, which are commercially available, are delivered with specific shapes (round, square, rectangular). Most of them, except some thin membrane, such as piezoelectric unimorphs or bimorphs [SITTI et al. 2001; TING et al. 2009], PZT-brass [LI, XIAOPING et al. 1999; OOIJEVAAR et al. 2012], cannot be reshaped during applying to feed a specific application need. Even if ordering a special shape of piezoelectric transducers from an industrial producer is possible, this is very costly and will finally increase the total budget of a project. The last issue but not the least concerns the piezoelectric ceramics is that they are discrete transducers, which are impossible to be distributed on a large area of a structural surface. This becomes a big issue in cases having single or multi-curvature structural surfaces, where a distributed transducer is more favorable.

2.5.3 Piezoelectric polymers

Piezoelectric polymers are polymers that display piezoelectric properties similar to those of quartz and piezoelectric ceramics [GIURGIUTIU 2008]. It is a group of piezoelectric composite, which consists the properties of polymers and also has piezoelectricity. The most popular piezoelectric polymer is polyvinylidene fluoride polymer (abbreviated as PVDF or PVF2). PVDF is a fluorocarbon which has excellent processability and chemical resistance [ROSEN et al. 1992a]. The discovery of a strong piezoelectric effect in PVDF dates back to the pioneer work of Kawai in 1969 [KAWAI 1969]. It was described as light, flexible, ruggedness, strong piezoelectricity and have a relatively low acoustic impedance [FURUKAWA and SAKURAI 1971; MURAYAMA et al. 1976; SACHSE and HSU 1988; SESSLER 1981]. The most distinct difference between PVDF and other polycrystalline piezoelectric materials is that the PVDF is a polymeric substance, therefore it is a good alternative in many applications. Two years later in 1971, pyroelectricity was discovered in the same polymer [BERGMAN et al. 1971; NAKAMURA and WADA 1971]. This discovery ignited many researches concerning the use of PVDF [SUSSNER and DRANSFELD 1979; TAMURA et al. 1975; WADA and HAYAKAWA 1976]. Later on, ferroelectricity was also confirmed in PVDF and its copolymers [LOVINGER 1983]. Since then, the science and technology of piezoelectric polymers has been dominated by polymers from the PVDF family, especially the copolymers of vinylidene fluoride and trifluoroethylene P(VDF-TrFE) [HEYWANG et al. 2008].

PVDF can be produced inexpensively in large sheets of thin films (thickness in the order of micrometers) [BLOOMFIELD and MARCUS 1988], it is a semi-crystalline high-molecular weight polymer consisting of long chains of repeating monomer (-CH2-CF2-), its structure is essentially head-to-tail (CH2-CF2-(CH2-CF2)n-CH2-CF2-) [PRIYA and INMAN 2009].

Figure 2.8(a) shows its molecular structure. PVDF is produced in a large thin sheet, which are stretched along the direction which most of the carbon chains run, this process poles the PVDF to generate piezoelectricity. In reality, the polarization is achieved by heating the plastic to about 100°C in oil, and subjecting to a high electric field of about 80MV/m [ROSEN et al. 1992a]. After poling, the hydrogen atoms which have net positive charges and fluorine atoms which have net negative charges are separated on opposite sides of the sheet. When an electric field as indicated in Figure 2.8(b) is applied across the PVDF sheet, the polymer expanded in the stretch direction because the positive hydrogen atoms are attracted by the negative side of the electric field, and the negative fluorine atoms are attracted by the positive side of the electric field, and vice versa (Figure 2.8(c)).

The most distinguished feature of the piezoelectric polymers is its high flexibility, low weight and low acoustic impedance comparing with normal piezoelectric ceramic sensors. The properties are especially attractive for applications involving single or multi-curvature structural surfaces, or applications involving Carbon Fiber Reinforced Polymer (CFRP), whose acoustic impedance is closer to the piezoelectric polymer than ceramics.
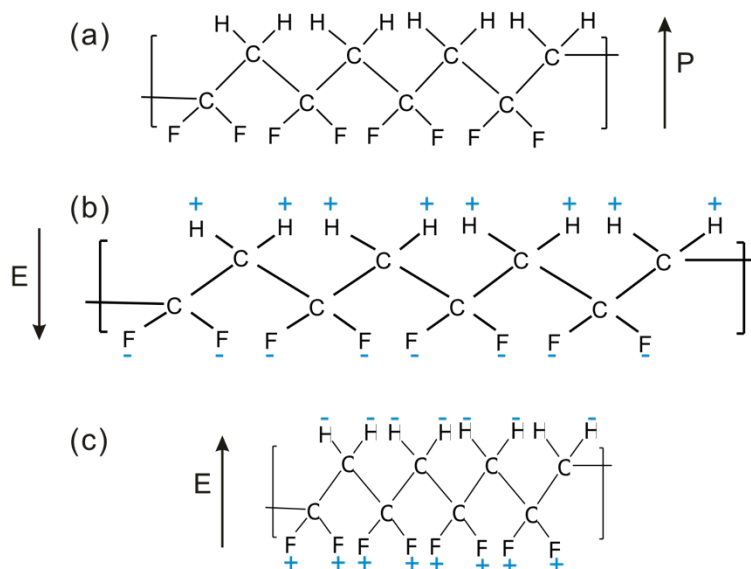

Figure 2.8 Molecular structure of PVDF [TASHIRO et al. 1981]

In the 1980s, another group of piezoelectric polymer, the piezoelectric paint, which is mainly made from piezoelectric ceramic powder and epoxy resin, entered into many researchers' view. Unlike the piezoelectric ceramic, which consists of ceramic synthesis solely, or PVDF, which is a semi-crystallized flexible polymer, the feature of the piezoelectric paint can be told from the name itself: it shows piezoelectricity, and is flexible and distributable similar to a paint in a natural meaning.

Piezoelectric paint is an uprising new smart material and has attracted many attentions in the past years. The fabrication and application of the piezoelectric paint, which will be presented in the following chapters, is one of the most important focuses of this dissertation. Before introducing the piezoelectric paint in the following chapters, a group of transducers named spatially distributed transducers are briefly introduced in the next section.

2.6 Spatially distributed transducers

The concept of distributed transducers is indeed not novel, one of them which is widely known is the fiber optic sensor. It is a sensor that uses an optic fiber as the sensing element, or relaying signals from a remote sensor to the electronics that processes the signals. A fiber optic sensor is useful for sensing seismic or pressure disturbances [ROWE 1984], environmental effects [UDD *et al.* 1988], strain, temperature, and many other quantities that can modify the fiber. Due to their lightness, flexibility, immunity to electromagnetic interruption and other properties, fiber optic sensors are used in SHM for sensing and damage detection [INAUDI 2007; LI, S. and WU 2007; MEASURES 2001], such as in bridges [MAASKAN *et al.* 1997; VURPILLOT *et al.* 1996], buildings [LAU, K.-T. 2003] and aircraft fuselages [GUO *et al.* 2011]. However, fiber optic sensors also have several major disadvantages, which cannot be ignored:

- Despite the fact that the installation cost of fiber optic sensors is dropping every year, the price of installation is still expensive, not to say the complicated installation methods, which requires very precise techniques [HUBTECHINSIDER 2009].

- The signal acquisition and conditioning devices are very bulky and expensive [THAKRAL and MANHAS 2011].

- The fiber is very fragile and susceptible to physical damages.

Since this work focuses on transducers with piezoelectricity, the fiber optic sensor is not included in the discussion. The spatially distributed transducers which are going to be discussed in this work are piezoelectric paint and Aluminum Nitride.

Piezoelectric paint is the solution to the above-mentioned obstacles, it is flexible, distributable and can be integrated into its host structure. It is not a completely new smart material, the research about it can be traced back to the 1980s. Over the years, new results of its investigation have been continuously published, which proved its promising usability as a smart material for applications which could not be fulfilled by traditional piezoelectric ceramics. Despite its light weight, its fabrication and installation price is much lower than the distributed fiber optic sensors, if a mass production is possible, the cost of piezoelectric paint is comparable to piezoelectric ceramics. The detailed investigation of piezoelectric paint will be discussed in following chapters.

3 Investigation on development and characterization of piezoelectric paint

3.1 Introduction

The main focus of this chapter is the development and characterization of piezoelectric paint. Since the piezoelectric paint is a composite material, it requires strict selection of materials and appropriate handling methods to produce it. To start with, the state-of-the-art of piezoelectric paint development over the years is reviewed. Followed, a chosen method is described for producing the piezoelectric paint. Since a new material cannot be used in applications without knowing its properties, the piezoelectric paint is characterized through different methods to obtain its elastic, mechanical, piezoelectric, and thermal properties.

3.2 Review of the development of piezoelectric paint

Piezoelectric paint is a composite piezoelectric material that is mainly comprised of tiny piezoelectric ceramic particles, which is used to provide the material with piezoelectricity, and polymer matrix, which is used to bind the ceramic particles together. Furthermore, it may also include other additives, such as defoamer, sovlent, plasticizer, which helps to enhance the properties of piezoelectric paint [LI, XIN 2009].

As indicated by the name, the piezoelectric paint possesses the features similar to a normal paint, for instance, flexible, distributable and conformable, meanwhile it has piezoelectricity which makes it very promising and attractive in many fields, such as vibration measurement [EGUSA

and IWASAWA 1993], structural health monitoring [EGUSA and IWASAWA 1998] and acoustic emission [LI, X. and ZHANG 2008], because it is able to provide favorable features which cannot be obtained by single-phase materials. The exploration history of the piezoelectric composite can be traced back to the late 1970s, when Newnham and his colleagues studies the connectivity of a two-phase piezoelectric composite [NEWNHAM *et al.* 1978]. Followed in the 1980s, several researchers studies fabrication of the piezoelectric composite [GINIEWICZ 1985; GURURAJA *et al.* 1980; HANNER *et al.* 1989; LEVINSON, L. M. and DEKKER 1988; NEWNHAM 1986]. In the work of Newnham *et al*, they prepared the composite paint from a water-based suspension electroceramics and polymer, sprayed the composite on a brass plate, dried in air at room temperature for 24 hours, and then placed it in a vacuum oven at 110°C for an additional 24 hours, then poled the sample under 10-15kV/mm. They also measured the average value of d_{33} by a Piezo d_{33}-meter. Han *et al.* used a colloidal processing method to improve the piezoelectric properties of a ceramic-polymer composites [HAN, K. *et al.* 1991; HAN, K. H. *et al.* 1990a; HAN, K. H. *et al.* 1990b]. They dissolved epoxy in a methanol solution and added ceramic powder to form a suspension, precipitated the powder-polymer coacervate from the suspension, after colloidal filtration, the coacervate was cold-pressed to form a powder-polymer composite, they summarized the method could produce composite with uniform microstructure and decrease air void formation, so that a higher poling field was possible. In addition, they also studied the effect of piezoelectric powder particle size on dielectric and piezoelectric properties.

Followed by the research works performed by Egusa and Iwasawa in the 1990s [EGUSA and IWASAWA 1993; EGUSA and IWASAWA 1994; EGUSA and IWASAWA 1996], they prepared the piezoelectric paint by using PZT ceramic powder as pigment and epoxy resin as binder, spread the mixture on an aluminum beam surface with a paint brush, dried in air at room temperature for around three days, used a screen mask to print electrodes on the paint surface, poled under 20-45kV/mm, and applied the thin film as vibration sensors. Later Egusa *et al.* also explored the health-monitoring capabilities of the piezoelectric paint [EGUSA and IWASAWA 1998].

Based on these works, improvements were done by the research group of Hale, who combined fine milled PZT powder with acrylic lacquer to make the piezoelectric paint, used air brushes to spray the paint on a surface, and poled the samples under 600V for one hour [HALE and TUCK 1999], they also characterized the piezoelectric paint through tensile test, dynamic test and environmental test [HALE 2004]. Followed Zhang *et al* reported the piezoelectric paint fabrication

and extended the application to in situ fatigue crack detection [ZHANG 2006a] and acoustic emission [LI, X. and ZHANG 2008]. M. Dietze and M. Es-Souni reported the fabrication of PZT-PVDF-TrEF composites by screen-printing method on indium-tin-oxide-coated(ITO) glass substrate, and characterized the film by SEM and X-ray diffraction [DIETZE and ES-SOUNI 2008]. They claimed that the method is cost-effective, however it is not clear in this paper why they used a ITO glass as substrate, which is very expensive in fact. Lau *et al.* embedded nano-sized PZT powder in P(VDF-TrFE) matrix to fabrication a 0-3 composites and studied its piezoelectric properties and hydrophone performance [LAU, S.T. *et al.* 1999], afterwards, lead titanate (PT) was also embedded into [P(VDF-TrEF) 70/30] matrix to form a 0-3 composites, spin-coating was used to form a thin film with thickness of 5μm [LAU, S. T. *et al.* 2004]. Kobayashi *et al* used a sol-gel spray technique to produce integrated ultrasonic transducers on structural surfaces for NDT and SHM, they tested the performance of this transducer in pulse-echo mode, and also explored the application of this high temperature ultrasonic transducers by firing the sprayed sol-gel up to 800°C [KOBAYASHI and JEN 2004; KOBAYASHI *et al.* 2009; KOBAYASHI *et al.* 2006; KOBAYASHI *et al.* 2007; WU, K.-T. *et al.* 2011; WU, KUO-TING and KOBAYASHI 2009].

Recently Payo and Hale proposed a method to characterize the piezoelectric paint under biaxial strain [PAYO and HALE 2010], they also analyzed how the polarization voltage, film thickness and PZT powder weight percentage effects the sensitivity [PAYO and HALE 2011a]. Payo and Hale summarized some advantages and disadvantages of the piezoelectric paint [PAYO and HALE 2010], such as being distributable, which means a large-area coverage, conformable and absence of a bonding layer if a spraying method is used. However there are also drawbacks that confine applications of the piezoelectric paint in the real field. One of the main disadvantages is that the physical properties are vague if no characterization is performed before use. In [HALE 2004] the measurement of d_{31} was demonstrated, however, the determination of its Young's modulus, which is an important parameter to calculate d_{31}, was poorly described. And the resulted Young's modulus was cross referenced by [PAYO and HALE 2010] to deduce d_{31}, which brought more uncertainties into the characterization results, because the fabrication of piezoelectric paint has not reached an industrial standard, its properties vary with the composition and conditions it subjects to. Another main disadvantage is the low piezoelectricity compared with traditional ceramic sensors, because of which the popularity is limited and the application field is narrowed.

The advantages that make piezoelectric paint very attractive can be summarized as:

- Distributable. Whether it is in a free-standing form or being directly sprayed on a surface, it can be distributable, so that covering a relatively large area is feasible than other piezoelectric transducers.

- Flexible. The existence of polymer phase in piezoelectric paint endues this great feature, which is widely favored in many applications involving uneven surfaces. A free standing piezoelectric paint can easily cover a one-dimensional single or multi-curved structural surface, furthermore, sprayed piezoelectric paint is able to layer on a surface regardless of the complexity.

- Ability to be integrated into a structure. This feature comes along with the distributability and flexibility. It is also the trend for future smart materials, if a transducer can be integrated as a part of a host structure, the sensor design can be considered in the structural designing stage.

- Adjustable properties. The material properties can be altered to adjust different applications by changing the composition ratio of ceramic-phase and polymer-phase, which means the sensor can have an acoustic impedance that matches the host structural at most.

- Competitive cost. The price of substances forming the piezoelectric paint is relatively low, e.g., PZT powder, polymer resin as well as other additives are commercially available with reasonable prices. In fact, the only factor that makes the piezoelectric paint expensive is the human resource involved, which means a lot of effort is used in making satisfactory samples and characterizing the samples. However, in the future, if this technology is mature enough to enable a mass production, the price will be very competitive compared with other piezoelectric transducers.

Besides the above-mentioned advantages, in fact, the piezoelectric paint is still an immature material under development. Many problems still exist that hold up its development and popularity, which need to be solved in order to make the piezoelectric paint a novel smart material that is competitive enough to be applied in SHM applications. The main problems are listed as follows:

- High quality piezoelectric paint is required. A high quality piezoelectric paint would mean smooth surface, evenly mixed ceramic powder and polymer, repeatable production and stable performance, all of them are essential for SHM applications. However, at this stage,

the piezoelectric paint is made from various methods, each having its own pros and cons, the quality of piezoelectric paint depends greatly on its fabrication method, for instance, a sprayed piezoelectric paint is easily broken through during polarization due to its poor mechanical quality.

- High piezoelectricity is required. A high piezoelectricity would mean high signal-to-noise ratio, high sensitivity, more application possibilities and fewer amplifiers involved. For most of the piezoelectric paint samples which have been discussed, the sensitivity is relatively humble, which means charge amplifiers are required and the applications are very limited.

- Characterization. A new material cannot be applied directly in SHM without knowing its properties, especially in real cases relating to the public safety. A systematic characterization is needed to investigate the piezoelectric paint properties in various aspects of view, e.g., surface morphology, mechanical properties, piezoelectric properties, bandwidth, thermal properties, etc. The characterized results can give end-users an accurate impression of how, when, and where to use the piezoelectric paint.

- Typical application for demonstration. Although piezoelectric paint has been used as vibration sensor, acoustic emission sensor and strain sensor, a typical application is still desired to demonstrate a combination of its advantages: flexible, distributable, easy to be shaped, and ability to be integrated into a structure.

The above-mentioned problems are the main focuses of the piezoelectric paint research works of this dissertation. To have a fundamental overview of piezoelectric paint, an illustration of its basic principle is presented in Figure 3.1. Generally, the piezoelectric paint can be divided into two categories according to the substrate on which it is applied. The first one is a non-conductive substrate (Figure 3.1(a)), in this case, a conductive electrode has to be prepared on the substrate before placing the piezoelectric paint on the surface for signal wire connection, the conductive electrode could be silver paint, conductive tape or other conductive materials which are easy to be applied as a thin layer. The second case is a conductive substrate (Figure 3.1(b)). In this case, the substrate itself can be adopted as one electrode, thus an extra conductive thin layer is not necessary. It should be noticed that no matter what kind of substrates the piezoelectric paint are adhered to, the bonding material should always be conductive. In addition, for a non-conductive substrate, a free-standing piezoelectric paint is to be prepared beforehand, on the contrary, a

conductive substrate has no requirement for the paint form, both a free-standing or sprayed piezoelectric paint is applicable.
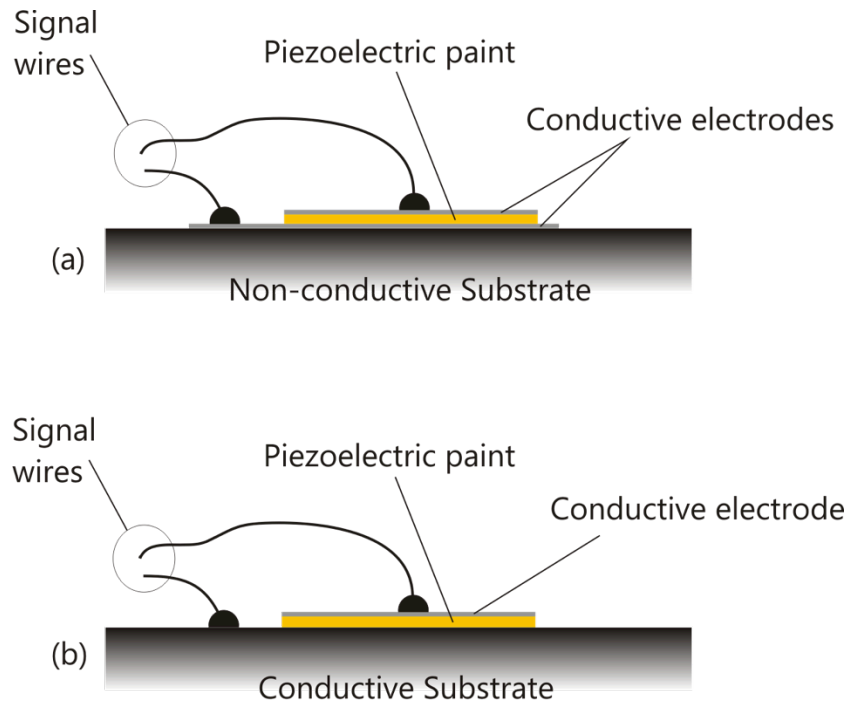

Figure 3.1 Basic principle of piezoelectric thick film on (a) non-conductive substrate and (b) conductive substrate

In the next sections, the fabrication technique of piezoelectric paint will be explored, two main techniques are reviewed, the spraying method and the tape casting method, both of which are designed for different applications. Afterwards the fabrication of piezoelectric paint is performed. The microstructure of piezoelectric paint is investigated by Scanning Electron Microscope (SEM). Material characterization is performed to investigate its material properties, which are indispensible for further applications.

3.3 Piezoelectric paint fabrication

3.3.1 Fabrication methods overview

A variety of methods has been previously and continuously reported for producing of piezoelectric paint through these years [EGUSA and IWASAWA 1994; HALE 2004; HANNER *et al.* 1989; NEWNHAM 1986; PAYO and HALE 2010; ZHANG 2006b]. However, these details reported in these works to formulate a step-by-step procedure to fabrication piezoelectric paint in a lab is

insufficient, furthermore, none of these works reported the accurate "recipe" of piezoelectric paint, either due to a patent issue [HALE 2004] or other unknown reasons.

In general, there are two groups of production method for the piezoelectric paint. The first kind is direct applying, which means directly apply the piezoelectric paint on the structural surface for sensing applications. This is usually realized by an air gun spraying, a manual brushing or a sol-gel technique. The advantages of this technique are easy-to-apply and can cover a large area of a host structure even with unsmooth surface, besides, the paint integrates very well with the host structure and dries out fast. However, drawbacks of the direct applying technique also cannot be ignored:

- It is limited to conductive substrate only, since the substrate has to be used as one of the electrodes for later polarization and signal wire connection. Direct applying is not feasible for non-conductive substrates, which are often meet in engineering applications, such as glass-fiber reinforced composite, concrete, wood, etc.

- Since the spraying is performed manually, the thickness of the paint is difficult to control, and the quality of paint almost always depends on the proficiency of the applying personal.

- As the sprayed paint has a poor quality, in order to avoid a dielectric break down, corona polarization is the only poling technique to be used to polarize the sample. The corona polarization is a non-contact poling technique, which requires a bulky, expensive and specialized equipment. If a sensor is to be sprayed on an immobile structure, a corona polarization is almost impossible.

Another group of applying technique is indirect applying, which means a free-standing piezoelectric paint is produced separately before utilizing, methods such as molding, screen printing or tape casting is adopted for this purpose. The practice of these methods are much more complicated compared with the direct applying method, since they involves various procedures and demand skillful techniques. The paint thickness can be accurately controlled with these methods, after fabrication, the sample could be shaped and adhered on a structure according to a specific application. Table 3.1 summarizes different fabrication methods of the state-of-the-art.

Above all these techniques, tape casting is the most effective method. Not like the molding or screen printing, whose outcome fully depends on the size of a mold or a screen mask, a tape

casting method can produce a large sheet of piezoelectric paint with a high quality. Tape casting is usually used in industry for thick film production. This method was firstly proposed by Howatt *et al* [HOWATT 1952; HOWATT *et al.* 1947], who used the method to produce thin ceramic sheets for capacitors. The major advantage of the tape casting process is that it is the best way to form a large-area, thin, flat ceramic or metallic part, which is virtually impossible to be pressed or extruded, the prime dried thickness range for tape casting is generally accepted as being from 0.025 mm to 1.27 mm [MISTLER and TWINAME 2000]. These above listed features are very attractive and suitable for producing a piezoelectric paint, therefore, it is chosen in this work for a high quality piezoelectric paint production.

First of all, a revised technique to adjust the specific task in this work is presented in Figure 3.2. The fabrication of piezoelectric paint involves few steps. Figure 3.2 illustrates the steps in a flow diagram. The process starts with mixing the piezoelectric ceramic powders with solvents for slurry preparation, this step is usually done in a ball milling machine; followed with substrate pre-treatment for tape casting, a pre-treated substrate would guarantee an easy-to-peel-off result and a high quality paint; after being casted, the piezoelectric paint is set aside for drying and peeled off from the substrate; finally, a conductive paint, such as a silver paint or a conductive tape, is applied on both sides of the green tape, followed is the sample polarization. The paint fabrication procedure is to be discussed in detail.

Table 3.1 Review of fabrication methods of piezoelectric paint and the state-of-art

Researchers and periods	Substances	Fabrication methods	Pros and cons
Newnham *et al* (1986)	PZT/PbTiO3, methyl methacrylate, hexyl acrylate and water	Spreading and casting on a brass plate; dried in air for 24hours, then in vacuum oven at 110°C for additional 24 hours; oil bath poling at 75°C	Easy to handle; but a low quality paint
Hanner *et al* (1989)	PZT/PbTiO3, acrylic copolymer and polyurethane	Spreading and casting on a brass plate; 24 hours drying in air; oil bath poling at 100°C	Easy to handle; but a low quality paint
Egusa and Iwasawa	PZT and epoxy resin (Epikoto	Spread with paint brush; 3 days drying; poling in air	Difficult to handle; fixed thickness and

|			
(1993)	1001)	at room temprature for 30min	size
Li *et al* (2000)	PZT and cement	Spreading and curing in concrete for 26 days; oil bath poling at 150°C	Easy to handle; but a low quality paint
Hale *et al* (2005)	PZT and acrylic paint	Spraying with air brush and firing; conventional poling at 60°C	Easy to handle; metal substrate; difficult to pole
Kobayashi *et al* (2007)	Unknown sol-gel	Spraying and firing by heat gun; corona poling at 120°C for 10 minutes	Easy to handle; metal substrate; difficult to pole
Zhang *et al* (2008)	PZT and epoxy resin	Spraying and curing for 3 days; oil bath poling at 70°C for 1 hour	Easy to handle; metal substrate; difficult to pole
Li	PZT and epoxy	Depositing on PVC plate and curing for 5 days; oil bath poling at 80°C	Long duration; free standing paint is obtained
Yang and Fritzen (2011)	PZT and epoxy resin	Tape casting and curing for 24 hours; oil bath poling at 30°C for 45 minutes	Adaptable on both non-conductive and conductive substrates; easy to pole; difficult to handle
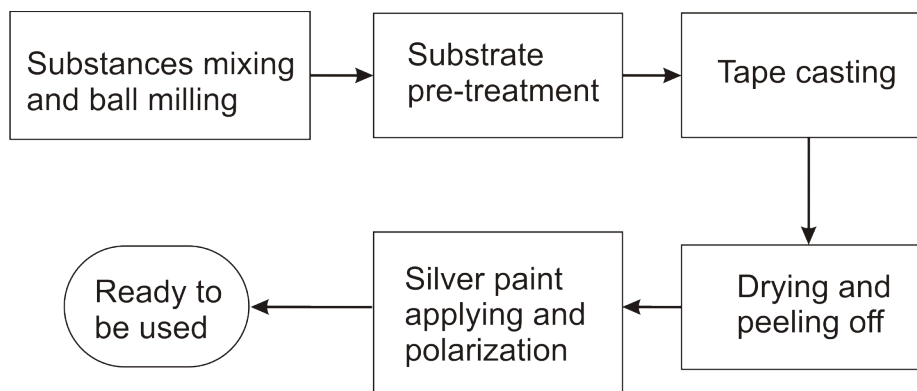
Figure 3.2 Flow diagram of piezoelectric paint fabrication process

3.3.2 Piezoelectric slurry preparation

Table 3.1 has shown the substances that comprise the piezoelectric paint in many previously published works, usually it is composed of piezoelectric ceramic powder and epoxy resin. The former is as a pigment and the later is as a binder, this composition is similar to a normal paint. The piezoelectric ceramic powder usually has a particle size under 20µm, among all of the piezoelectric materials, PZT powder is by far the most popular substance. In addition, the choice of a polymer binder is also very crucial, it determines whether a high quality sample can be obtained or not.

The piezoelectric ceramic powder used in this study is a commercial product, the powder is mainly comprised of PZT, and doped with appropriate ratio of ZrO2, PbO and TiO2 [SUNNYTEC 2012]. The material properties of PZT powder are described in Table 3.2.

Table 3.2 Material properties of the PZT powder used for making piezoelectric paint [SUNNYTEC 2012]

Density (kg/m^3)	Dielectric constants $(\varepsilon_{33}^T/\varepsilon_0)$	Piezoelectric Charge constant (pC/N)		Piezoelectric Voltage constant $(10^{-3}Vm/N)$		Coupling coefficients (%)		
		d_{31}	d_{33}	g_{31}	g_{33}	k_p	k_t	k_{31}
7600	2300	-200	450	-11.1	22.1	71	51	38

The mixed powder is twice pelletized by spraying during the production process, so that the particle size is controlled within 1µm [SUNNYTEC 2010]. The binder chosen in the study here is mainly comprises of n-propyle acetate, combining with other plasticizer and solvent. A quantity named weight percentage ($wt\%$) is used to quantify the ceramic powder ratio in the piezoelectric paint. Weight percentage is defined as,

$$wt\% = \frac{m_p}{m}\%$$

(3-1)

where m_p is the weight of piezoelectric ceramic powder in the slurry, and m is the whole weight of slurry. An ideal assumption would be: the more piezoelectric ceramic powder in a slurry, the

higher sensitivity the piezoelectric paint would have, however, this assumption is not applicable in a real experiment, because a high weight percentage beyond a threshold will only lead to a ceramic powder saturation, thus will cause a sample with low quality. Therefore, there is always a trade-off between a high sensitivity and a high quality, the appropriate weight percentage is found out in experiments by try-and-error.

To accurately control the milling time, speed and force effectively, a ball milling technique is chosen to mix the powder and the binder. The milling machine is Pulverisette 5 (Figure 3.3).

Figure 3.3 Ball milling for piezoelectric paint fabrication

The milling vessel is carefully chosen as a marble jar, and the milling balls are Zirconia balls with a diameter of 5mm, both of them are hard, dielectric and inert to chemical reactions, so that no pollutions will be brought into the samples. The mixture is ball milled with a speed of 250rpm, which gives enough energy to mix the ceramic powder and solvent but also not too high to polymerize the slurry. Many experimental trials have shown that the ball milling time for at least one hour and a half is necessary, less than this the ceramic powder cannot be completely and evenly distributed in the polymer matrix, which leads to precipitation and air voids when casting. The prepared slurry is set aside for further processing.

3.3.3 Tape casting method

While many advanced materials are featured with novel properties that are useful in a variety of applications, economic methods to produce these materials in large volumes with a good quality are necessary for a broad commercial acceptance [DENNIS 2007]. Generally, the tape casting method is a popular and important ceramic form technique which is widely used by industries to produce thin sheets of flexible tape. It produces thin films inexpensively and scaleablely, and is widely accepted due to its suitability, simplicity and low implementation cost when compared with the other available methods, such as dry pressing, slip casting, or injection molding. Therefore, the tape casting method has been adopted to manufacture a variety of multi-layer ceramic package products, as well as non-ceramic, polymer and metal applications [DENNIS 2007]. Nowadays, with the development of smart materials, the tape casting method is showing its advantages in new fields.

The principle of tape casting is simplified in Figure 3.4. As could be seen, the piezoelectric slurry is distributed on a glass substrate, which has been made hydrophobia, this pretreatment ensures an easy peeling-off of samples after casting and drying without any physical damage. Experimental trials in this work have shown that the substrate pretreatment is indispensible, if a high quality piezoelectric paint is desired. In general, the hydrophobia treatment is realized in several steps. First of all, the glass plate is washed by deionized water to remove dusts and greases on the surface, afterwards leaving it completely dry. To remove the organic compounds on the plate surface, it is boiled in a mixture of hydrochloric acid and ammonia for ten minutes, then washed by deionized water and dried completely again. Finally, the plate is dipped into methylene dichloride for ten minutes, then set aside, dried and put in an oven with 80°C for 12 hours. Afterwards, the glass plate is entirely hydrophobia.
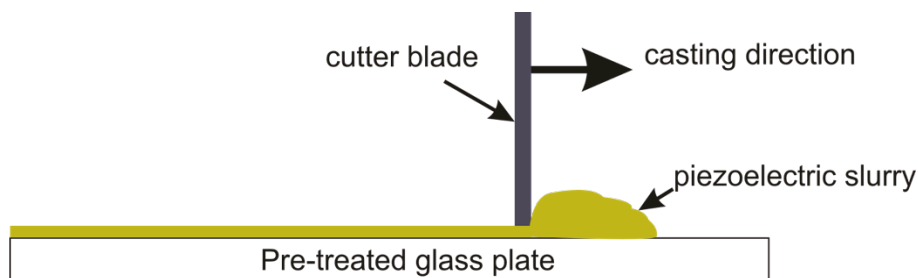

Figure 3.4 Schematics of tape casting

As shown in Figure 3.4, the slurry is casted on the glass substrate by a cutter blade moving from one end of the substrate to another. By doing this a thick piezoelectric layer is evenly distributed on the substrate surface, with thickness of approximately 10 to 20 μm. The casted layer is dried in a fume hood for few minutes. The procedure is repeated until a desired thickness is achieved. To accurately and effectively handle this process, a simplified lab applicator was built. Figure 3.5 shows the lab applicator.
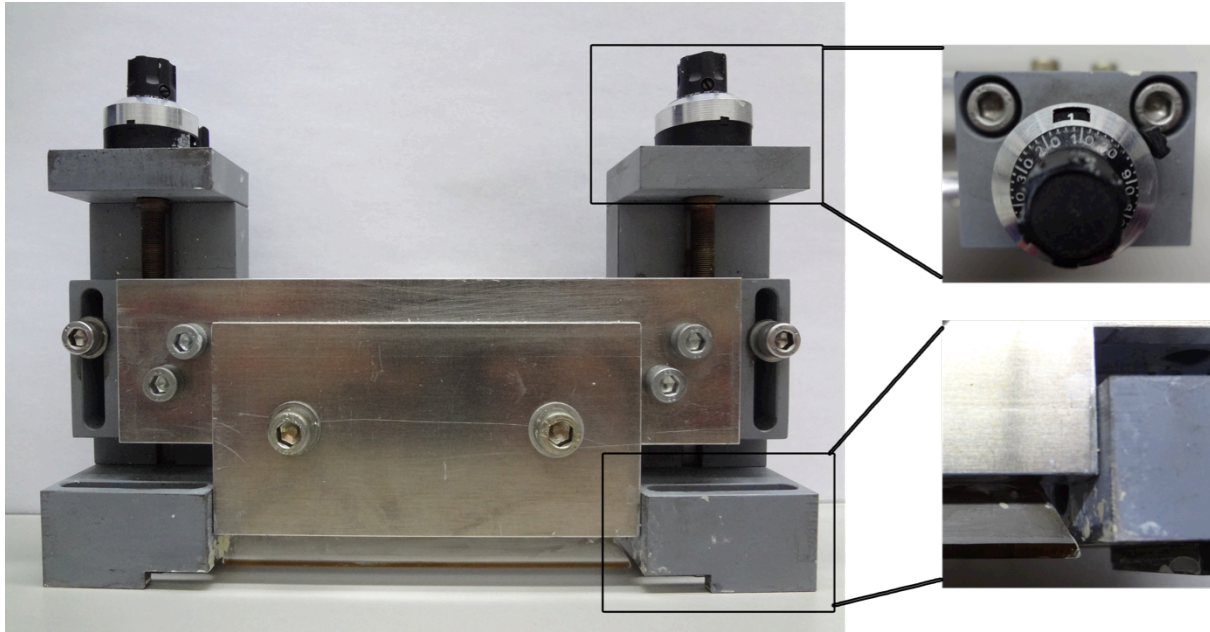

Figure 3.5 Simplified lab applicator for piezoelectric paint

It mainly comprises two parts: the casting part, which is made of a blade (Figure 3.5 down right corner), and a thickness control part, which is made of a tunable screw (Figure 3.5 upper right corner). By each casting round, the thickness of the layer can be controlled by tuning the left and right screws simultaneously, so that the height of the blade, which is connected to the two screws, can be adjusted. The resolution of the tuning screw is 10μm, this is more than enough for controlling the piezoelectric paint thickness. The simplified lab applicator is low cost, easy to build, and it can produce a large sheet of free-standing piezoelectric paint, the size of which simply depends on the length of the blade and the substrate. By choosing a blade rigorously, the paint surface can be smoothly distributed with good quality. After being set aside for a complete drying of twelve hours, the paint can be peeled off from the glass plate and is ready for poling. Figure 3.6(a) shows a dried free-standing green sheet, and Figure 3.6(b) demonstrates its flexibility, as could be seen the piezoelectric paint conforms well on the steel tube without any

damage. Further analysis of the microstructure of the paint will be performed in the characterization section.
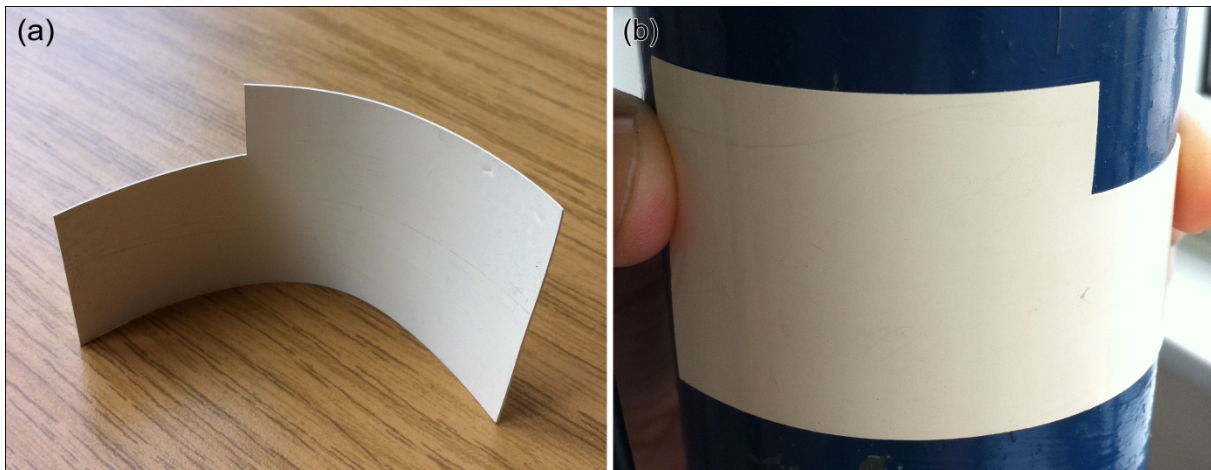

Figure 3.6. (a) A piezoelectric paint sample (b) a piezoelectric paint conforming on a steel tube

3.3.4 Polarization

The dried piezoelectric paint is ready for poling. The polarization is a very important stage for piezoelectric transducers fabrication, only after which the piezoelectricity can be induced. Basically, due to the dielectric differences between the piezoelectric ceramic (high dielectric property) and polymer (low dielectric property), poling of a composite including a polymer matrix with 0-3 connectivity is especially difficult, since most of the applied electric field will go through a low dielectric phase [WALLER and SAFARI 1988]. If a dielectric break through happened at a local spot which is weaker than the rest of the region, it would stop further polarization because of short circuits. Sa-Song *et al* solved this dielectric difference by adding carbon, germanium or silicon into PZT powder [SA-GONG *et al.* 1986], Sakamoto *et al* doped 0.5%-2.0% amount of carbon powder (volume percentage) into PZT powder [SAKAMOTO *et al.* 2001], the purpose of these doping is to create a continuous electric flux path between PZT grains [LI, XIN 2009]. However, by adding conductive particles into a piezoelectric composite to help the poling process is still controversial, since it will also decrease the dielectric property of the product [CUI *et al.* 1997; CUI *et al.* 1999].

Generally, there are two different methods for polarization, one is the conventional DC poling, another is a corona discharge poling. The former involves poling the green sheet by directly contacting both sides of the surface to a high electric field. Because the green sheet is non-

conductive, conductive electrodes have to be added on the sample surfaces. This method mainly requires a high voltage power supply which is easily available, however, the piezoelectric paint must have a high quality with as less flaws as possible, otherwise dielectric break down will be easily induced, thus the poling process will be interrupted. Another poling method, named corona discharge poling, was proposed by Waller *et al* to polarize piezoelectric composites in 1988 [WALLER and SAFARI 1988], it is used in industries to polarize PVDF and other electro-optic materials. The corona discharge poling is realized by partially breaking down of air around a poling needle, and initiated by a discharge in an inhomogeneous electric field, so that electric charges are distributed on the sample surface without further help of conductive electrodes. This method avoids dielectric break-down caused by partial flaws, and therefore is very suitable for samples with low quality or samples whose conductive electrodes have to be removed after poling. However, bulky, expensive and professional equipments are required to perform corona poling, therefore it is rarely used in piezoelectric paint researches for polarization due to the cost and availability.

The polarization method used here is conventional DC direct poling, because the casted piezoelectric paint has a high quality which is proved by a microstructure investigation (the details are discussed in section 3.5). Figure 3.7 shows the schematics of the polarization method. A conductive silver paint is applied on both sides of a green sheet as electrodes, to reach the best conductivity, a commercial conductive paint G3682 containing very fine silver flakes (approximately 8μm) and methylisobutylketone [PLANO-GMBH] was evenly applied on the green casted sheet for polarization and further applications. Furthermore, annealed silver wires with 99.99% purity and 0.127mm diameter are used to connect the surface electrodes to a DC power supply, because the silver wire has an excellent conductivity. A high electric field is applied across the piezoelectric paint, the polarization direction is indicated in the figure. The arrow points to the surface which is subjected to a negative polarity, and the tail points to a positive polarity.
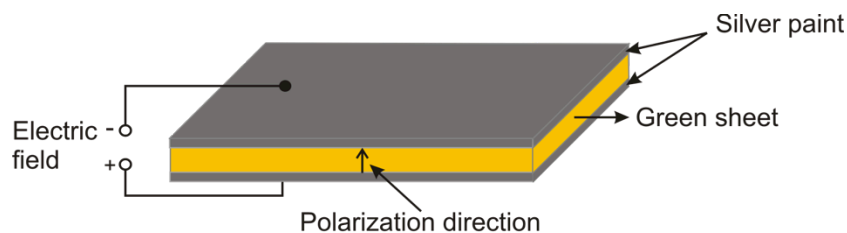

Figure 3.7 Schematics of piezoelectric paint polarization

To accelerate the poling process and obtain an optimized polarization result, the prepared green sheet is poled in heated silicon oil within a controlled temperature up to 40°C (Figure 3.8). Because a heating process can increase the mobility of molecules, the rotations of dipoles are made easier. It is not suggested to polarize the piezoelectric paint in an alleviated temperature without any control, because the polymer phase will be aged under a high temperature. In this case, a high voltage amplifier P350 from Physics Instrument was used to apply a maximum of 5kV/mm high electric field through the piezoelectric paint. To convert the dipoles in the piezoelectric paint progressively, the polarization voltage was controlled to start from 800V/mm and increased sequentially with a rate of 100V every five minutes, this gave enough time to stabilize the oriented dipoles. After reaching a maximum poling voltage, another half an hour was taken to continue poling the sample. In a poling process, the maximum poling voltage is restrained either by the limitation of a power supply, or by the maximum voltage a piezoelectric sample can withstand.
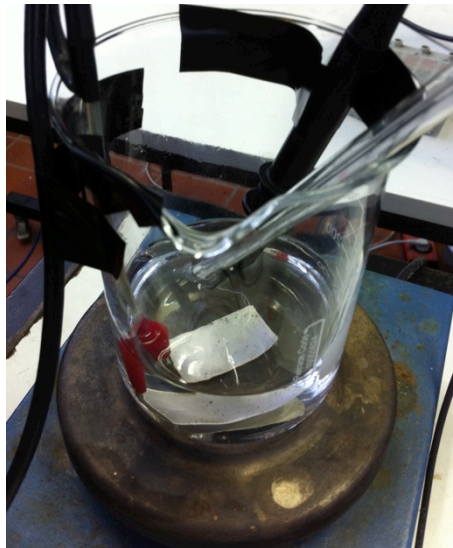

Figure 3.8 Oil bath polarization of piezoelectric paint

Cautions must be aware that by placing the piezoelectric paint in a maximum poling field without starting from a moderate value will result in dielectric break-down (Figure 3.9), the same consequence happens when poling a poor quality piezoelectric paint with local flaws. The dielectric break-down issue will be analyzed in detail in the next sections.

Figure 3.9 Dielectric break down during polarization

3.4 Weight percentage, volume percentage and density

3.4.1 Theory and experiments

During the piezoelectric composite production, two quantities were often mentioned: one is weight percentage (*wt*%) and another is volume percentage (*vol*%). In the work of Furukawa *et al.*, this two quantities were converted by making an assumption of the epoxy resin density [FURUKAWA *et al.* 1976], in a later work of Furukawa, a mole percentage was used [FURUKAWA 1989]. Klein *et al* produced a composite piezoelectric paint with a volume percentage of 60-70% by their simple spreading technique [KLEIN *et al.* 1986], although the PZT concentration was really high, it is hard to tell from the results that how good the quality of the composite is. Gururaja *et al* produced a PZT-rod polymer with 5-30 *vol%* of PZT [GURURAJA, SCHULZE, CROSS, and NEWNHAM 1985; GURURAJA, SCHULZE, CROSS, NEWNHAM, *et al.* 1985]. Esuga *et al.* developed a piezoelectric paint with 53% volume fraction [EGUSA and IWASAWA 1993; EGUSA and IWASAWA 1996]. Hale *et al.* produced a piezoelectric paint with a high weigh concentration up to 70% PZT by a scraping technique [HALE and TUCK 1999]. The weight percentage of PZT was also 70% in Zhang's experiment [ZHANG 2006a], this value was claimed as equaling to 24% volume percentage, however it was not clear how these two values were related. The PZT fraction ratio was not clear in the work of Kobayashi *et al*, who applied a sol-gel technique [KOBAYASHI *et al.* 2007].

In previously reported works, sometimes the weight percentage and volume percentage were mixed together and brought much confusion for a clear understanding. The weight percentage has been defined in Equation (3-1), it is a percentile used when preparing the piezoelectric paint, to quantify how many PZT powder has been added into the slurry. This value is a popular quantity to be used when producing the piezoelectric paint, because measuring the weight is more appropriate than measuring the volume, under the circumstance that the substances involve not only solvent, but also the solid PZT powder, which are not compressed, but loosely distributed.

The volume percentage used to describe the volume percentile of the PZT powder in a green sheet can be defined as,

$$vol\% = \frac{m_p/\rho_{piezo}}{Vol}\%$$
(3-2)

where ρ_{piezo} is the density of PZT powder, in this case here it is provided by the producer as $7800 kg/m^3$, Vol is the volume of a sample, m_p here is the weight of PZT powder in the sample and is measured by sintering a sample up to 450°C, so that all the polymer substances is gasified, leaving only the PZT whose weight can be accurately measured afterwards. The density of piezoelectric paint can be calculated as m/Vol. If m_p is known, the density of polymer phase can also be calculated,

$$\rho_{polymer} = \frac{m - m_p}{Vol - m_p/\rho_{piezo}}$$
(3-3)

In order to output a satisfactory quality, after many experimental trials the maximum weight percentage was selected as 60%. A higher value will make the handling of the slurry extremely difficult, at least by the method introduced in this work here, therefore a higher weight percentage will not be considered here.

3.4.2 Results and discussion

Three samples with weight percentage of 40%, 50%, 60% were taken as examples to define their volume percentage and density, this three groups of sample will also be used to investigate their microstructures, connectivity, elastic property and piezoelectric property. The sample dimension was measured by a digital micrometer with 0.001mm precision, the weight was measured by a

weighing scale with 0.0001g precision. The measured and calculated results are listed in Table 3.3. In Table 3.3 several important information can be obtained.

Table 3.3 Weight percentage and volume percentage of the piezoelectric samples

Sample weight percentage before sintering ($wt\%$)	40%	50%	60%
Dimension (mm)	20×20.5×0.44	20×20.5×0.44	20×20×0.42
Weight before sintering (g)	0.5515	0.6742	0.6766
Weight after sintering (g)	0.4397	0.5899	0.6105
weight percentage after sintering ($wt'\%$)	79.73%	87.50%	90.23%
volume percentage ($vol\%$)	32.07%	43.03%	44.53%
Paint density (kg/m^3)	3057.10	3737.25	4027.38
Polymer density (kg/m^3)	912.32	820.19	753.95

1.) In fact, the weight percentage has to be classified as weight percentage before sintering ($wt\%$), and weight percentage after sintering ($wt'\%$), usually the weight percentage mentioned in references is the weight percentage before burning out the polymer substances from a sample. Weight percentage after sintering is much higher than before sintering. The reason is: a small part of the solvent in the slurry volatilized during processing, and the rest of the solvent dried out after the sample was casted;

2.) It is mentioned in publications that the volume percentage is approximately half of the weight percentage [ZHANG 2006a], this conclusion is only true when the weight percentage after sintering is referred. The maximum volume percentage which can be realized by the method introduced here is approximately 44%.

3.) A piezoelectric paint is much lighter than the PZT powder used to produce it, since the density of piezoelectric paint is only approximately half of the pure PZT powder, the result proves that making the piezoelectric distributable is reasonable, and it is more suitable in weight-sensitive applications than a traditional PZT ceramic. The estimated paint density and polymer density is very useful for various calculations.

3.5 Investigation of the piezoelectric paint microstructure

After the fabrication, the piezoelectric paint is to be characterized for further applications. The microstructures of free-standing paint films are studied under SEM, the elasticity constant and piezoelectric constant is to be measured, from which future calculations could benefit.

One of the main reasons that the piezoelectric paint is very favorable is due to its attractive material properties: both piezoelectric active and flexible, which cannot be offered by a single-phase material, neither piezoelectric ceramics nor polymer solely. The research focus in this section is to investigate the micromechanical structures of the casted piezoelectric paint. Because it is difficult to evaluate the piezoelectric paint quality from a macro point of view, SEM is used to observe its particle connectivity and surface morphology.

3.5.1 Connectivity of piezoelectric composites

Piezoelectric composites can be categorized according to their connectivity (e.g.: 0-3, 1-3, 2-2) [NEWNHAM *et al.* 1978]. Connectivity is defined as the number of dimensions through which the material is continuous. Newnham *et al* have developed the connectivity theory of composite to describe a two-phase composite [NEWNHAM *et al.* 1978]. He concluded that there are ten important connectivity patterns for two diphase solids, ranging from a 0-0 unconnected checkerboard like pattern to a 3-3 pattern, which both phases are three dimensionally self-connected [NEWNHAM *et al.* 1978].These ten patterns are 0-0, 0-1, 0-2, 0-3, 1-1, 2-1, 1-3, 2-2, 2-3 and 3-3, as shown in Figure 3.10. The first number indicates the piezoelectric particle phase and the second indicates the polymer phase. As shown in Figure 3.10, each piezoelectric active phase or polymer phase has a zero, one, two or three dimensional connectivity to itself. Connectivity is directly related to the piezoelectric ceramic powder volume percentage. Yamada *et al.* studied a high content PZT/polymer composite with volume fraction up to 67%, they observed the relationship between PZT volume fraction and dielectric constant, as well as Young's modulus

[YAMADA *et al.* 1982]. To simulate the formation of 1-3 connectivity, Jayasundere *et al.* proposed a 0-3/1-3 connectivity model [JAYASUNDERE *et al.* 1994]. Li established an analytical model to illustrate the connectivity problem and concluded that the piezoelectric charge constant is higher with 0-3/1-3 connectivity than 0-3 connectivity alone [LI, XIN 2009].
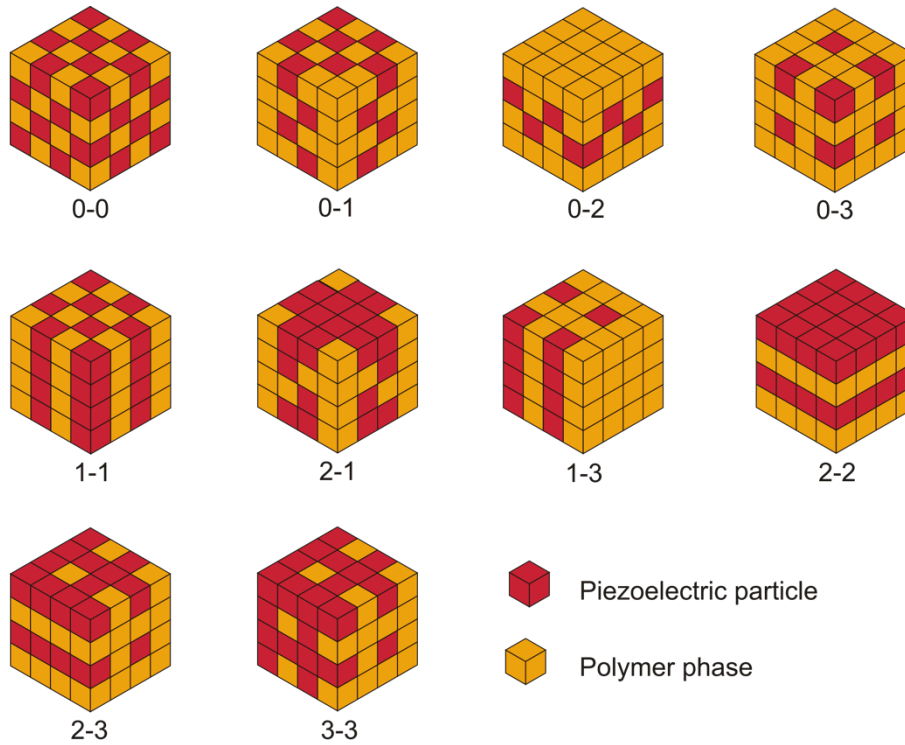

Figure 3.10 Connectivity of diphase piezoelectric composites [NEWNHAM *et al.* 1978]

Although several analytical models have been established to predict the connectivity problems of piezoelectric paint, only few works have investigated the microstructure of piezoelectric paint, the morphology of piezoelectric paint was not clearly presented in these works. This is the problem to be discussed in the next section.

3.5.2 Surface morphology investigation

In this section, the surface morphology and the transverse microstructure of prepared samples is investigated by a Scanning Electron Microscope. SEM is a kind of electron microscope that observes and characterizes heterogeneous organic or inorganic materials on a nanometer to micrometer scale [GOLDSTEIN *et al.* 2003]. It is widely used in scientifically area to study the topology of materials.

Three samples with 40%, 50% and 60% weight percentage are selected to investigate how their ceramic particles are distributed in the polymer phase and their bi-phase connectivity problem. Figure 3.11 is a SEM micrograph of the three samples. It could be seen that the size of most piezoelectric particles is under 1μm. The sample with 40 $wt\%$ has the lowest particle density (Figure 3.11(a)), which is defined by the number of ceramic particles per unit area, this value increases with the increase of PZT powder weight percentage (Figure 3.11(b)) and (Figure 3.11(c)).

The 50 $wt\%$ sample is taken as an example to investigate piezoelectric paint surface morphology. Figure 3.12 is a smooth sample surface and its enlargement, Figure 3.12(a) shows the smoothness of the sample, without any air void or flaw (the small dots in the picture are nothing but dusts). Figure 3.12(b) is its enlargement, it clearly shows that all the piezoelectric ceramic are evenly distributed in the continuous polymer phase. Some connection of the two phases belong to the simplest composite type, the "0-3" connectivity. However it could be seen that many of the piezoelectric particles are in contact with each other, which forms a "1-3" connectivity pattern. It has been reported experimentally and theoretically that the "1-3" connectivity can produce higher piezoelectricity, which is due to the continuously chained piezoelectric particles [EGUSA and IWASAWA 1993; LI, XIN 2009]. It is also possible that few piezoelectric particles are in contact in all directions, which forming a "3-3" connectivity. However, for this bi-phase piezoelectric composite, the dominant connectivity is still "0-3" and "1-3" connectivity.
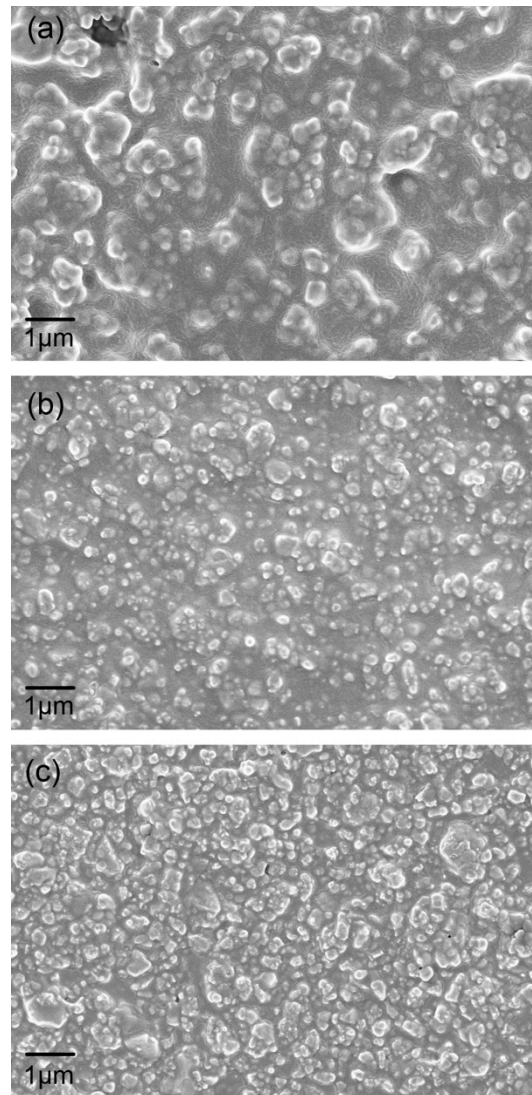
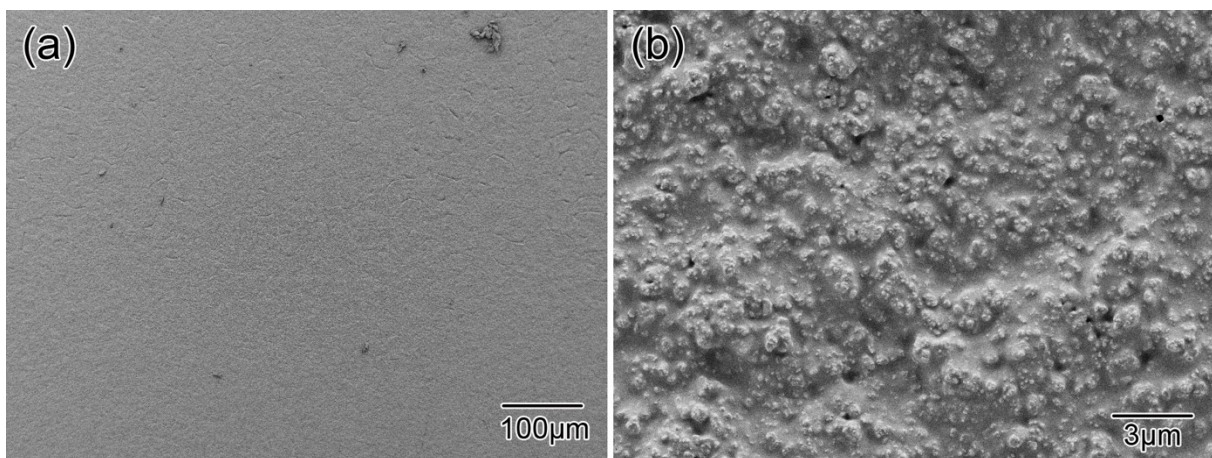**Figure 3.11 SEM of (a) 40%*wt* (b) 50%*wt* and (c) 60%*wt***

Figure 3.12 SEM micrographs of (a) a smooth sample surface and (b) its enlargement

As having been explained during the piezoelectric paint fabrication process, false handling or high ceramic powder concentration will result in flawed piezoelectric paint, which makes a successful polarization impossible. Figure 3.13 is a failed sample with 65 $wt\%$, comparing with the qualified sample from Figure 3.12, this sample has an unsmooth surface and many ravines, as well as some partial severe breakage, they are the air voids and are greatly unwanted. The sample shown in Figure 3.13 was investigated closely under SEM, the results is shown in Figure 3.14. In Figure 3.14(a), the discrete dark parts in the image are air voids, they are distributed all over the sample. The enlargement Figure 3.14(b) clearly shows the structure of air voids, the polymer breaks at the paint surface, and a ravine is created.

The causes of air voids are diverse, but excessive PZT powder concentration is the main reasons. Generally, the higher the weight percentage, the higher the pigment-to-binder ratio, thus the thicker the slurry. A thick slurry with insufficient solvent causes low adhesive strength between the piezoelectric particles, thus leads to film breakage during drying. After many experimental trials, the maximum weight percentage was selected up to 60%. Another main reason causing air voids is false handling during processing. For instance, pouring the slurry out from a milling jar rashly, shaking the slurry unnecessarily, or casting the film too fast, all of these may bring air bubbles into the slurry, and some air bubbles were trapped in the film during casting, thus becoming air avoids after drying.
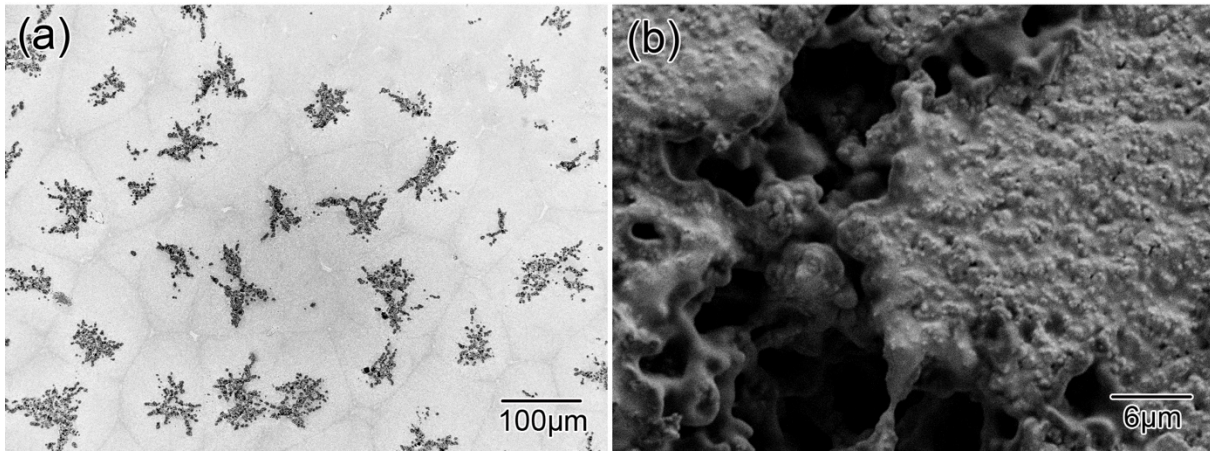

Figure 3.13 A low quality sample

Figure 3.14 SEM micrographs of (a) a failed sample and (b) its enlargement

When performing direct poling, a conductive paint is applied on both sides of the thin film as electrodes. The conductive paint is a silver flocculating agent which comprises fine silver particles (approximately 8μm), therefore it can infiltrate into the air voids easily. The air voids along with infiltrated silver particles change the dielectric permittivity of the paint, and finally lead to dielectric break down when poling. Even if the paint might be polarized under very low voltage, this would only induce very low piezoelectricity or no piezoelectricity in the worst case, which cannot reach the prerequisite as a sensor or actuator. In this case the corona poling, which is a non-contact polarization method, is also unsuitable, because the air voids have already reduced the effective thickness of the paint substantially, thus the physical strength of the paint has been compromised.

Besides the surface morphology, the paint cross section is also investigated. Figure 3.15 is a sample whose surface is covered with a conductive paint. The enlargement of the cross section is shown in Figure 3.15(b). They are densely and evenly distributed in the polymer matrix, the dominant connectivity pattern is the "1-3" connectivity. This quality avoids the issue of conductive paint infiltration, thus ensuring a successful polarization which is essential for applications. It can be concluded from Figure 3.12 and Figure 3.14 that with appropriate PZT powder concentration and handling procedure, the tape casting method can produce high quality piezoelectric thin films.
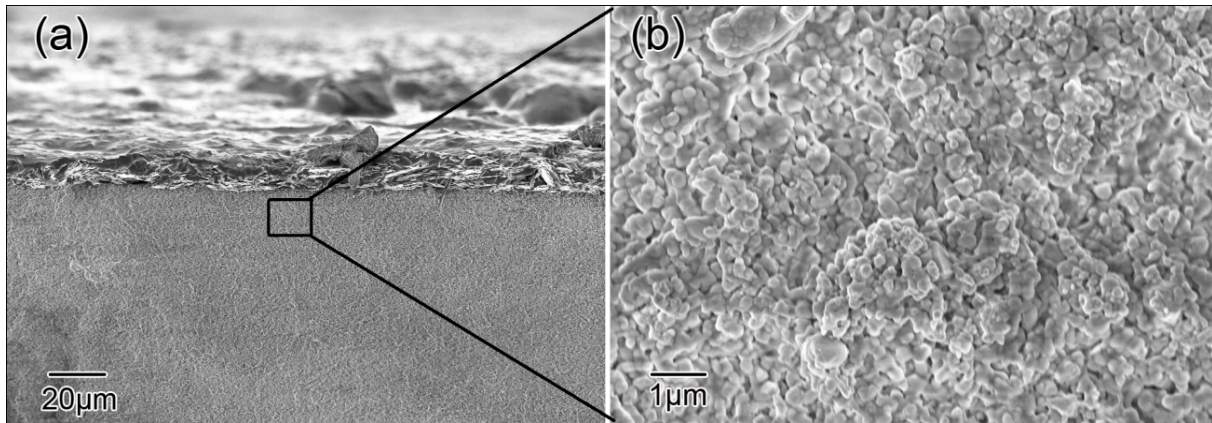
Figure 3.15 (a) SEM micrographs of a piezoelectric paint cross section and (b) its enlargement.

3.6 Elastic properties

3.6.1 Normal tensile test

Tensile tests were performed to characterize Young's modulus of the piezoelectric paint. The modulus of elasticity is an important parameter for a better understanding of the piezoelectric paint and further applications. Few reported works have estimated the Young's modulus of the piezoelectric paint. Li *et al.* used an analytical model to predict the Young's modulus with different volume percentage [LI, X. and ZHANG 2008], Hale described a tensile test to measure the value [HALE and TUCK 1999], however due to the thin and soft physical properties of the piezoelectric paint, the experimental measurement lacked detailed description and verification.

It was introduced in the section 3.3 that the tape casting method can produce high quality free standing piezoelectric paint in large area, therefore it makes possible to measure the Young's modulus by using a tensile test. The original sample has a dimension of $100mm\times25mm$, it is shaped according to DIN standard: Preparation of plastic materials for tensile testing [NORMUNG 2003]. The sample was shaped manually by using a scalpel, Figure 3.16 shows the prepared sample with dimensioning.

Since the piezoelectric paint is soft and thin, direct placing it in a traditional tensile test machine and adjusting it properly would be very difficult and might bring damages beforehand. To solve this problem, an extra clamp was designed to be placed between the specimen and tensile test machine grips. A load cell was applied between the upper part of the extra clamp and the tensile head to measure the stress. Figure 3.17 is the experimental setup. It should be noticed that the

placement of samples requires extra precaution, this is to avoid twisting and initial stress or strain, which might affect the measurement result. As the sample was stretched, forces exerted by the machine and displacement of the samples were recorded, these data were used to construct a stress-strain curve, through which the elastic modulus could be calculated.
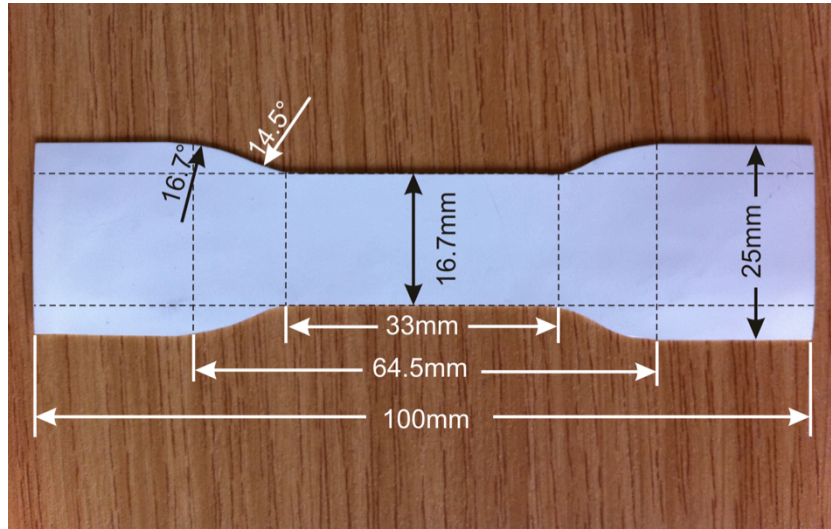

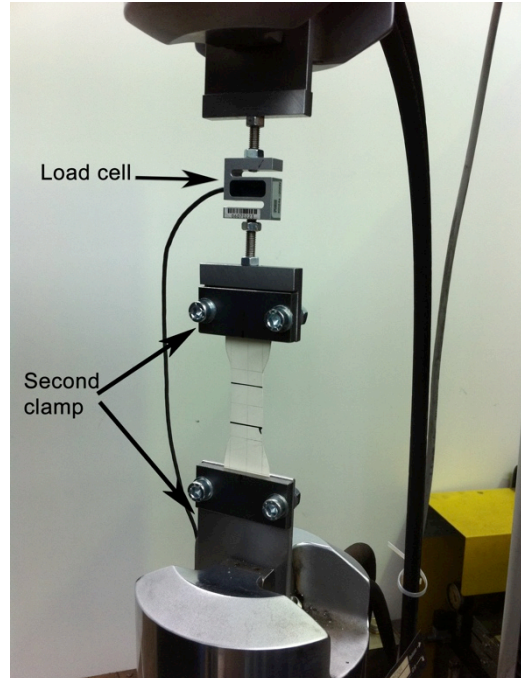**Figure 3.16 Dimension of a tensile test sample**

Figure 3.17 Tensile test experimental set up

Three groups of sample were chosen for the tensile test, each group had five samples, the weight percentage of the three groups was 40%, 50% and 60% respectively, the ambient temperature

was room temperature. Table 3.4, Table 3.5 and Table 3.6 list the measured Young's modulus of each sample, as well as the mean and variance of each group. The sample number in the table is in accordance with the number marked in Figure 3.18. Figure 3.18 shows the three groups of sample after testing.

Table 3.4 Measured results of samples with 40 $wt\%$

Sample number	1	2	3	4	5
Thickness (mm)	0.376	0.418	0.42	0.422	0.39
Cross section (m^2)	6.392e-6	7.106e-6	7.14e-6	7.174e-6	6.63e-6
E (MPa)	40.66	36.27	28.34	20.68	25.53
Mean and variance of E	E=30.29$\pm$8.1 MPa				

Table 3.5 Measured results of samples with 50 $wt\%$

Sample number	6	7	8	9	10
Thickness (mm)	0.438	0.448	0.430	0.424	0.414
Cross section (m^2)	7.446e-6	7.616e-6	7.31e-6	7.208e-6	7.038e-6
E (MPa)	10.28	25.76	20.92	35.79	39.12
Mean and variance of E	E=26.37$\pm$13.50 MPa				

Table 3.6 Measured results of samples with 60 $wt\%$

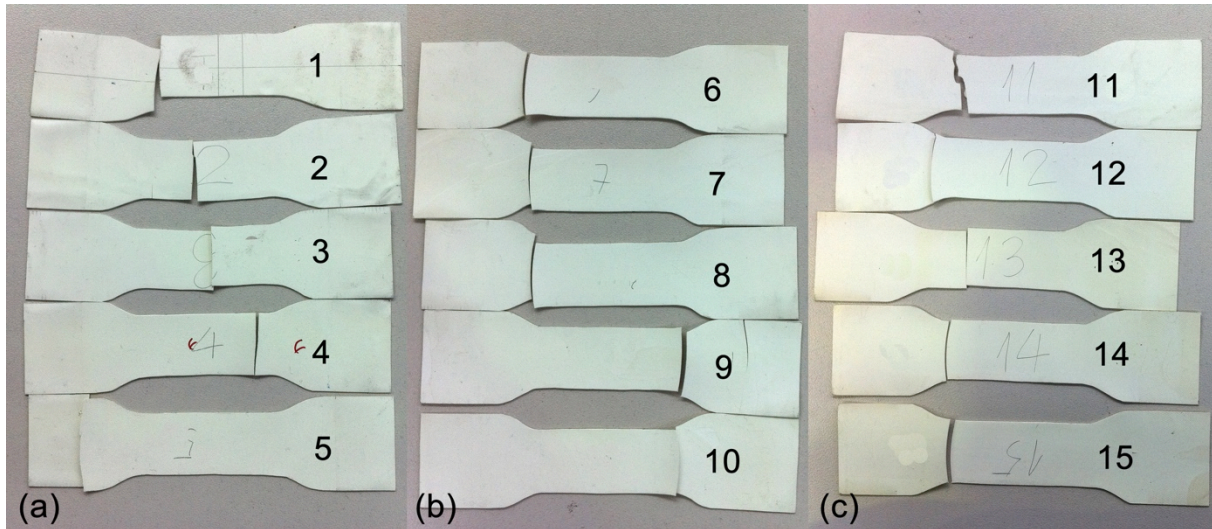| Sample number	11	12	13	14	15
Thickness (mm)	0.45	0.48	0.398	0.384	0.39
Cross section (m^2)	7.65e-6	8.16e-6	6.766e-6	6.528e-6	6.63e-6
E (MPa)	9.80	9.47	7.30	7.73	8.04
Mean and variance of E	8.47$\pm$1.22 MPa				

Figure 3.18 Three groups of tested samples (a) 1 - 5 with 40 *wt%* (b) 6 - 10 with 50 *wt%* (c) 11 - 15 with 60 *wt%*

The listed results show that the mean value of Young's modulus of the samples decreases with the increase of PZT powder concentration. In order to make these results more visual and direct, all the data points are plot in Figure 3.19.
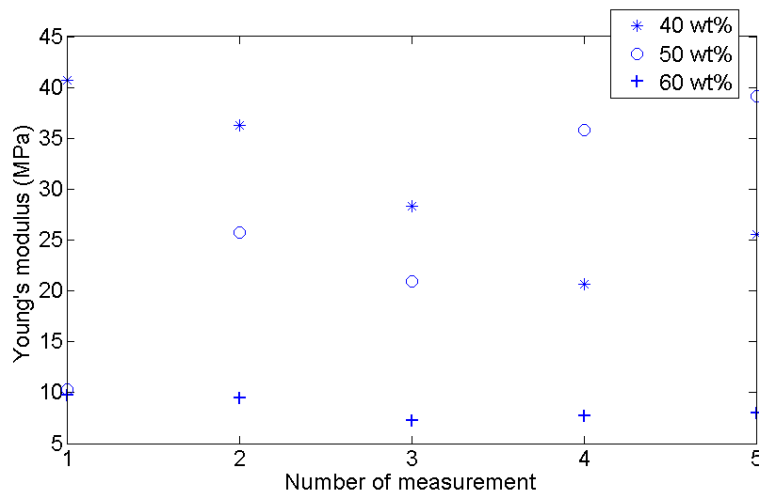

Figure 3.19 Plot of all tensile test measurements

It could be seen that the piezoelectric paint with 40 *wt%* has the highest Young's modulus, and the value decreases with the increasing of piezoelectric powder concentration. This is due to that the higher the PZT powder concentration, the less binder a sample has, so the connection force between particles in the piezoelectric paint is smaller. It could also be seen that the variation of Young's modulus among a same group has a high fluctuation, this is caused by the temperature influence and measurement error, as the tensile test machine is not designed for measuring elastic

modulus of polymer materials. In fact, to accurately quantify the elastic modulus of the piezoelectric paint by using a traditional tensile test technique is very difficult, but the value gives a reference for future calculations, furthermore this technique is low cost and the equipment is easily available.

Figure 3.20 is the stress-strain curve of a 50wt% sample. The initial portion of the curve in Figure 3.20 is incompatible with Hooke's law, this is induced by a placement error, because it was very difficult to adjust the sample in the machine with zero stress and strain. However as the sample elongated, the stress and strain showed linearity, the slope of the linear portion in the plot is the elastic modulus, which is calculated as $\Delta T / \Delta S$. There are more issues that can be discussed by observing Figure 3.18. It can be seen that for most of the stretched samples, the breaking points are not located in the geometric center of the samples as supposed, but break at the notch of the samples. The reasons are mainly due to: a.) the sample is very soft, by which a traditional tensile machine is not completely suitable, because it is very difficult to adjust the applied force properly and accurately, b.) since the piezoelectric paint is fabricated manually, there might be minor flaw in the sample, the region with minor flaws will be more fragile than the other region, c.) the samples are shaped manually by a scalpel, therefore it is very difficult to keep the cutting perfectly smooth, especially at the notched area, therefore deformations are easily induced at the notched area at higher stresses.
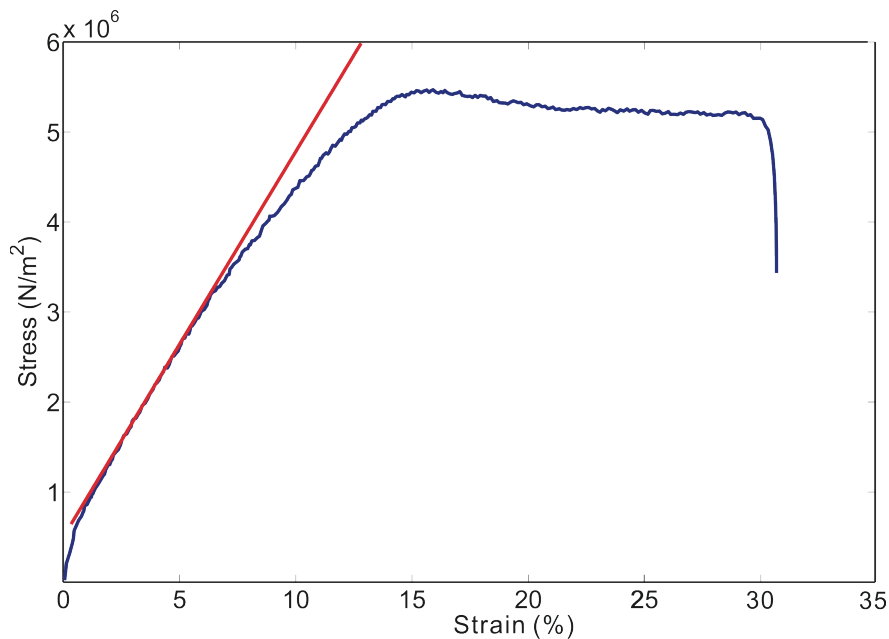

Figure 3.20 Induced stress-strain curve of 50 *wt*% sample

3.6.2 Tensile test validation

Because a traditional tensile test machine has many limitations for measuring the elastic modulus of piezoelectric paint polymer materials, a professional technique was adopted to verify the measured results. Instron is a professional materials testing technique used to measure the material properties of polymeric materials, it produces accurate results, but is also very expensive. The sample with $50wt\%$ was taken for the Instron tensile test, it has a dimension of $20mm\times 20mm$. Three different locations on the sample were chosen randomly to measure the elastic modulus. Figure 3.21 shows the measured stress-strain curve. The sample has an average value of 24.48MPa, which is close to the average value documented in Table 3.5. It can be observed from Figure 3.21 that the third test deviates slightly from the first and second test, which might be due to a manufacturing error or sample flaws. The measured result verifies the tensile test performed in the last section, and proves that with proper handling, the method discussed in the last section can be used to quantify the elastic modulus of piezoelectric paint.
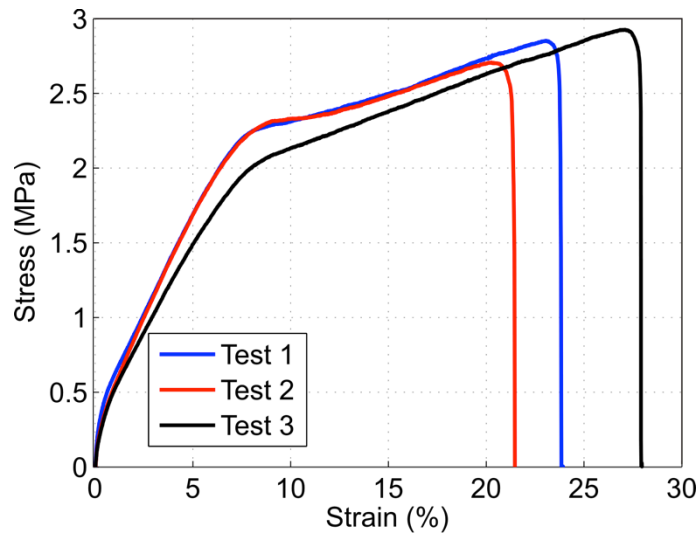

Figure 3.21 Tensile test by Instron

3.7 Piezoelectricity characterization

3.7.1 Analytical model

To quantify the piezoelectric constants of a piezoelectric material is very important, because the result determines how the material can be used in applications. Among the piezoelectric properties, piezoelectric charge constant is one of the most important values to evaluate the

piezoelectricity. Generally, the charge constant d_{33} can be obtained easily by a d_{33}-meter [PIEZOTEST 2004]. However, in many engineering applications that involve the measurement of an in-plane strain, e.g. acoustic emission, vibration, a more important parameter to be known is the piezoelectric charge constant d_{31}. If numerical calculations are considered, d_{31} is almost always a must-known parameter. In addition, this value directly indicates the piezoelectric properties of the material. In order to utilize the piezoelectric paint for further applications, its d_{31} is to be characterized.

Payo and Hale discussed the measurement of d_{31} by using a biaxial strain method [PAYO and HALE 2010; PAYO and HALE 2011b]. Since this method is very cost-effective which only requires a few easy-to-get equipments, it is adopted here to determine piezoelectric charge constant and sensitivity of samples. To deduce d_{31}, first of all, an analytical model of the piezoelectric paint is considered. Figure 3.22 shows the coordinate system and the piezoelectric paint polarization direction.
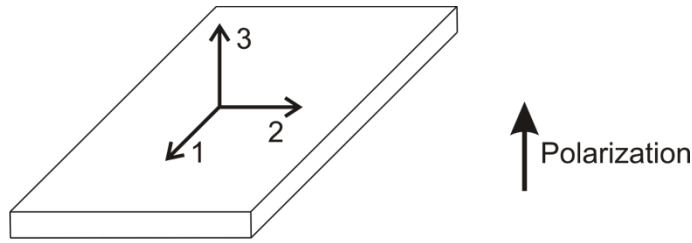

Figure 3.22. Coordinate system and the piezoelectric paint polarization direction.

Assuming that the piezoelectric paint is under low mechanical stress, by which the material behavior can be considered linear, and that the piezoelectric paint is isotropic in in-plane direction, because the piezoelectric paint is poled in the out-of-plane direction, the electric displacement could be rewritten as,

$$D_3 = d_{31}\sigma_1 + d_{32}\sigma_2 \qquad\qquad (3\text{-}4)$$

where σ_1 and σ_2 are the two in-plane stresses. Due to the isotropic assumption, we can deduce $d_{31} = d_{32}$, therefore

$$D_3 = d_{31}(\sigma_1 + \sigma_2) \qquad\qquad (3\text{-}5)$$

and,

$$D_3 = \frac{q}{A_e}$$
(3-6)

where q is the collecting of charges on the paint surface and A_e is the paint area covered by a silver paint electrode. Therefore the electric displacement would be obtained from measuring the charges and the paint area. Considering again the Hooke's law,

$$\begin{bmatrix} \sigma_1 \\ \sigma_2 \end{bmatrix} = \frac{E}{1-\nu^2} \begin{bmatrix} 1 & \nu \\ \nu & 1 \end{bmatrix} \begin{bmatrix} s_1 \\ s_2 \end{bmatrix}$$
(3-7)

and the sensitivity of the piezoelectric paint can be related by the electric displacement and the biaxial strains,

$$S = \frac{D_3}{s_1 + s_2}$$
(3-8)

3.7.2 Piezoelectric constant d_{31}

Basically, the piezoelectric sensors are used either as axial sensors or flexural sensors. An axial sensor senses a force exerted parallel to the direction in which the piezoelectric ceramic element is polarized, and generates an electric energy signal in the same direction [APC_INTERNATIONAL_LTD 2002]. Since the mechanical strain and the received electric signal are both the same to the polarization direction, the axial sensors are also called d_{33} sensor [APC_INTERNATIONAL_LTD 2002]. A flexural sensor also measures a force exerted in the polarization direction of the sensor, but the force causes the ceramic element to bend along the plane perpendicular to the direction of polarization. Therefore flexural sensors are also named d_{31} sensor [APC_INTERNATIONAL_LTD 2002].

By combining equation (3-4), (3-6) and (3-7), we get the relationship between d_{31} and the sensitivity as,

$$d_{31} = \frac{S(1-v)}{E} \hspace{4cm} \text{(3-9)}$$

or the relationship between d_{31} and the biaxial strain as,

$$d_{31} = \frac{q(1-v)}{A_e E(s_1 + s_2)} \hspace{3cm} \text{(3-10)}$$

where E has been measured in the last section, therefore if S is known, d_{31} could be calculated from (3-10).

Measurement of S

As indicated in (3-8), the sensitivity of the piezoelectric paint could be deduced if the electric displacement and the biaxial strain could be measured simultaneously. This was realized by adhering a $50wt\%$ piezoelectric paint on a 0.5mm thick aluminum cross, on the same position but another side of the cross, a rosette strain gauge was applied (Figure 3.23).
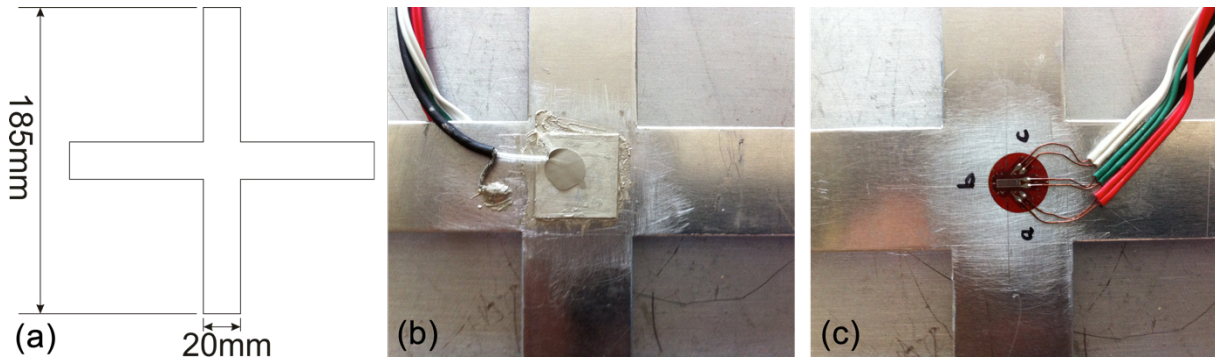

Figure 3.23 (a) Geometry of aluminum cross (b) A piezoelectric paint is adhered on one side of the aluminum cross and (c) a strain gauge is adhered on another side of the aluminum cross

The strain gauge is used to measure the biaxial strains s_1 and s_2. A test bed which is similar to the one described in [PAYO and HALE 2010] is constructed. The test bed consists of two $200mm \times 200mm \times 6mm$ plates, in between the plates there are eight steel bars which are placed between the plates as shown in Figure 3.24.
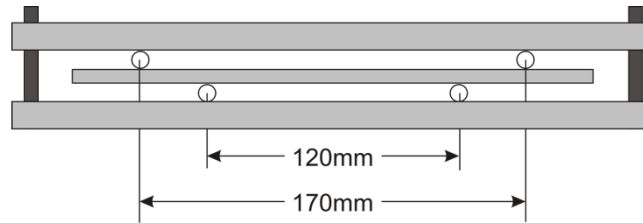
Figure 3.24 Side view of the test bed

Figure 3.25 is the assemble schematics of the test bed. To constrain the in-plane movement between the upper and lower plates, four bolts are applied at their corners, the aluminum cross is placed between the two plates as shown in the figure. This positioning ensures that the bending moment on the piezoelectric paint is constant.
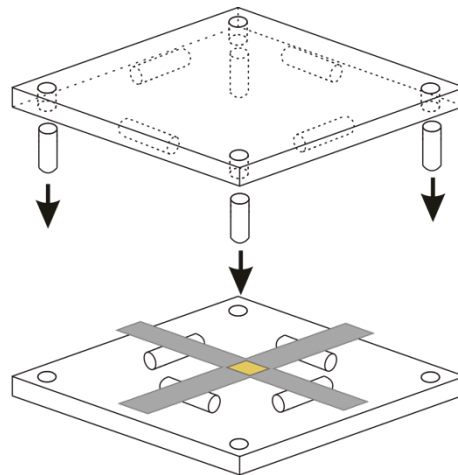

Figure 3.25 Assembly schematics of the test bed

Figure 3.26 shows the experimental setup together with signal acquisition devices. An impact was introduced on the aluminum plate by a hammer with rubber tip, the output signal of the piezoelectric paint went to a charge amplifier, and the signal of the strain gauge went to a four-channel carrier-frequency amplifier, the outputs of the two amplifiers were measured by a handyscope HS4.
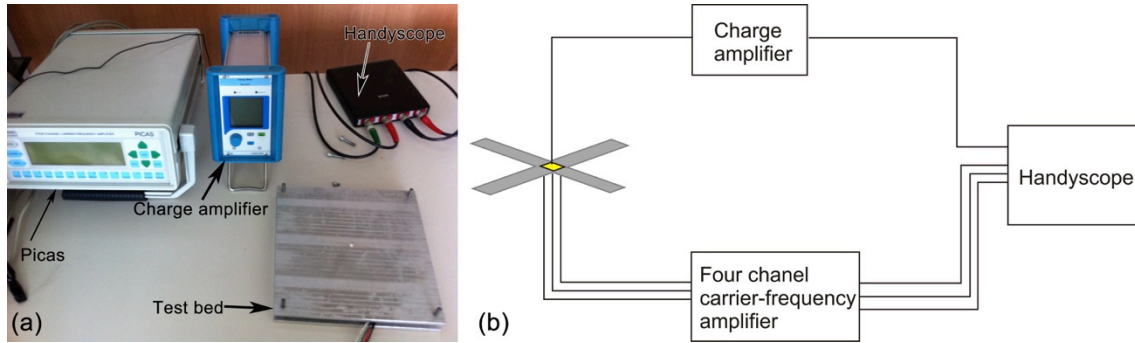
Figure 3.26 Experimental setup for the signal acquisition

Figure 3.27(a) and (b) are the output charges measured from the piezoelectric paint and strains measured by the rosette strain gauge in three directions respectively.
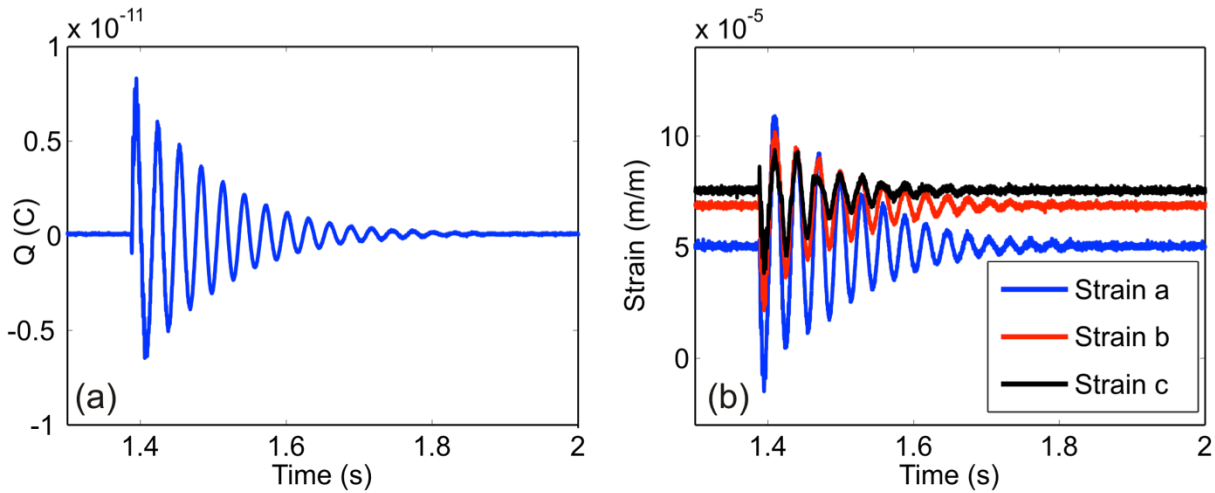

Figure 3.27 (a) Output charges from piezoelectric paint and (b) output strains from rosette strain gauge

The principal strains s_1 and s_2 can be calculated from the experimental data as [SHARPE 2008]

$$s_{1,2} = \frac{s_a + s_c}{2} \pm \frac{1}{\sqrt{2}}\sqrt{(s_a - s_b)^2 + (s_b - s_c)^2} \qquad (3\text{-}11)$$

and electric displacement D is

$$D = \frac{Q}{A_e} \qquad (3\text{-}12)$$

where s_a, s_b, s_c are outputs from the rosette strain gauge. Figure 3.28(a) and (b) show the calculated sum of principal strains and the electrical displacement respectively from equation

(3-11**)** and (3-12**)**. Although these two quantities are in different scale, their responses to the impact are very similar. The similarity indicates that the piezoelectric paint can be used as strain transducers, only that the piezoelectric paint cannot recognize a strain direction. The relationship between the sum of the principal strains and the electric displacement is plot in Figure 3.29. By applying a linear regression, the sum of principal strain and electrical displacement shows almost linearity in the measuring range, thus the sensitivity S can be calculated by measuring the slope. In this case, S has a value of 1.96×10^{-4} $((C/m^2)/(m/m))$.
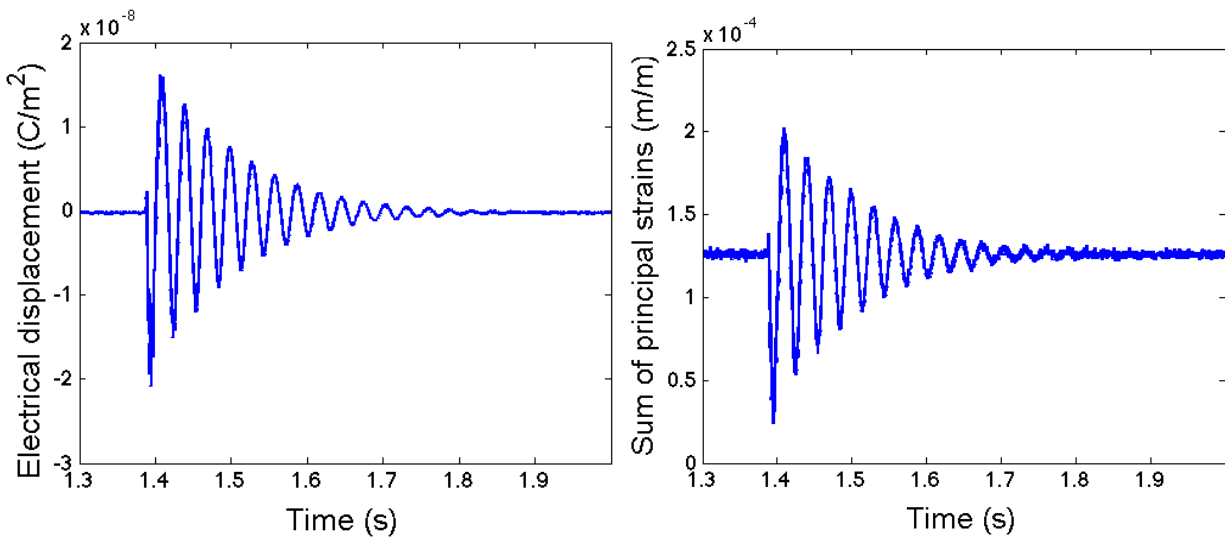

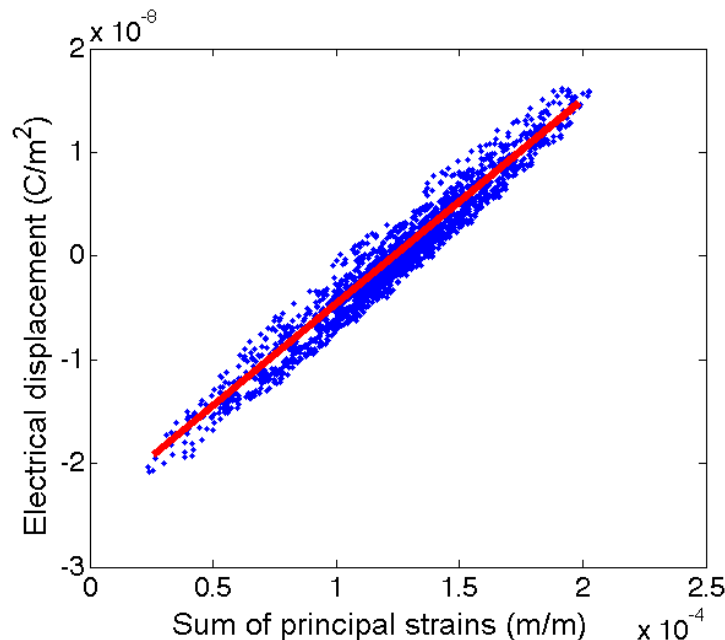**Figure 3.28 (a) Electrical displacement and (b) sum of principal strain**

Figure 3.29 Relationship between the sum of the principal strains and the electrical displacement

Since for most well-known polymers their Poisson's ratio are between 0.25 and 0.35 [GREAVES *et. al.* 2011], the Poisson's ration of piezoelectric paint is assumed as 0.3. By replacing E and S back into equation (3-9), the estimated d_{31} is 5pC/N. This result is close to the d_{31} predicted by Li (4.4pC/N) [LI, XIN 2009], in which he used a percolation based mixed model to predict the piezoelectric constants. The result obtained from the experiment here and from Li's is comparable based on three main reasons: a.) Li also used a $50wt\%$ piezoelectric paint, b.) the PZT powder Li used in his experiment is similar to the PZT powder used in this work, c.) the piezoelectric paint in both cases are made by tape casting method.

3.8 Piezoelectric paint refinement

The previous section has discussed the characterization process of piezoelectric paint, the results have shown that through comparing with other traditional sensors, the piezoelectric charge constant of the piezoelectric paint is relatively low. This disadvantage compromises the superior features of the piezoelectric paint: flexibility and conformability, and makes the piezoelectric paint less attractive in NDT and SHM. Due to this reason, applications of piezoelectric paint in real fields are still very limited, in another word, if the piezoelectricity of the piezoelectric paint could be enhanced, its popularity would be increased, and its application in SHM will be expanded as well.

Therefore, another issue concerning the investigation of a high quality piezoelectric paint is the piezoelectricity enhancement. There is not much work concerning the piezoelectricity enhancement of piezoelectric paint. The most popular way of increasing the sensitivity of piezoelectric paint is by increasing its weight percentage. However, Hale *et al.* has shown that the improvement of sensitivity was very limited by increasing the weight percentage of piezoelectric powder, and there was no evidence that a PZT concentration greater than 75% by weight gave any improvement in sensitivity [HALE and TUCK 1999]. Moreover, it has been proved in section 3.5 that an excessive concentration of PZT powder will contribute nothing beneficial but only compromising the quality of piezoelectric paint. Feenstra *et al.* promoted a method of enhancing active piezoelectric 0-3 nanocomposites through electrocspun nanowires, their experimental results showed that the piezoceramic wires produce 0-3 nanocomposites with as high as 300% increase in electromechanical coupling [FEENSTRA and SODANO 2008]. However, since this method used another completely difference technique, it will not be adopted here.

The piezoelectricity enhancement method described here is by refining the PZT powder. This is realized by sintering the PZT powder at high temperature, usually above 900°C at a predefined heating/cooling rate. By sintering the PZT powder in a high temperature, the organic species and other impurities within micro pores are removed, in addition, a high temperature sintering will form a perovskite phase PZT and densification [GU, Y. W. *et al.* 2008], so that the particles are fused to form a monolithic sintered structure and crystal grains are increased. Two cases were considered for the enhancement process.

Case one:

Sintering the piezoelectric powder up to 900°C for four hours with heating/cooling rate of 5°C/min. The enhanced PZT powder was used to fabricate samples with 50 $wt\%$, the sample was characterized with a same technique. Figure 3.30 is the measured principal strains vs. electrical displacement scatter plot. The resulted d_{31} has a value of 34.8pC/N, which is approximately seven times of the unrefined sample.
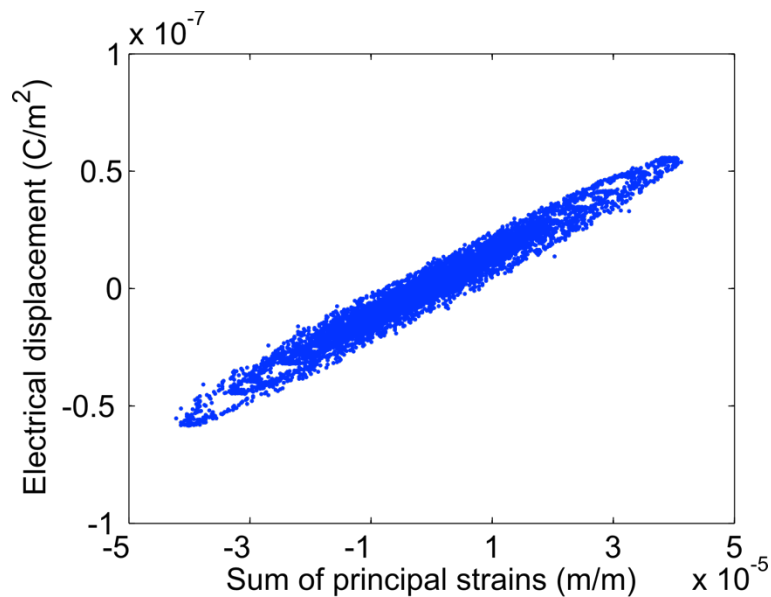
Figure 3.30 Sum of principal strains vs. electrical displacement in case one

Case two:

In this case, the sintering temperature was increased to 950°C and the sintering time was extended to eight hours. This is to check if by increasing the sintering temperature and time could increase the piezoelectricity of the paint. The enhanced PZT powder was also used to fabricate samples with $50wt\%$. Figure 3.31 is the resulted sum of principal strains and electrical

displacement. The resulted d_{31} deduced from Figure 3.31 is 120pC/N, this value is comparable with that from a PZT-5A ceramic [APC_INTERNATIONAL_LTD 2002].

By successfully enhancing the sensitivity of piezoelectric paint, its applications can be expanded effectively and broadly. The applications of refined piezoelectric paint will be discussed in the next chapter.
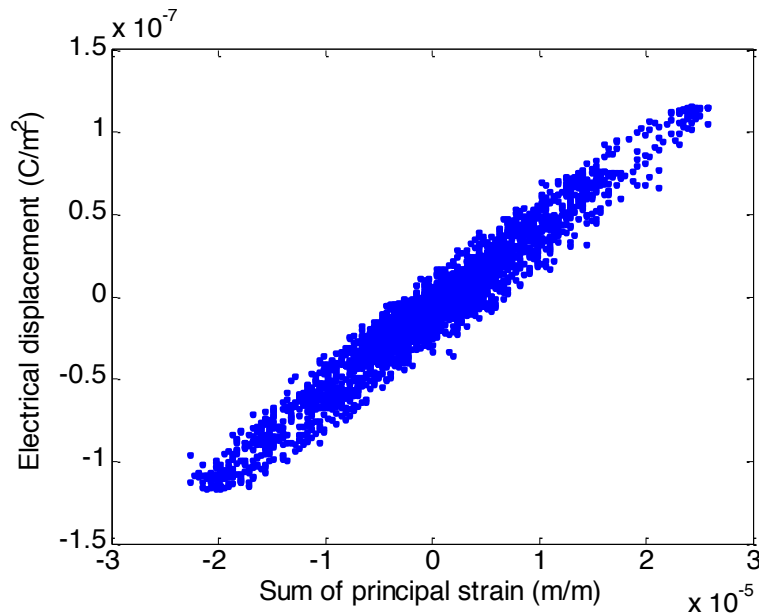

Figure 3.31 Sum of principal strains vs. electrical displacement in case two

3.9 Thermal property characterization

3.9.1 Thermal gravimetric analysis (TGA)

The aim of a thermal gravimetric analysis is to investigate the changes in weight of a substance in relation to the changes in temperature [DUVAL 1963]. It is usually measured under a controlled temperature program in a controlled atmosphere. In this case, the purpose of TGA is to observe the thermal stability of the piezoelectric paint. This measurement is to quantify the weight loss of the piezoelectric paint due to the decomposition of the plasticizer with the increase of temperature, as the loss of plasticizer affects the physical properties of the piezoelectric paint. TGA measurement helps to predict a product performance and improve a product quality.

A piezoelectric paint sample with 50 *wt%* was subjected to TGA. The sample was placed in a small electrically heated oven with a thermocouple to accurately measure the temperature. The heating temperature started from 30°C and went up to 1000°C. The weight of the sample was

recorded simultaneously and converted to residue mass fraction, which is defined as the original mass divided by a residue mass at various temperatures. Figure 3.32 is the measured thermogravimetric curve. As could be seen, the sample went through a significant mass reduction starting from 215.7°C, this was due to the decomposition of polymers at this temperature. After 315.6°C, the sample experienced a quasi-stable stage until 719.9°C, from which all the decomposed polymer started to gasify. The thermogravimetric analysis indicates that the principle working temperature of piezoelectric paint should be below 215°C. In fact, in real applications, the temperature should be much lower than the value, because high temperature will accelerate the polymer aging.
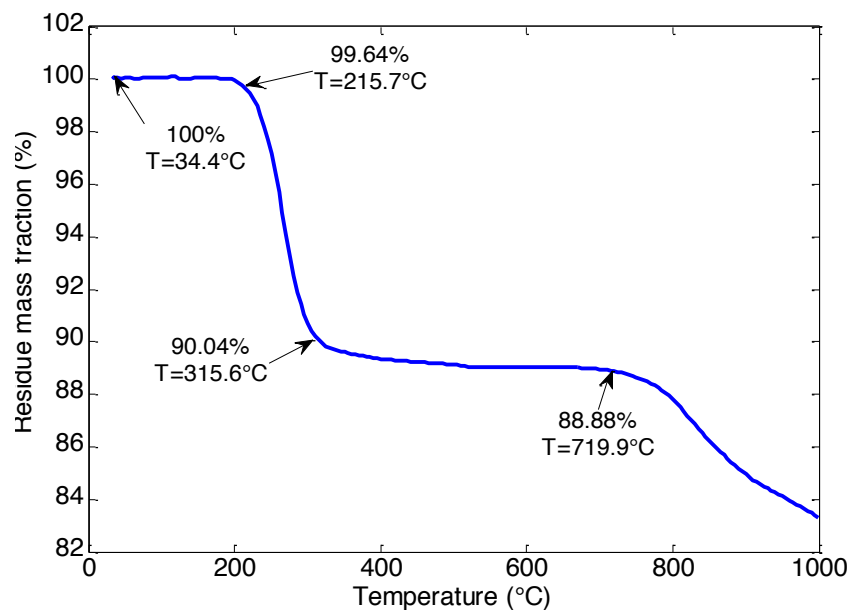
Figure 3.32 Thermogravimetric analysis curve of piezoelectric paint

3.9.2 Effect of frequency and temperature on dielectric properties

Several important dielectric properties, including impedance, admittance, permittivity, conductivity and capacity were investigated as a function of temperature (25°C-45°C) and frequency (10Hz-1MHz). In this case, the silver paint was replaced by a spray coated gold layer as electrodes on the sample surfaces (Figure 3.33), so that the weight and thickness of electrodes can be ignored in this experiment, meanwhile, it is able to provide an excellent conductivity.

Figure 3.33 Samples used for electrical properties characterization
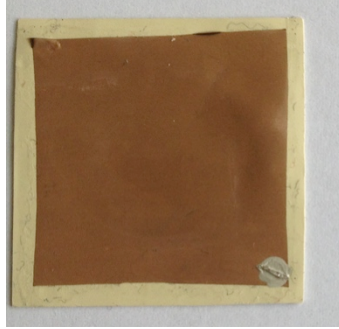
The samples were characterized by a frequency analyzer with heating and cooling options, which is specially designed for polymer related materials. In the first experiment, the sample was heated from room temperature (25°C) to 50°C, and cooled back to the room temperature, the stabilization time for each temperature was five minutes. The admittance, impedance, conductivity and permittivity, as well as the phase angle are presented in Figure 3.34 and Figure 3.35. As can be informed from Figure 3.34 and Figure 3.35, the admittance (Figure 3.34(a)), impedance (Figure 3.34(b)), conductivity (Figure 3.34(c), capacitance (Figure 3.35(a)), permittivity (Figure 3.35(b)) and phase angle (Figure 3.35(c)) changes as the temperature changes. The capacitance, permittivity increases with the increase of temperature, since as the temperature increases, the orientation of dipoles is facilitated, through which the dielectric constant is increased [YADAV *et al.* 2010]. Meanwhile, when a single curve at a specific temperature point is studied, the capacitance and permittivity decreases with the increase of frequency. The variation of phase angle clearly shows how the admittance, impedance and conductivity varies with temperature, as could be seen from Figure 3.35(c), when the temperature increase from 35°C to 45°C, or decrease from 45°C to 35°C, below the frequency of 1kHz, the curves of phase angle fluctuate in this range, this is due to the glass transition of the polymer phase, under which the molecule orientation changes with the cooling and heating process.

In addition, the sample was swept from 10kHz to 50kHz at room temperature, Figure 3.36 shows the resulted impedance. The impedance curve indicates that the piezoelectric paint is not suitable to be applied in an electro-mechanical impedance method, which usually utilize the resonance of a piezoelectric component [PARK *et al.* 2008]. For the piezoelectric paint, the resonance is severely damped by the polymer-phase.
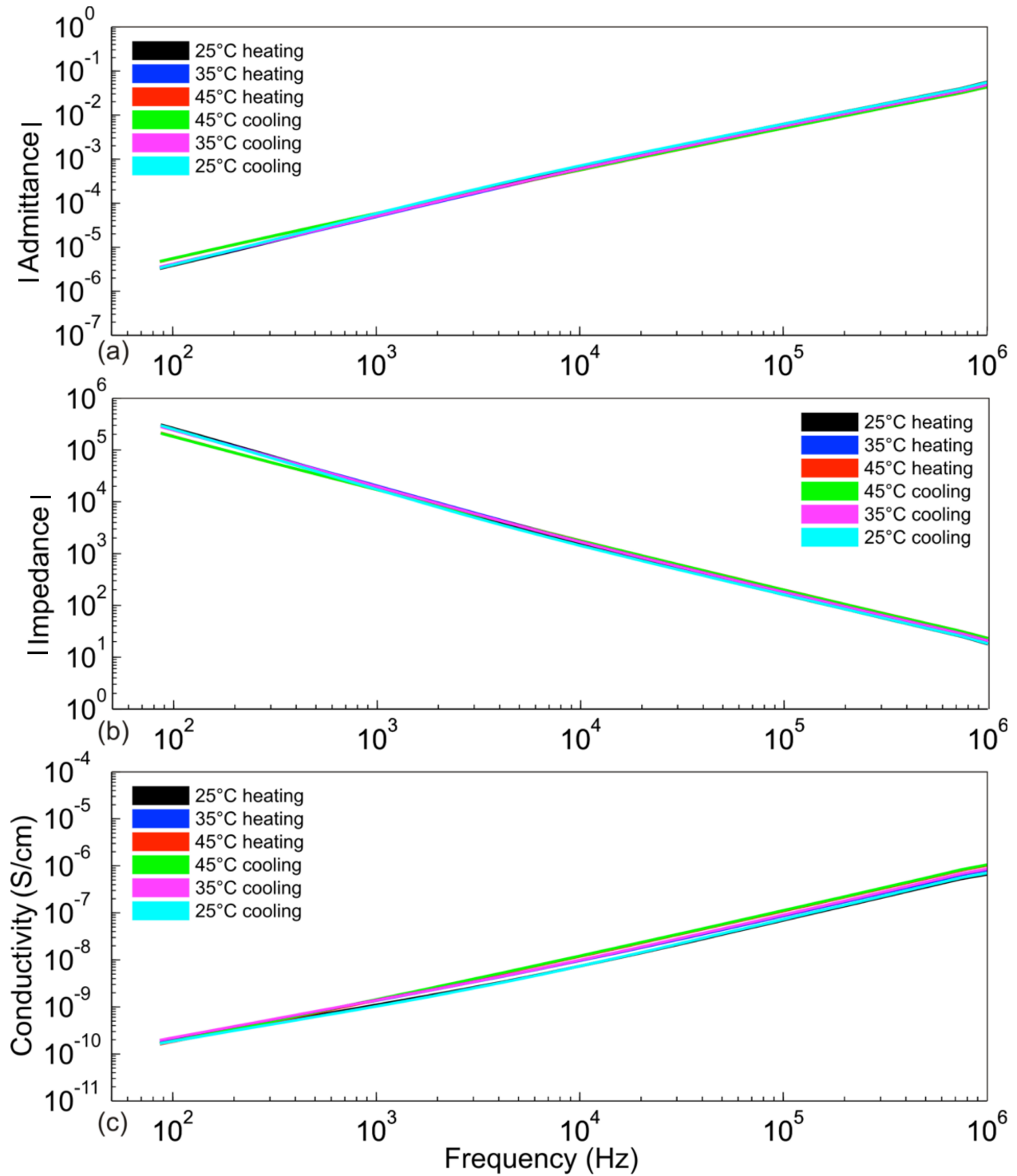
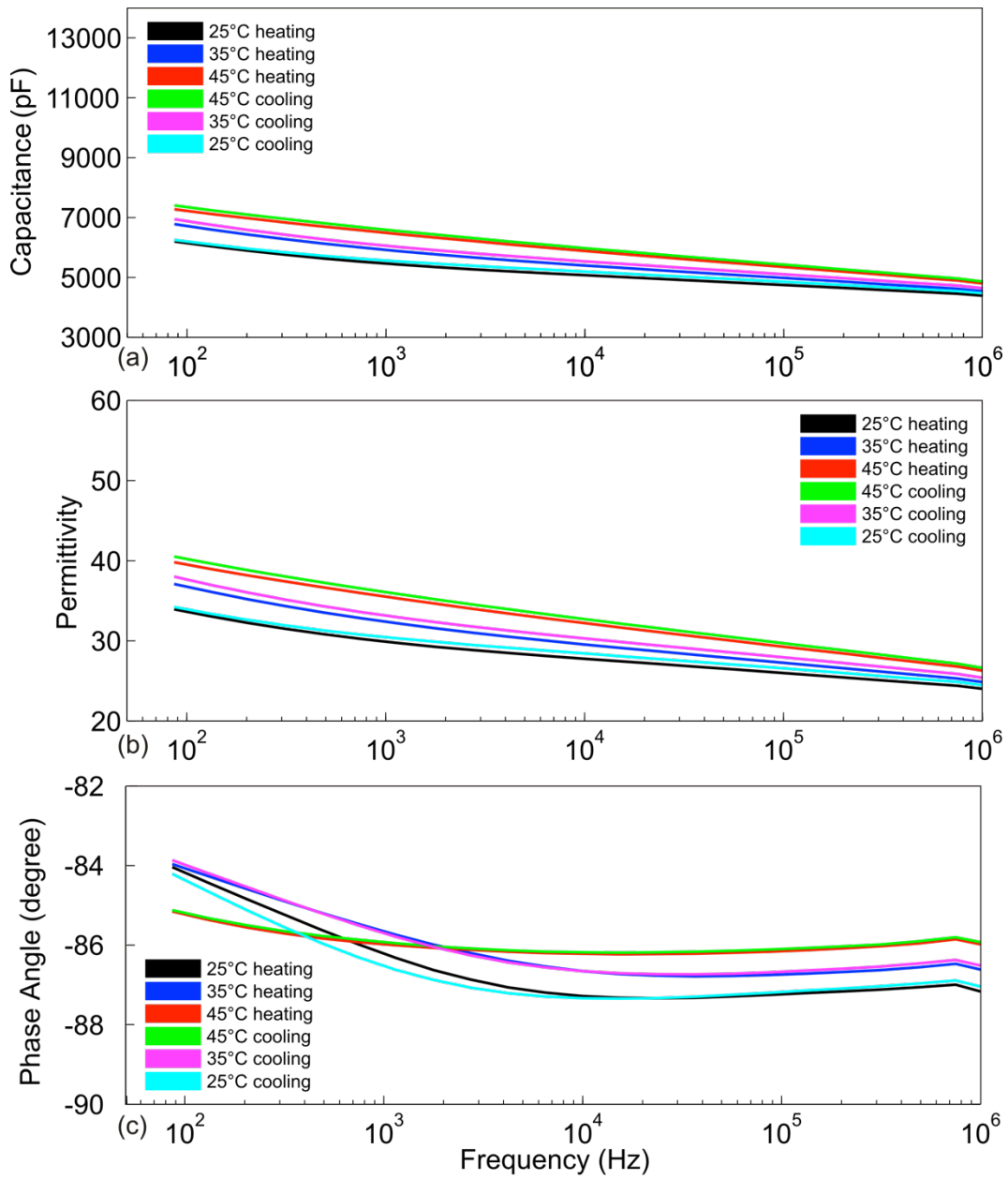**Figure 3.34 Magnitude of (a) Admittance (b) impedance and (c) conductivity of piezoelectric paint sample**

Figure 3.35 (a) Capacitance (b) permittivity and (c) phase angle of piezoelectric paint sample
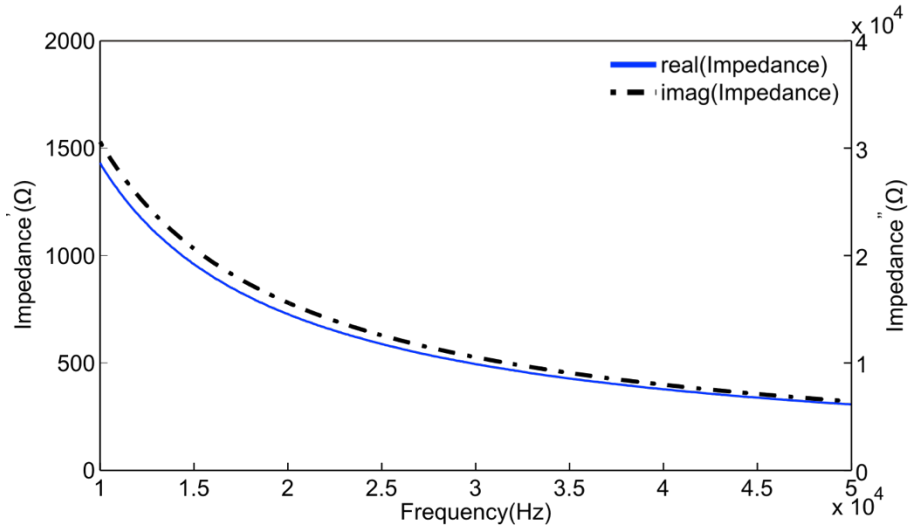
Figure 3.36 Frequency sweep of piezoelectric sample from 10kHz to 50kHz

3.9.3 Active sensing at various temperatures

In this section, the piezoelectric paint is implemented as sensors in active sensing, with the temperature varies from a room temperature (25°C) to 75°C. As shown in Figure 3.37, two transducers, the piezoelectric ceramic and the piezoelectric paint are applied on an 400mm× 150mm×2mm aluminum plate. The piezoelectric ceramic functions as the actuator, it is a commercial product (PIC155) from PI Ceramic with a dimension of 20mm×20mm×1mm, the dimension of piezoelectric paint is 30mm×30mm×0.2mm, the geometric center distance between the two transducers is 200mm.

Figure 3.37 Piezoelectric ceramic and paint on an aluminum plate

The plate was placed in an oven for heating purpose. The ventilation system in the oven was switched off, otherwise the sensing signal would be severely disturbed. Although the oven used

in the experiment has a temperature sensor itself, it is not accurate enough to determine the temperature near the plate, therefore two temperature sensors were adhered on the aluminum plate for the temperature measuring purpose. The two temperature sensors were connected to a Series T900 process-controlled temperature measurement instrument (Figure 3.38), which can be directly connected to a Handyscope for signal acquisition.

Figure 3.38 Series T900 process-controlled temperature acquirement instrument

The plate was placed in the oven and heated from 25°C to 75°C, with a heating rate of 5°C/min. As an actuator, the piezoelectric ceramic was sending ultrasonic signals from 25kHz to 30kHz repeatedly. A handyscopte HS4 was recording the received signals from the piezoelectric paint directly. In this case, a charge amplifier was absent since it can cause charge saturation in a long time duration measurement, this is also a main drawback of using charge amplifiers. Fortunately, the piezoelectric paint after sensitivity enhancement has a piezoelectricity which is high enough to be directly measured without using a charge amplifier, this experiment also shows the importance of the refinement and improvement of the piezoelectric paint.

Figure 3.39 shows the input signal, it is a wavelet with peak-to-peak amplitude of 10V. Figure 3.40 to Figure 3.42 are the responses of the piezoelectric paint during heating at the frequency of 25kHz, 27.5kHz and 30kHz respectively. It could be seen that with the increase of the signal frequency and the temperature, the amplitude of the piezoelectric paint increased 1mV approximately.
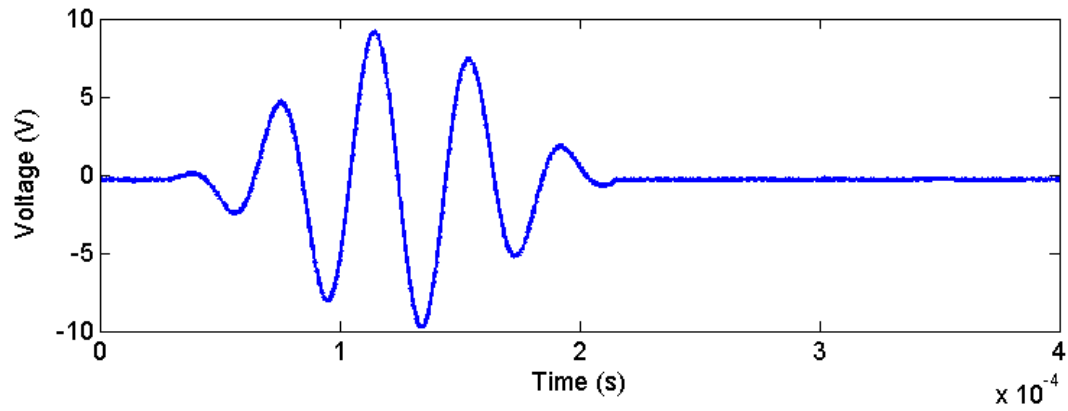
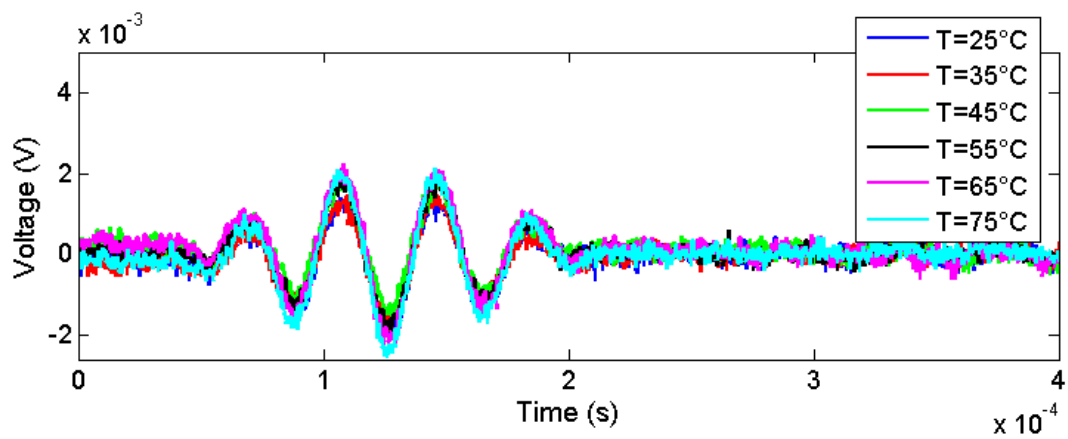**Figure 3.39 Input wavelet signal at 25kHz for active sensing**

Figure 3.40 Response of piezoelectric paint at 25kHz - heating
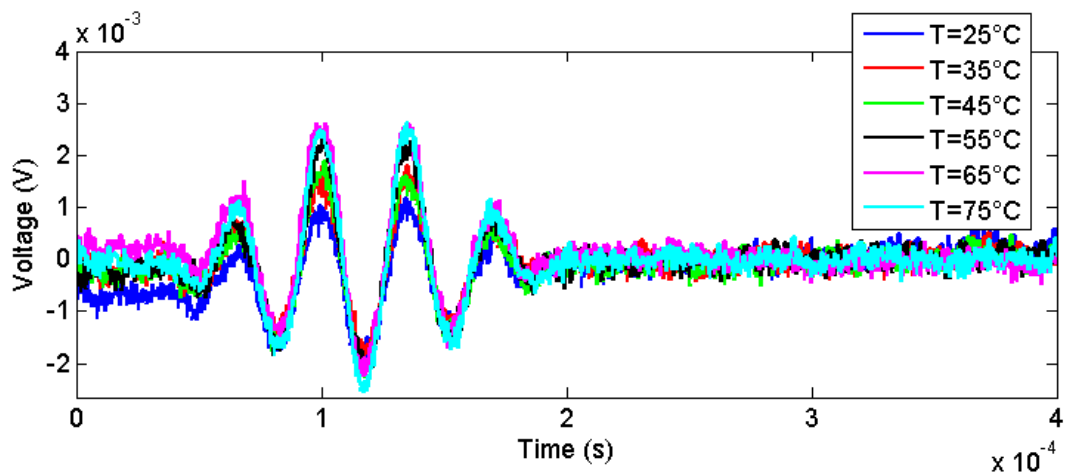

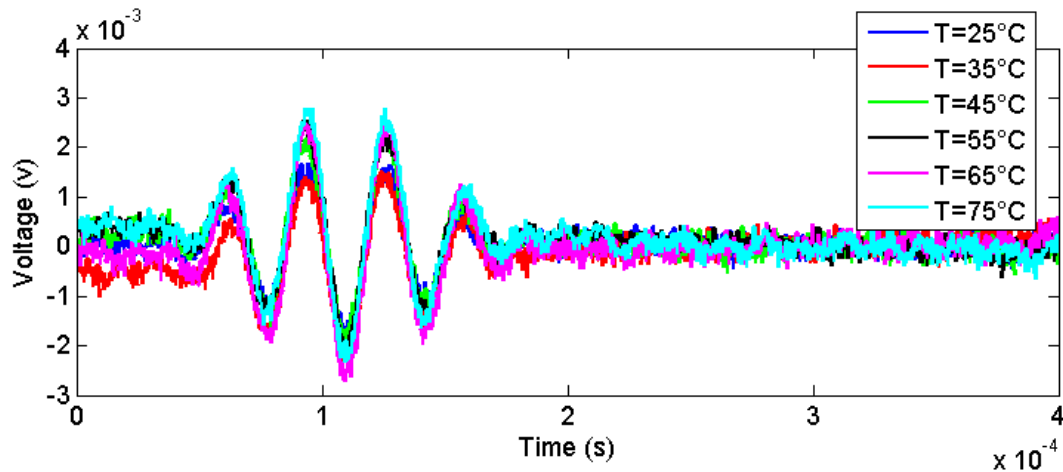**Figure 3.41 Response of piezoelectric paint at 27.5kHz - heating**

Figure 3.42 Response of piezoelectric paint at 30kHz - heating

During the cooling process, the cooling rate was also controlled at approximately 5°C/min, this was realized by stopping the heating function and leaving the oven door unlocked. Figure 3.43 to Figure 3.45 are the responses of the piezoelectric paint during cooling at the same frequency of 25kHz, 27.5kHz and 30kHz respectively. These three figures show that the variation of response from piezoelectric paint is higher at a high frequency. At higher frequency the response of the piezoelectric paint varies more with the influence of temperature. Also a higher temperature reduces the sensed signal.

Torres [TORRES 2014] did a similar experiment with two PZT ceramics – one as an actuator and another as a sensor, his results also shows that a varying temperature can modify the shape of the time histories. Since he used a PZT ceramic as the sensor, which has very high piezoelectricity compared with the piezoelectric paint, it can be clearly seen in his results that the sensed signal is right shifted under a higher temperature. For the piezoelectric paint, the signal shifting can hardly be observed due to the low signal-to-noise-ratio. Additionally, the right-shifted signal is reduced, its shape is modified as well, by comparison it can be seen that this response is similar to the response from the piezoelectric paint.

From the heating and cooling experiment, it can conclude that the signals of the piezoelectric paint can be influenced by a temperature variation. Therefore although its physical properties can withstand temperatures up to 200°C, it is not suggested to use the piezoelectric paint at its temperature limit.
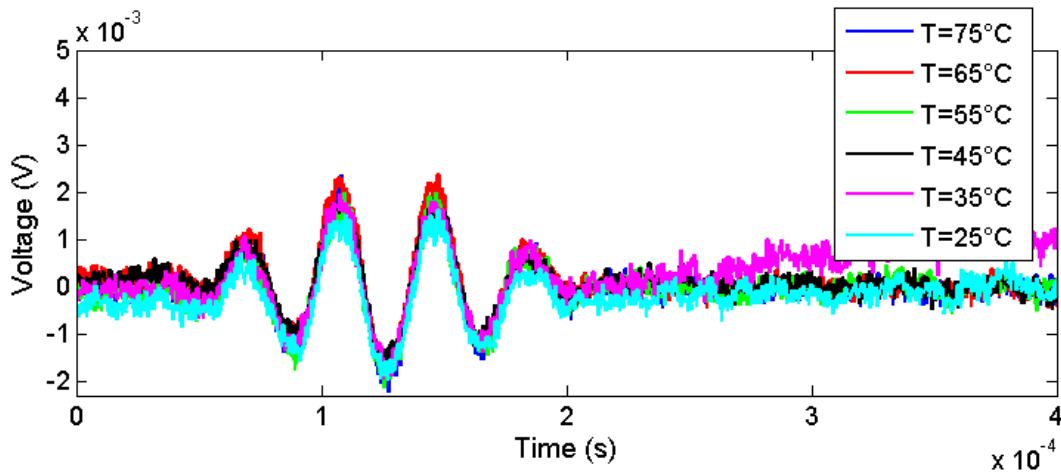
Figure 3.43 Response of piezoelectric paint at 25kHz - cooling
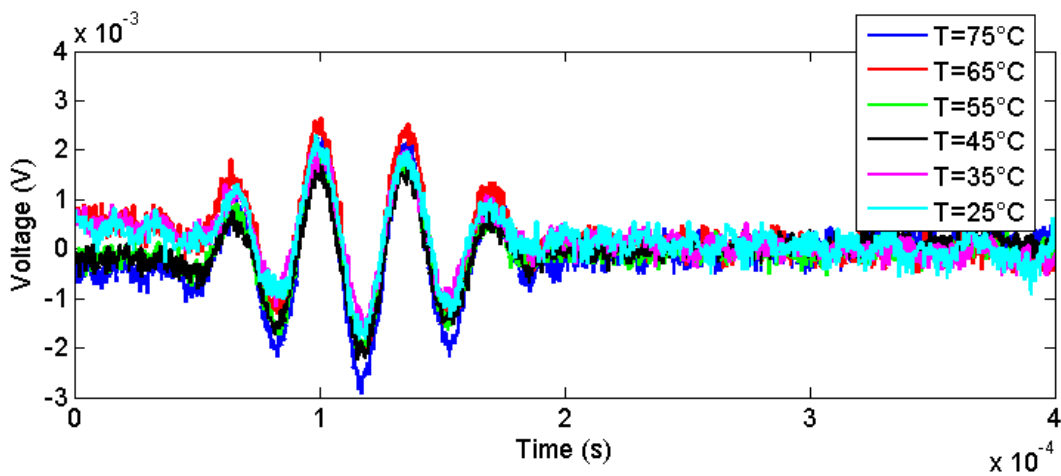
Figure 3.44 Response of piezoelectric paint at 27.5kHz - cooling
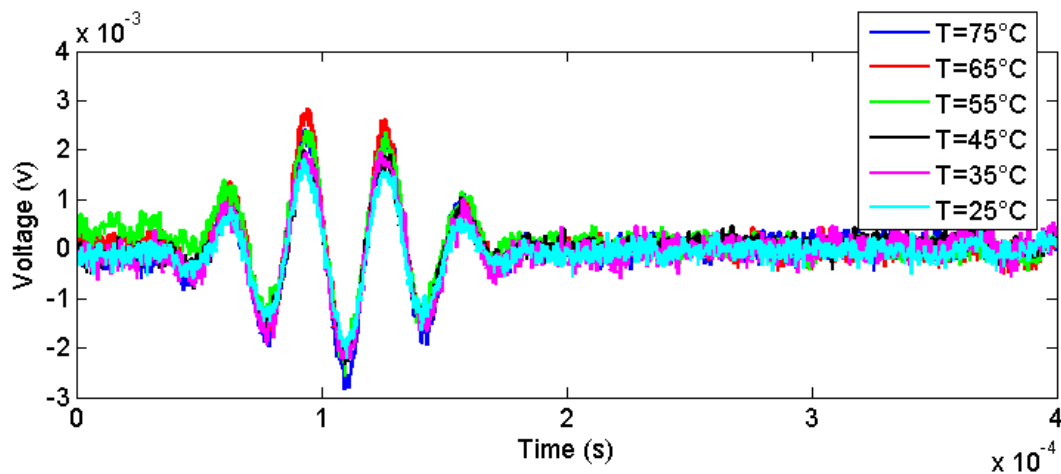
Figure 3.45 Response of piezoelectric paint at 30kHz - cooling

3.10 Conclusion

In this chapter, the fabrication of the piezoelectric paint was investigated. Difference fabrication methods were compared at the beginning, continued with a detailed description of the method invented in this work. After fabrication, its properties in different aspects were studied, including its morphology, elastic properties, piezoelectricity as well as its thermal properties. In order to characterize these properties, different experiments were designed and carried out. This study helps a better understanding of the piezoelectric paint, especially for experimental applications. The characterized results enable a profound understanding of the material, and ensure effective applications of it.

4 Application of piezoelectric paint as spatially distributed sensors

4.1 Application of piezoelectric paint as spatially distributed modal sensors

4.1.1 Introduction

In the last chapter, the fabrication and characterization of the piezoelectric paint was investigated. The results have presented an underlying knowledge about many aspects of the piezoelectric paint. The successful fabrication and characterization of the piezoelectric paint in lab motivates and enables many applications in Structural Health Monitoring and Non-Destructive Testing.

Like the exploration of many other smart materials, the final aim is to put the new material in service for practical applications, especially those that can prove the superiority of the material itself. A variety of research works have proved that the piezoelectric paint is a promising smart material in the sensing field [HALE 2004; LI, X. and ZHANG 2008; ZHANG 2006b]. In this chapter, applications are going to be demonstrated concerning using piezoelectric paint in different cases.

Conventionally, the piezoelectric materials are usually crystals or ceramics, which are well known for their brittleness. Due to this property, they can only compose point sensors with a small dimension, which are also known as discrete sensors. These point sensors/actuators, such as accelerometers, piezoelectric active wafers, will react or induce force, displacement or acceleration at a local point in a structure [TZOU, H.S. and ANDERSON 1992]. For the point

sensors, no prior knowledge of the host structure is necessary beforehand, however, the sensor design is also not be able to be integrated into a host structure.

In vibration control, the method of using discrete sensors/actuators to control the vibration of flexible structures has been discussed by Balas [BALAS 1978], these control strategies often suffer from actuator/observer spillover due to the residual models which leads to instabilities in the closed-loop system. Therefore, the idea of performing distributed control has been discussed widely [BAILEY and HUBBARD 1985; BURKE and HUBBARD 1987; COLLINS et al. 1994; CRAWLEY and LUIS 1985; GU, Y. et al. 1994; HANAGUD et al. 1985; HUBBARD and MILLER 1987; PLUMP et al. 1987; PREUMONT et al. 2002; SUNG et al. 1990; TZOU, H.S. 1989; TZOU, H.S. and GADRE 1988; TZOU, H. S. and TSENG 1990]. However, these works only achieved limited success in terms of obtaining a high damping. With the discovery of piezoelectric effects from PVDF in 1969, extensive research works concerning applying it have been encouraged and explored. For the modal sensors, one of its main advantages is that the structural information known a priori could be integrated into the sensor design [TZOU, H.S. and ANDERSON 1992]. The pioneer work of using PVDF in distributed modal sensors was performed by Lee and Moon [LEE and MOON 1989], they demonstrated the critical damping control of a one-dimensional cantilever plate successfully, which was made from PVDF thin film. Preumont *et al* discussed and demonstrated the construction of spatial filters in structural control and applied a new electrode concept by porous distributed electrode [PREUMONT et al. 2004; PREUMONT et al. 2002]. Chen *et al* implemented an optically reconfigurable modal sensors for a cantilever beam by using a chemical method [CHEN et al. 2011]. The use of spatial filters was also expanded into vibration-based damage detection [DERAEMAEKER and PREUMONT 2005] and structural health monitoring [FRISWELL and ADHIKARI 2010], along with the discussion of modal sensors/spatial filters for rectangular plate structures [DONOSO and BELLIDO 2009a; DONOSO and BELLIDO 2009b; JIAN and FRISWELL 2007; TANAKA and SANADA 2007].

Although the idea of building spatially distributed modal sensors have been continuously discussed since the late of the 1980s [COLLET et al. 2003; FRISWELL 1999; FRISWELL 2001; VASQUES and RODRIGUES 2008], the real experimental trials are still very limited, and most of them were realized by adopting PVDF, which is commercially available on the market. No work has reported the utilizing of piezoelectric paint as modal sensors. This is mainly due to the special requirement of materials and the complexity of shaping of the modal sensor, as well as the

immaturity of the piezoelectric paint technology. With the successful production and characterization of the piezoelectric paint in the last chapter, the investigation of applying it as spatially distributed modal sensors is performed.

Generally, using the piezoelectric paint as spatially distributed modal sensors will benefit from the following advantages:

- The piezoelectric paint is flexible and distributable, therefore it is easily to be produced in a large thin sheet with a free-standing form, as a result it can cover a large area of a structural surface.

- The piezoelectric paint is a polymeric smart material, which is very soft and therefore can be shaped into desired forms without structural damage, the shaping of it is quite simple comparing with other piezoelectric ceramics, especially for shaping into a more complicated form. This feature is a prerequisite for implementing it as spatially distributed modal sensors.

- Production of the piezoelectric paint is inexpensive, and the sensor properties can be tailored by altering the ratio of constituents in the piezoelectric slurry. This is an advantage over the PVDF, whose properties cannot be customized according to a specific application requirement.

- The surface electrode of a modal sensor can be realized easily by applying a thin layer of silver paint on the piezoelectric paint surface, or by spraying coating method.

- Comparing with PVDF, an optimized piezoelectric paint has a much higher piezoelectricity.

This section investigates the use of piezoelectric paint as spatially distributed modal sensors. To begin with, the theoretical backgrounds behind are to be introduced in the next subsection. Following will be implementation of the theory in experiments, as well as results and discussion. The difference between the theoretical modal sensors and experimentally developed modal sensors are compared, followed with sensitivity analysis which explains the error obtained between theory and experiments. Afterwards, a series of optimization methods are introduced and applied on the modal sensor for a better performance.

4.1.2 Analytical description of modal sensors for a one-dimensional Euler beam

For designing a distributed piezoelectric modal sensors, one of the most important parameters is the surface electrode pattern of the piezoelectric layer [TZOU, H.S. 1989], which collects all the charges being generated due to the mechanical vibration of a structure, this process is also known as spatial domain integration. Various methods can be used for the surface electrode patterning, such as etching the surface electrode of the piezoelectric layer to a desired shape, which was adopted by Lee *et al.* [LEE and MOON 1989], or sputtering a patterned electrode on the piezoelectric green sheet before poling.

For the case of piezoelectric paint, since the surface electrode is achieved by spreading a conductive paint on the surface, the surface electrode pattern can be implemented by cutting the piezoelectric paint itself, this method is the simplest of all the mentioned above. Another important parameter involved is the polarization profile of the piezoelectric layer, this can be achieved by re-poling the piezoelectric material [COLLINS 1990]. For the piezoelectric paint, it can be achieved easily by changing the polarization direction of the piezoelectric paint, in addition, the piezoelectricity can be tuned by altering the composition of the two phases. In this section, the finding of the two parameters will be discussed in detail.

A cantilevered beam is shown in Figure 4.1, which can be considered as a fundamental element of a distributed structure. Assuming that the deformation of the beam is small enough so that the shear deformation is much smaller than the transverse deformation, so that the beam will not extend or contract after deformation, and the lines perpendicular to the mid-plane remain after deformation. Therefore the beam can be considered as an Euler beam, whose shear stresses can be ignored. Considering the transverse vibration of the beam, the bending moment M_b is calculated as [INMAN 2001],

$$M_b(x,t) = E_b I_b(x) \frac{\partial^2 w(x,t)}{\partial x^2} \tag{4-1}$$

where E_b is Young's modulus of the beam, $I_b(x)$ is the cross sectional area moment of inertia about the z axis of the beam and $w(x,t)$ is the transverse displacement of the beam.
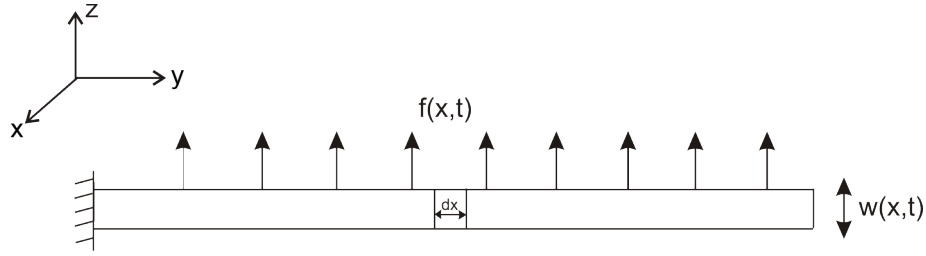
Figure 4.1 A cantilevered beam in transverse vibration

The transverse vibration of beams with a constant cross section has been well described by Timoshenko *et al.* [WEAVER *et al.* 1990],

$$E_b I_b \frac{\partial^4 w(x,t)}{\partial x^4} + \rho A_b \frac{\partial^2 w(x,t)}{\partial x^2} = f(x,t) \tag{4-2}$$

where x is the spatial coordinate, t is the time, $f(x,t)$ is the distributed transverse force, ρ, E_b, I_b and A_b is density, Young's modulus, second moment of area and cross section of the beam respectively. According to the Euler-Bernoulli beam assumption, the extensional strain component is described as,

$$\varepsilon_{11}(x,z,t) = -h_b \frac{\partial^2 w(x,t)}{\partial x^2} \tag{4-3}$$

where z is the spatial coordinate in the transverse direction, h_b is the half thickness of the beam. For piezoelectric materials, if plane stress is considered, according to equation (2-6), the conventional equation of the sensing behavior in the transverse direction is:

$$D_3 = e_{31}\varepsilon_{11} - \epsilon_{33}^T E_3 \tag{4-4}$$

where e_{31} is the piezoelectric stress constant, ϵ_{33}^T is the dielectric constant under constant stress, D_3 is transverse displacement and E_3 is transverse electric field. Assume the electric field is zero, this leads to,

$$D_3 = e_{31}\varepsilon_{11} \tag{4-5}$$

According to Gauss's law, integrating the electric displacement over the electrode area A_e on the piezoelectric material and replace (4-3) into (4-4) gives the induced charge,

$$q(t) = -e_{31}h_b \int_{A_e} \frac{\partial^2 w(x,t)}{\partial x^2} dA_e \tag{4-6}$$

and is equal to,

$$q(t) = -e_{31}h_b b_b \int_0^{l_b} \mathcal{F}(x) \frac{\partial^2 w(x,t)}{\partial x^2} dx \tag{4-7}$$

where

$$\mathcal{F}(x) = \int_{-h_b/2}^{h_b/2} F(x,y)P_0(x,y)dy \tag{4-8}$$

is the spatial sensitivity function of an arbitrarily shaped piezoelectric sensor, b_b and l_b are the beam width and length respectively, $F(x,y)$ is the surface electrode pattern and $P_0(x,y)$ is the polarization profile, which is designated as either positive or negative. The transverse deformation $w(x,t)$ can be decomposed into the modal summation:

$$w(x,t) = \sum_{m=1}^{\infty} A_m(t)\phi_m(x) \tag{4-9}$$

where $A_m(t)$ and $\phi_m(x)$ are the m-th modal coordinate and mode shape. Substitute (4-9) into (4-7) induces,

$$q(t) = -e_{31}h_b b_b \sum_{m=1}^{\infty} \int_0^{l_b} \mathcal{F}(x) \frac{d^2 \phi_m(x)}{dx^2} A_m(t)dx \tag{4-10}$$

Since a one-dimensional beam is a self-adjoint system, the modes are orthogonal to each other. This gives the principle of designing a modal sensor [LEE 1992]. The mode shape of a one-dimensional cantilever beam is known as [BLEVINS 1979],

$$\phi_m(x) = \cosh\left(\frac{\lambda_m x}{l_b}\right) - \cos\left(\frac{\lambda_m x}{l_b}\right) - \sigma_m[\sinh\left(\frac{\lambda_m x}{l_b}\right) - \sin\left(\frac{\lambda_m x}{l_b}\right)] \tag{4-11}$$

According to the fact that,

$$\int_0^{l_b} \frac{d^2\phi_m(x)}{dx^2}\frac{d^2\phi_n(x)}{dx^2}dx = \delta_{nm}(\lambda_n^4/l_b^3) \tag{4-12}$$

where δ_{nm} is the Kronecker delta. Since $\mathcal{F}(x)$ has been proved to be proportional to the modal strain distribution along the length of the beam, it could be chosen as,

$$\mathcal{F}(x) = \alpha_n \frac{d^2\phi_n(x)}{dx^2} \tag{4-13}$$

where α_n is a normalization factor. Substituting (4-12) and (4-13) into (4-10) obtains the modal sensor equation,

$$q(t) = -(e_{31}h_b b_b \alpha_n \lambda_n^4/l_b^3)A_n(t) \tag{4-14}$$

Equation (4-14) indicates that the induced charge on the piezoelectric material is only proportional to a single modal coordinate of the beam, therefore only a particular modal coordinate is measured. In addition, the sensing voltage can be calculated accordingly,

$$v(t) = \frac{q(t)}{C_p} = \frac{-(e_{31}h_b b_b \alpha_n \lambda_n^4/l_b^3)A_n(t)}{C_p} \tag{4-15}$$

where C_p is the capacitance of the piezoelectric paint, it is defined in terms of the piezoelectric paint area and thickness as

$$C_p = \epsilon_{33}^T A_e/h_p \tag{4-16}$$

Figure 4.2 shows the calculated surface electrode pattern and polarization profiles of the normalized first and second modal sensors. Figure 4.2(a), (b) and (c) represents the first, second and third mode modal sensor respectively. In this figure the beam size is normalized, therefore it is dimensionless. The blue area is the surface electrode pattern, which is also the shape of the piezoelectric paint. The "+" and "-" sign marks the polarization profile of the respective part. For the first mode sensor (Figure 4.2(a)), the whole sensor has a same polarization profile, this is different from the second (Figure 4.2(b)) and third mode sensor (Figure 4.2(c)), which are composed of piezoelectric paint with both "+" and "-" polarization profile. It can be concluded

that with the increasing of modes, the shape of the modal sensor is becoming more complex, which also means it is more difficult to fabricate them. Therefore, only the performance of first and second mode modal sensors will be demonstrated in the next section.
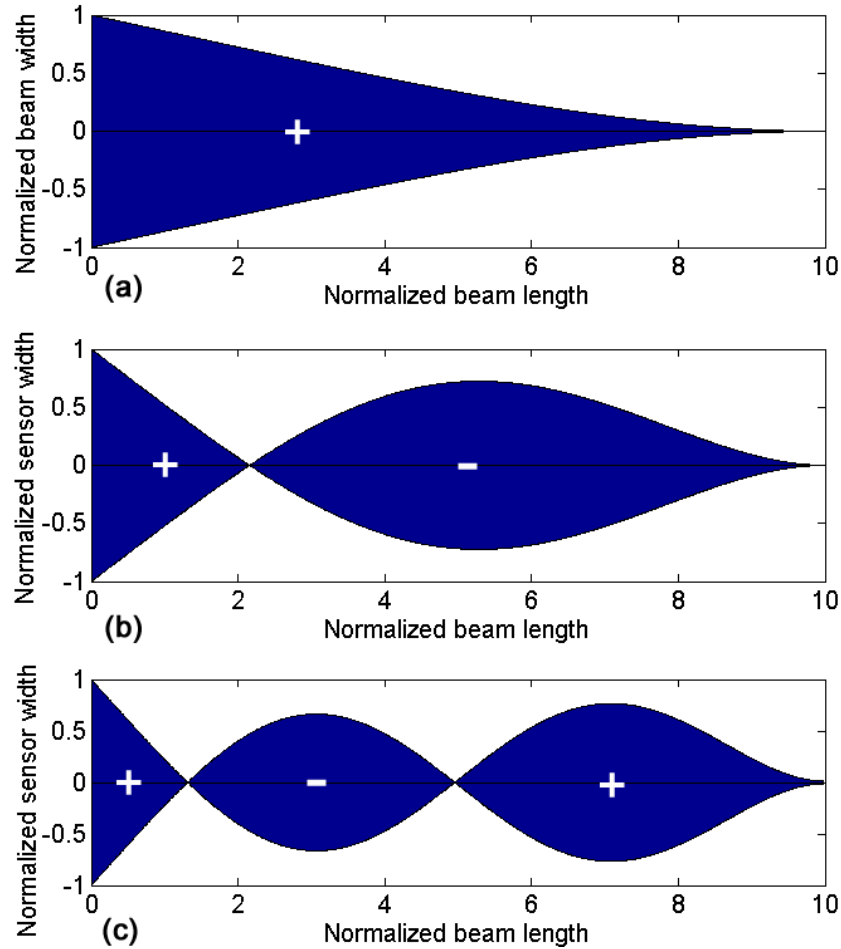
Figure 4.2. Surface electrode pattern and polarization profiles of (a) first mode sensor (b) second mode sensor and (c) third mode sensor

4.1.3 Experiment and discussion

4.1.3.1 Experimental and results

To verify the results, two modal sensors were built for a spring steel beam having a dimension of $130mm \times 10mm \times 0.5mm$ (length*width*thickness). The effective length of the beam is 100mm, an extra length of 30mm is designed for clamping. The theoretical natural frequency of the first and second mode of the beam is 41Hz and 259 Hz respectively. Figure 4.3 shows the experimental setup of the two modal sensors. The piezoelectric paint used in this case is a sample

with $50wt\%$. It was cut manually according to its calculated shape in the last section, and carefully glued on the beam by a strong conductive epoxy from Chemtronics. During the adhering process, short circuit should be avoided, as the piezoelectric paint is very thin, the remnant bonding chemicals is easily attached to the edge of the piezoelectric paint, thus making the upper electrode conductive to the beam. According to Figure 4.2(a), the first modal sensor comprises only a single piece of piezoelectric paint, contrarily, the second modal sensor is comprised of two pieces with opposite polarization direction, as showed in Figure 4.3(b). These two parts are connected through a 1cm silver wire, showed by the enlargement on the upper right corner of Figure 4.3(b). The beam is clamped on a shaker from TIRAvib, and stimulated by a sinusoidal wave from 1Hz to 300Hz. It should be noticed that shielded cables must be used to reduce electronic noise. The output of the modal sensor is connected to a charge amplifier, a handyscope HS4 is used to acquire the measured signals.
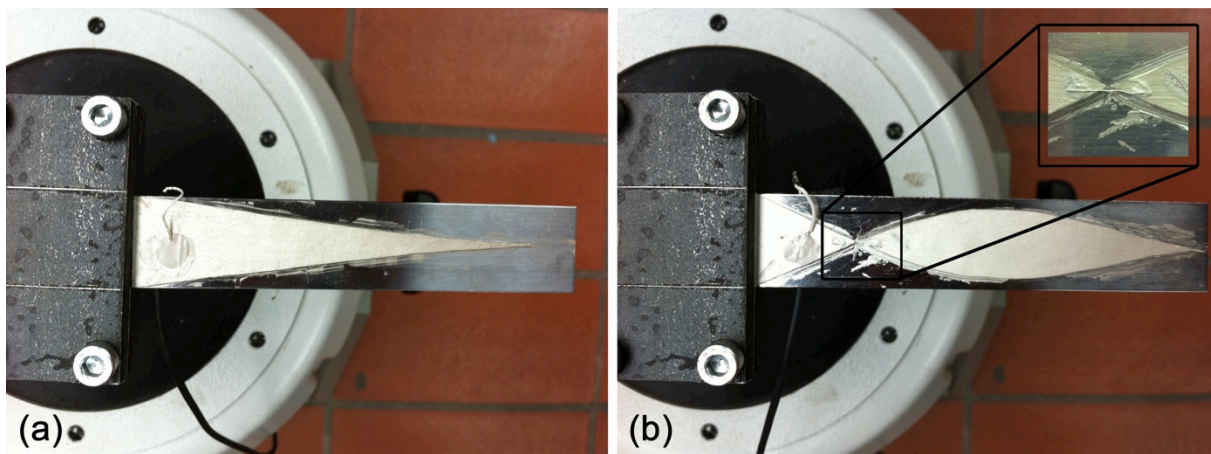
Figure 4.3. Experimental setup of (a) first modal sensor and (b) second modal sensor

Figure 4.4 is the frequency response of the two modal sensors. The output of the modal sensors, which is the charge Q, is measured by a charge amplifier. Since a charge amplifier is in fact a charge integrator, it collects all the charges being generated on the sensor surface. As can be seen, the first modal sensor has an obvious response at 37.66Hz, and the second modal sensor has one at 219.10Hz. The results are very close to their predicted natural frequencies. However, a small resonance of 224.90Hz can also be investigated from the first modal sensor (Figure 4.4(a)), as well as the second modal sensor with 36.13Hz (Figure 4.4(b)), these results are not predicted by the theory. Lee firstly encountered this unexpected resonance in his modal sensor/actuator experiment [LEE 1992], and defined this phenomena as the mode leak through.
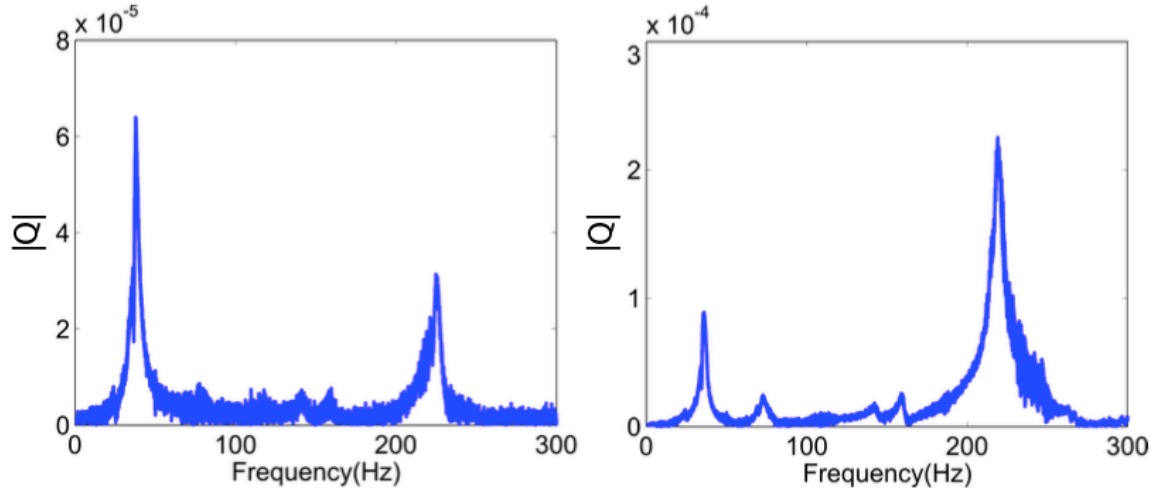
Figure 4.4. Frequency response of (a) first modal sensor and (b) second modal sensor

4.1.3.2 Discussion

Generally, one of the most important causes of mode leak through is the sensor geometric error. The sensor geometric error indicates the difference between the real modal sensor and the predicted modal sensor, it happens because the shaping of the piezoelectric paint by a knife manually produces many inaccuracies, for instance, it is difficult to cut the edge of the modal sensor perfectly smooth; the end tip of the modal sensor is too tiny to be properly handled and therefore is easily damaged. In addition, some small area of the modal sensor is not fully covered with silver paint, and is hardly recognized afterwards.

The sensor designed thus far is only considered as perfect, which means there is no fabrication tolerance when shaping the piezoelectric paint to the expected shape. However, in reality, the geometric errors are unavoidable, especially for cutting the sensors manually. The former sections have already demonstrated the leak through problems of modal sensors. Considering the sensor has a geometric error which is described by $\delta_e(x)$, the output charge generated by the ith mode can be [FRISWELL 1999]

$$q_i(t) = -e_{31}h_b b_b \int_0^l [\mathcal{F}(x) + \delta_e(x)] \frac{\partial^2 w(x,t)}{\partial x^2} dx \qquad (4\text{-}17)$$

therefore the error generated by $\delta_e(x)$ is

$$e_i = -e_{31}h_b b_b \int_0^l \delta_e(x) \frac{\partial^2 w(x,t)}{\partial x^2} dx \qquad \text{(4-18)}$$

If the sensor is sensitive to the kth mode, then the error can be described as [FRISWELL 1999],

$$e_i = \frac{e_{31}h_b b_b \delta_0}{q_k} \int_0^l \left| \frac{\partial^2 w(x,t)}{\partial x^2} \right| dx \qquad \text{(4-19)}$$

where δ_0 is the manufacturing tolerance, which is given as a percentage of the maximum sensor width. Lee and Moon has also concluded that the edges of the surface electrode pattern would cause a discrepancy between theory and experiments [LEE and MOON 1989].

Figure 4.5 and Figure 4.6 shows typical imperfections of the modal sensors with the help of an optical microscope. Figure 4.5(a) is a modal sensor whose edge is not fully covered by the silver paint (the bright particles), consequently, it in fact changed the original sensor shape because the generated charges are only collected from the sensor surface where it is covered by the conductive paint; Figure 4.5(b) shows a damaged sensor tip, this damage was caused during the cutting process, because the sensor tip is too tiny to be handled properly by hand, therefore inaccuracies were brought into the experimental process.
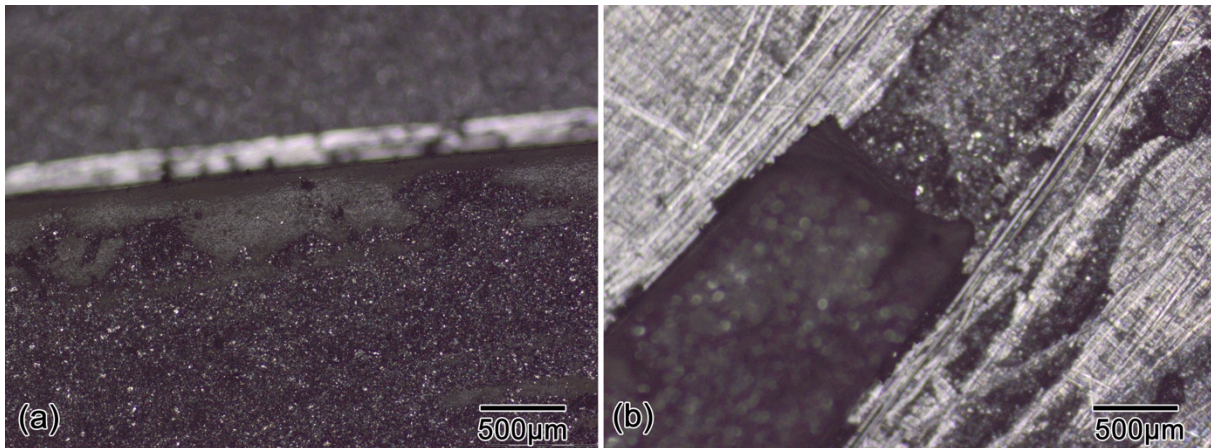

Figure 4.5.Optical microscope investigation of (a) a modal sensor edge (b) a damaged modal sensor tip

Figure 4.6(a) shows a partial cut edge of the modal sensor, which is severely unsmooth compared with its theoretical counterpart. Figure 4.6(b) shows the same problem at the sensor tip.
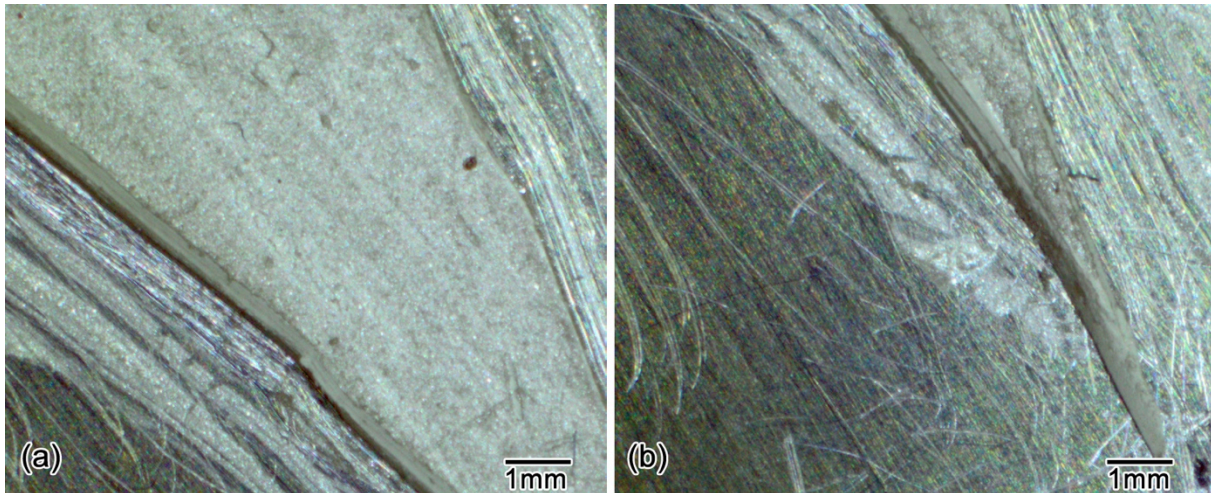
Figure 4.6 (a) a cut modal sensor tip and (b) a modal sensor cut edge.

Another main reason that induces the mode leak through is the sensor placement. All the sensors are cut to the desired shape before adhering on the beam, the mismatch between the desired placement and the real placement is unavoidable when fixing the sensor on the beam surface. Clark and Burke discussed the practical limitations of achieving shaped modal sensors in their work in the 1990s [CLARK and BURKE 1996]. They pointed out that the deviation between predicted and measured modal sensor is observed as a result of inaccuracy in placement of the sensor on the structure. The error of placement is a critical issue related to the experimental realization of the modal sensors. Clark and Burke has demonstrated that a small error in sensor positioning would caused a significant contribution from other modes [CLARK and BURKE 1996].

4.1.4 Modal sensor optimization

The last section has discussed the problems which might cause the mode leak through, the analysis has demonstrated that the realizing of a modal sensor experimentally to match a theory is not easy. However, some improvements are still worth trying. By building a modal sensor, one of the most difficult problems is sensor shaping. Since the piezoelectric paint can only be subjected to a low temperature, it is impossible to shape it by a traditional precision cut method, such as laser cutting. Instead, the method used there is another way around, by using a traditional cutting method to produce a mold, which has the same shape as the modal sensor, then cut the piezoelectric paint by stacking the mold on it and follow the edge line. By this way the geometric error can be controlled to the lowest. Figure 4.7 show the aluminum molds used for the first and

second modal sensors. It is produced by transferring the sensor shape data from Matlab into AutoCAD, and processing it by a digitally controlled machine tool.

Figure 4.7 Aluminum molds used for modal sensor shaping

In addition, the piezoelectric paint used in the optimization is a refined one. As having been shown in section 3.8, a refined sample could provide much higher signal-to-noise ratio. By performing a same experiment as described in section 4.1.3.1, the resulting sensor responses are shown in Figure 4.8. Figure 4.8(a) clearly shows that with the optimized shaping method, the mode leak through problem was significantly reduced, especially for the first modal sensor, which response almost only to the first mode, there is only a trivial response to the second mode. Figure 4.8(b) still shows an obvious mode leak through for the second modal sensor. This could be explained that the first modal sensor has the simplest shape of all modal sensors, therefore it is the easiest to be processed. When the mode increases, even for the second modal sensor of a cantilever beam, the shape becomes very complicated, as well as the polarization profile. Furthermore, the sensor placement also brings errors to the results.
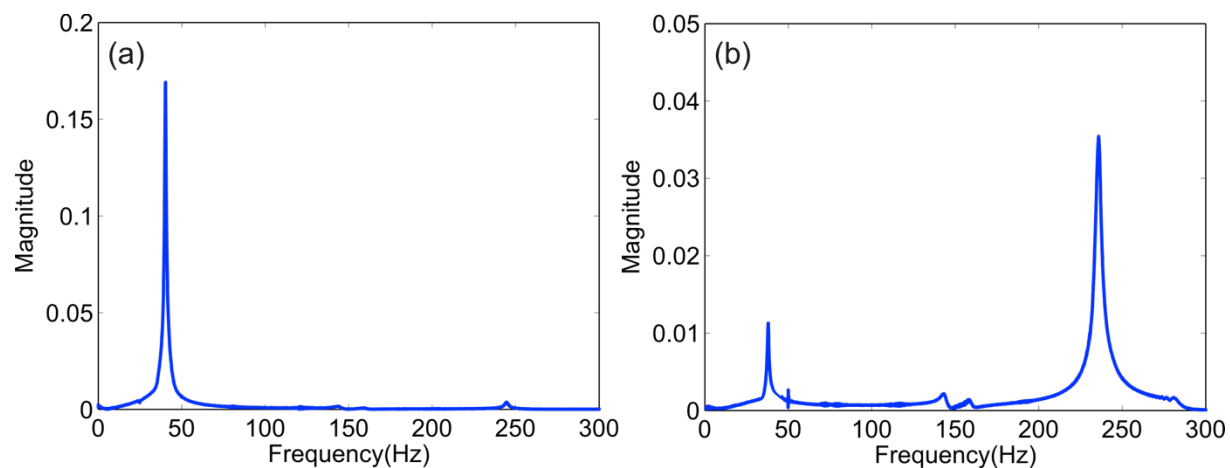

Figure 4.8 Frequency response of optimized (a) first modal sensor and (b) second modal sensor

Although the mode leak through problem cannot be completely gotten rid of in experimental modal sensors, it can be significantly reduced with proper optimization methods. From Figure 4.8 it can also be noticed that the refined piezoelectric paint has a much better performance than the unrefined one.

4.1.5 Conclusion

Section 4.1 explores the application of piezoelectric paint as modal sensors, the piezoelectric paint fabrication is briefly introduced at the beginning, followed by the theories of modal sensors and experimental verification. The piezoelectric paint is flexible, distributable and easy to be shaped. In addition, its polarization profile could be conveniently changed just by placing it up-side-down. The experimental results show that although the mode leak through exists, the piezoelectric paint is still a very promising composite for spatially distributed modal sensors.

The experimental implementation indicates the difficulty of achieving very accurate modal sensors which have responses only to specific modes. This issue is the sensitivity problems of modal sensors. In general, the accuracy of a modal sensor is influenced by many factors, for instance, the accuracy of sensor placement on the beam, the accuracy of sensor shaping, whether the sensor thickness is constant in the transverse direction, all of the above mentioned problems will affect the sensitivity of a modal sensor.

However, it could be seen that even with this rough handling process, the modal sensor still has an obviously greater response to its expected mode. If the handling process is improved, the modal sensor will produce better performance without doubt. The experimental results show that although the mode leak through exists, the piezoelectric paint is still a very promising composites for spatially distributed modal sensors.

4.2 Applications of piezoelectric paint as integrated and distributed sensors in Structural Health Monitoring

4.2.1 Introduction

The former section has described one important application of piezoelectric paint as modal sensors in vibration control. Besides be using as modal sensors, applications of piezoelectric

paint in many other fields are also very promising. This section is going to demonstrate that the quality refined piezoelectric paint is ready to be used in other fields in SHM.

In practical SHM, distributed sensors, which belongs to an inspection system, are attached to an existing structure or integrated directly within a newly fabricated structure. In either case, the integrated and distributed sensors become part of the host structure, and subjected to similar or identical environment conditions as the host structure [BOLLER *et al.* 2009].

With the advanced features of piezoelectric paint having been uncovered, its potential as integrated sensors in SHM is promising. Since the piezoelectric paint is light weighted and flexible, and having a controllable thickness, it can be integrated as part of a structure without compromising the whole structural integrity, especially structures with undulate surfaces, for instance, pipelines, rotor blades, etc. The other sensors, such as the piezoelectric ceramic, is hard, brittle, and difficult to be integrated. Furthermore, because the piezoelectric paint is cost-effective, it can be distributed on a structure to cover a large area, and can be dismantled or replaced easily without bringing any damage to a surface. Hale has tested the weathering problem of piezoelectric paint by placing it in field trials for three years, the result came out was quite positive -- that the piezoelectric paint did not show significant deterioration at a typical location on a bridge [HALE 2004].

There are only few works involving the application of piezoelectric paint as integrated vibration sensors. Esuga and Iwasawa investigated the piezoelectric paint as vibration modal sensors [EGUSA and IWASAWA 1994], in this work, they sprayed the piezoelectric paint on an aluminum beam at averaged positions, and used a shaker to analysis the modes of the beam. Hale applied a thick film piezoelectric paint as shock and vibration sensor for a bridge [HALE 2004].

One of the applications to use piezoelectric paint as integrated vibration sensors is modal analysis. Modal analysis is the study of measuring and analyzing the dynamic behavior of a structure under an excitation. The traditional transducers to perform a modal analysis involves accelerometers, load cell, or laser vibrometer. They are mounted on a structural surface and dismounted after measurement. To use the piezoelectric paint in modal analysis, they are adhered on a surface before measuring and can be left on the surface after the modal analysis for future data acquisition or structure condition interrogation.

In order to demonstrate the effectiveness of the piezoelectric paint as integrated vibration sensors, its performance under an external vibration was compared with a strain gauge and a piezoelectric ceramic sensor, respectively.

4.2.2 Comparison of piezoelectric paint with strain gauge and piezoelectric ceramic under external excitation

4.2.2.1 Comparison on a flat surface

This is realized by adhering a paint patch on an aluminum cross head (Figure 4.9(c)), at the same position but another side of the cross, a rosette strain gauge (Figure 4.9(b)) or piezoelectric ceramic (Figure 4.9(a)) is applied.
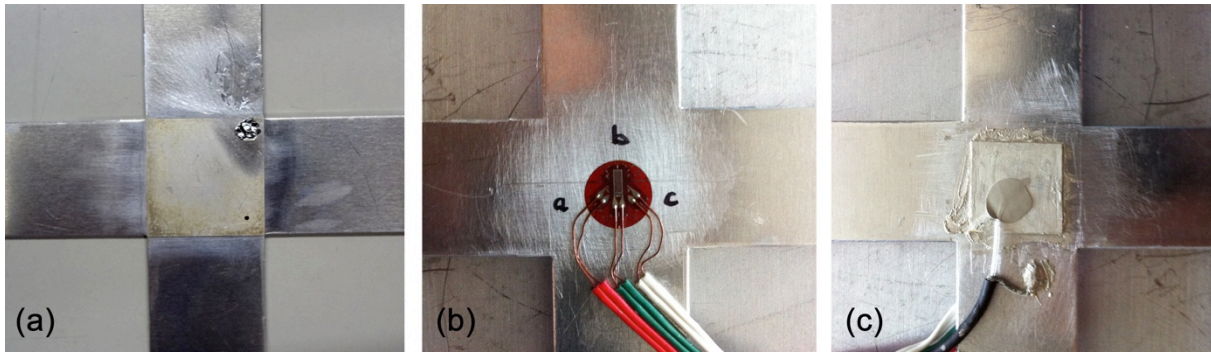
Figure 4.9 Placement of (a) piezoelectric ceramic (b) rosette strain gauge and (c) piezoelectric paint on an aluminum cross head

Figure 4.10 is the side view of the experimental setup. In Figure 4.10, the two parallel plates outside are fixed together with the frame, and the two parallel plates inside are attached to the shaker. The cylinder rolls are used to restrain the movement of the cross. As the shaker vibrates, only the inner part of the cross, which is equipped with different sensors, vibrates with the shaker. The principal strains of the rosette strain gauge can be calculated by equation (3-11). The charges generated on the piezoelectric paint surface and the principal strains measured by the strain gauge is,

$$q = \frac{d_{31}EA}{1 - v}(s_1 + s_2) \qquad \text{(4-20)}$$

where A, d_{31}, E, v is constant, they are the area, piezoelectric charge constant, Young's modulus and Poisson's ratio of the piezoelectric paint respectively. Therefore the charge q is proportional to the sum of the principal strains, and so does the output voltage of the piezoelectric paint.
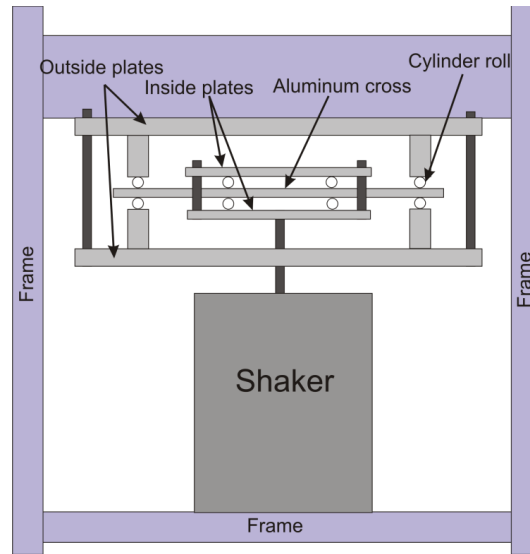
Figure 4.10. Experimental setup of vibration

Figure 4.11 compares vibration signals from the rosette strain gauge and the piezoelectric paint at a frequency of 50Hz, although the outputs of them are in different unit and scale, their reactions to the vibration are the same.
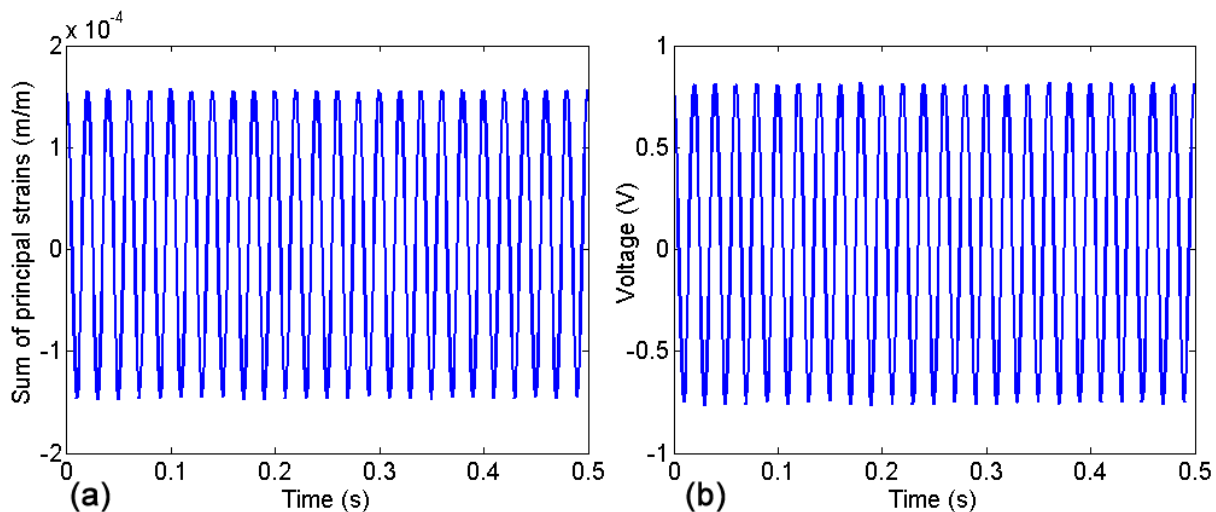
Figure 4.11. Output of rosette strain gauge (left) and piezoelectric paint (right) under 50Hz vibration

Similarly, Figure 4.12 is the normalized voltage signals from the piezoelectric ceramic and the piezoelectric paint at 50Hz. Figure 4.12(a) shows the two sensors under vibration, and Figure

4.12(b) shows the reaction of the two sensors under an impact. As can be seen, with proper amplification conducted by a charge amplifier, the piezoelectric paint has similar behavior as the piezoelectric ceramic. Figure 4.13 is the normalized output voltage of the piezoelectric ceramic and piezoelectric paint at a frequency sweep from 10Hz to 100Hz. Figure 4.13(b) is the magnification of part of the signal. Figure 4.12 and Figure 4.13 shows that the piezoelectric paint is competitive at measuring a vibration signal, under the condition that the sensor signal is properly amplified.
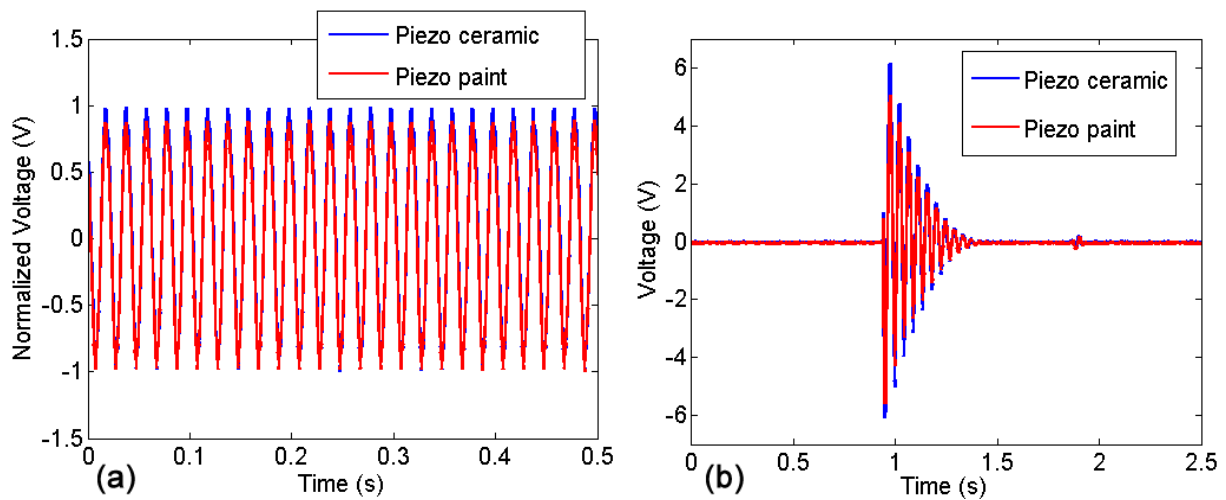
Figure 4.12. Normalized output of piezoelectric ceramic and piezoelectric paint at 50Hz vibration
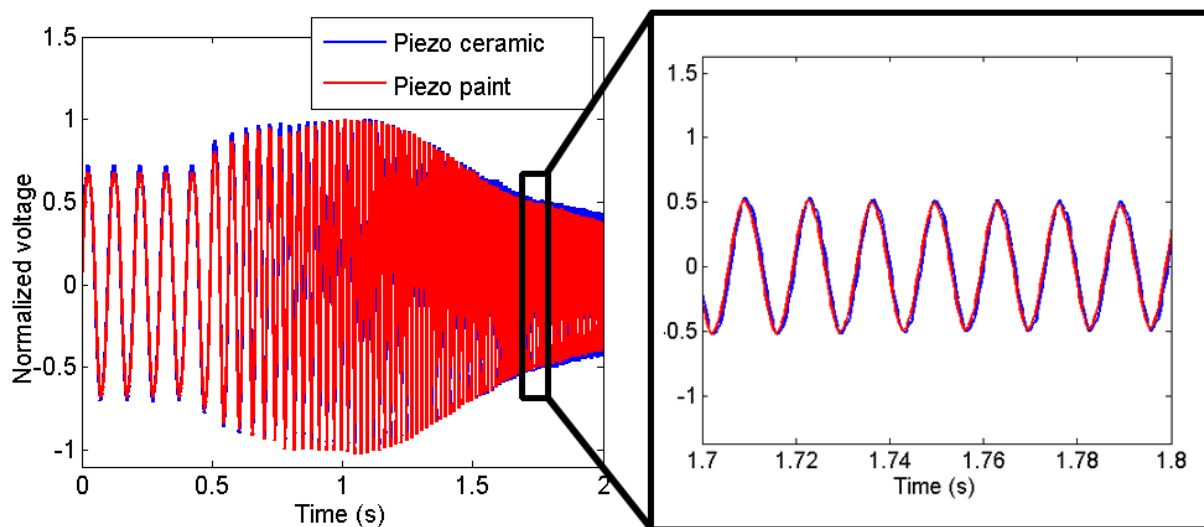
Figure 4.13. Normalized output of piezoelectric ceramic and piezoelectric paint from 10Hz to 100Hz

4.2.2.2 Comparison on a curved surface

A piezoelectric paint and strain gauge is adhered at the bottom of a tripod for sensing comparison on a curved surface. Piezoelectric ceramic is absent in this case since it cannot be attached on a curved surface. Figure 4.14 shows a steel tripod and the placement of piezoelectric paint and strain gauge on it, the bottom of the tripod is fixed on a concrete foundation. Figure 4.15 is the normalized output of the piezoelectric paint and strain gauge deduced by an impact on the tripod.
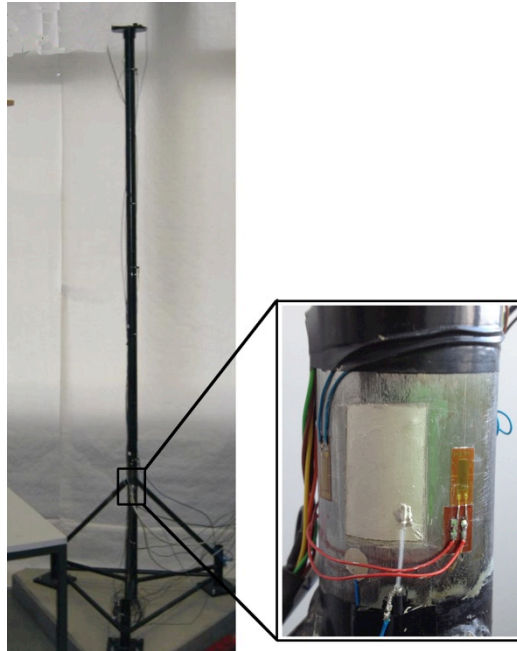
Figure 4.14 Placement of piezoelectric paint and strain gauge on a steel tripod
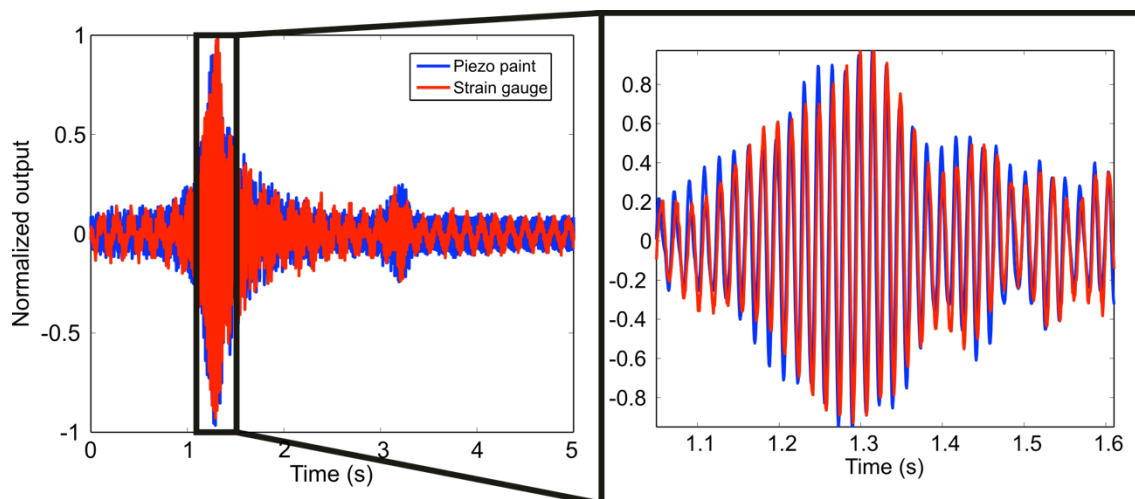
Figure 4.15 Normalized output signal of piezoelectric paint and strain gauge

From Figure 4.15 it can be seen that the two sensors have similar performances under the external excitation. The slight difference is caused by their location difference on the tube, as well as electronic noises on the piezoelectric paint.

4.2.3 Experimental modal analysis by using piezoelectric paint

Experimental modal analysis is the process of determining a dynamic model for a mechanical system. It produces a modal model that includes natural frequencies, modal dampings and mode shapes [SILVA 2007]. Due to the thin, light weight, flexible and low-cost properties of the piezoelectric paint, it suits very well as an integrated vibration sensor for a mechanical system.

This experiment presented here studies the piezoelectric paint as integrated vibration sensors for a cantilevered beam. Experimental modal analysis was performed to find out the natural frequencies, damping ratios and mode shapes of it. The results were compared with a finite element analysis results. Afterwards a simulated damage was introduced into the beam, the damaged case and the baseline was compared.

In this experiment, a $300mm \times 300mm$ steel beam with 3mm thickness is taken for the impact modal analysis, its E is $205GPa$ and ρ is $7700kg/m^3$. Two piezoelectric paint patches with dimension of $30mm \times 20mm$ are integrated on the beam surface. Figure 4.16 shows the dimension of the beam and placement of the two paint sensors. The beam is impacted at the marked 17 points shown in Figure 4.16(b), the paint sensors reside at another side of the beam to avoid being damaged. A LMS test lab is adopted for the input and output measurement and the post-processing.
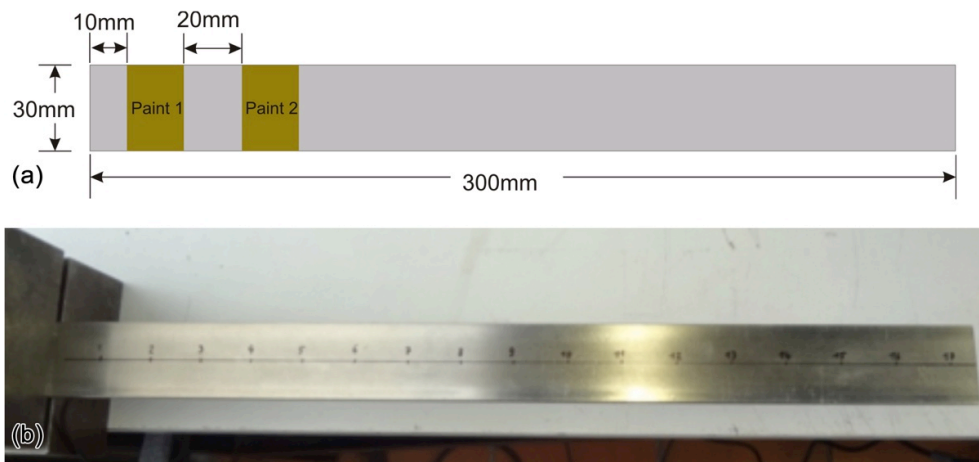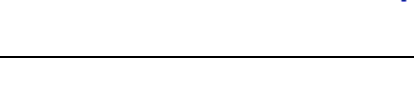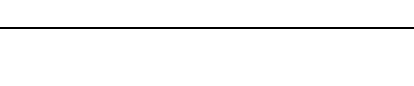
Figure 4.16. Beam dimension and placement of the piezoelectric paint

Table 4.1 is the measured natural frequency, modal damping and mode shape of the first five modes. It also compares the natural frequencies from experimental modal analysis and finite element analysis (FEA). The mode shapes from the experiment are also very close to the mode shapes obtained from the numerical calculation. The discrepancies between the two can be minimized by improving the impact skill and a modal updating.

Table 4.1. Mode shapes obtained by FEA and experiment

Modes	Natural frequency (FEA)	Natural frequency (Experiment)	Damping	Experimental modal analysis results
Mode 1	18.48Hz	18.56Hz	1.6%	
Mode 2	115.79Hz	114.64Hz	0.73%	
Mode 3	324.00Hz	320.48Hz	0.35%	
Mode 4	634.70Hz	624.05Hz	0.39%	
Mode 5	1049.00Hz	1026.48Hz	0.47%	

Followed, a damage is introduced to the beam by cutting its edge. The saw-cut is shown in Figure 4.17, the damaged point is 8cm from the clamping edge and has a length of 1cm. The impact modal analysis is repeated on the damaged beam, the results are presented in Table 4.2.
.
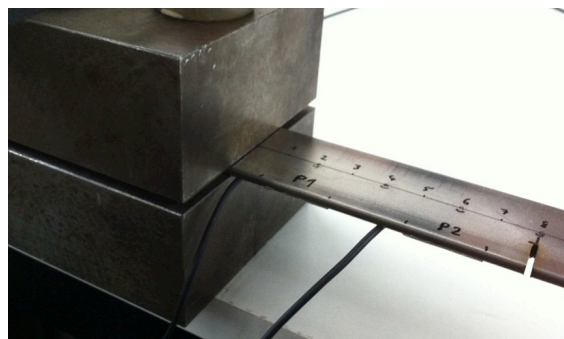
Figure 4.17. Saw-cut on the beam

Table 4.2. Experimental modal analysis results of damaged beam

Modes	Natural frequency	Damping	Variation
Mode 1	18.25Hz	1.25%	1.24%
Mode 2	113.87Hz	0.98%	1.66%
Mode 3	318.59Hz	0.51%	1.67%
Mode 4	617.56Hz	0.5%	2.70%
Mode 5	1021.73Hz	0.64%	2.60%

4.2.4 Conclusion

By comparing Table 4.1 and Table 4.2 an obvious decrease of the natural frequencies and increase of damping can be observed, the introduced damage decreased the stiffness of the beam. The resulted experimental data clearly proves that the piezoelectric paint is able to accurately measure a vibration compared with the other two sensors. By introducing the saw-cut damage and comparing the modes with the baseline, the piezoelectric paint was proved to be effective in distinguishing a damaged case. The results indicate the usefulness of the piezoelectric paint as integrated vibration sensors, and promote the application of it as vibration-based sensors in NDT and SHM.

To conclude, this chapter discussed that using the piezoelectric paint as integrated vibration sensors has many advantages, one of the most distinguished is that the piezoelectric paint is light and flexible, therefore it can be integrated on a structure as part of it, which suits very well for a single or double curved structural surface; in addition, the sensor design can easily be integrated into applications, therefore a specific application need can be feed. Comparing to a strain gauge, the piezoelectric paint is less sensitive to temperature changes, therefore it is more suitable to be used in a field application. With a mass production method, the cost of the piezoelectric paint can be very competitive compared with a traditional piezoelectric transducers and strain gauge. However, the piezoelectric paint cannot be applied in high temperature applications due to its polymer phase, this problem will be addressed in the next chapter.

5 Aluminum Nitride as distributed transducers in high temperature applications

5.1 Motivation

In the last chapters, the production of a flexible piezoelectric paint and its application in SHM has been discussed in detail, and the thermal property of the piezoelectric paint has been also demonstrated. It shows that the piezoelectric paint can only be applied in an environment which is not higher than 200°C. If a piezoelectric element is heated to its Curie point, the domains becomes disordered and the element becomes completely depolarized [MORGANCERAMICS 2009]. At another hand, the traditional piezoelectric ceramic also cannot endure high temperature applications. Generally the Curie temperature of traditional piezoelectric ceramics is between 170°C to 340°C [NOLIACCERAMIC]. And the operating temperature of a piezoelectric ceramic is about half of its Curie point, operation outside the temperature limitation may cause partial or total loss of the polarization, consequently resulted in a diminishing or loss of the piezoelectricity [MORGANCERAMICS 2009]. Therefore it is not suitable for applications involving temperature above 600°C.

On the other side, in high temperature applications, the requirement for materials is quite selective and critical. Because the environment of high temperatures applications is much more complex than at a room temperature, many chemical substances become active and they may

bring contaminations into the environment and cauterize a structural surface. Under these circumstances, most metals will inevitably oxidize over a wide range of conditions [YOUNG, D. J. 2008]. Therefore, one of the greatest challenges is to monitor the status of mechanical components, since unnoticed corrosions may cause imponderable lost to a whole system.

In recent years, the γ-TiAl has received great attention as a very promising material in the field of aerospace and industrial gas turbine engine applications [HARDING and JONES 1999], it has also been used in formula one racing engines, and been tested and applied in a variety of components [APPEL *et al.* 2011]. Because it retains high specific strength and high specific stiffness at elevated temperate, which is especially important for applications as vibration components [HARDING and JONES 1999]. In addition, its density is less than half of traditional nickel-based super-alloys, this feature will not only reduce the weight of a system significantly, but also in accordance with the demand to future materials, which is improved thermodynamic efficiency and ecological compatibility [APPEL *et al.* 2011]. Dimiduk assessed γ-TiAl with other aerospace materials [DIMIDUK 1999], and some of the highlights are listed here:

- high specific strength (exceeds those of polycrystalline nickel alloys at all temperatures and even those for titanium alloys greater than 500K)
- high specific modulus (50%-70% greater than that for titanium alloys and retain their stiffness to high temperature)
- low density
- high melting point (1460°C)
- good structural stability
- greater oxidation and corrosion resistance than titanium alloys
- high ignition resistance (compared with conventional titanium alloys)

However, γ-TiAl also has few drawbacks, the most critical problem is its relatively low ductility, low fracture toughness, low fatigue growth resistance and low wear resistance. Therefore it has a limited damage tolerance and its lifetime will intensively reduce if extrinsic damage is presented [HARDING and JONES 1999].

Based on these circumstances, protection layers are expected to be coated on the γ-TiAl surface for corrosion protection, thermal insulation and wear protection. It would be much more promising if the protection layers can be used as sensors to monitor the status of the whole

systems, thus forming an online SHM system. These protection layers are realized by the combination of nanocrystalline diamond and Aluminum Nitride (AlN), which form a multifunctional layer for γ-TiAl, thus the whole systems is written as AlN/Diamond/γ-TiAl.

In general, this research presented here focuses on investigations of this multilayer system AlN/Diamond/γ-TiAl, since both AlN and diamond has many prior features which are very favored in high temperature SHM applications. In the following sections, the problem will be discussed in detail. In the next section, the theoretical background of AlN, nanocrystalline diamond and Surface Acoustic Waves (SAW) will be reviewed. Followed with section and 5.4, which are the main part of this chapter, they discussed the calculation of SAW propagation on a piezoelectric multilayer system and the finite element simulation. Section 5.6 demonstrates the damage detection procedure of the multi functional layer system.

5.2 Background review

5.2.1 Review of nanocrystalline diamond

For many scientific and technological applications, diamond is a very attractive material due to its outstanding mechanical, electrical, thermal, and optical properties [NEBEL and RISTEIN 2003; NEBEL and RISTEIN 2004; PHILIP et al. 2003]. It has very high hardness and stiffness, which makes it a very desirable material in mechanical applications [NEBEL and RISTEIN 2003], therefore, the diamond thin film is very useful as a hard and wear resistance coating. In this work, the nanocrystalline diamond is expected to be deposited on the γ-TiAl surface, which functions as a wear resistance layer.

Meanwhile, diamond has the highest acoustic phase velocity (10750m/s) [ELMAZRIA et al. 2006; MORTET et al. 2008], when combined with piezoelectric film such as AlN [MORTET et al. 2003], is very attractive for high frequency surface acoustic wave devices [HRIBŠEK et al. 2010; LAMARA et al. 2004]. Using diamond in multilayered SAW structure has the following significant benefits: high frequency up to 5GHz, high coupling coefficient up to 1.2%, small temperature deviation, high power capacity as well as small device size [HRIBŠEK et al. 2010], however, like every coin has two sides, disadvantages also exists, including complex design, and deposition of a piezoelectric layer with appropriate orientation [HRIBŠEK et al. 2010]. Besides,

diamond has an extremely high chemical stability, therefore it is an ideal material for making sensors which will be working in a harsh environment [SPECHT *et al.* 2004].

5.2.2 Review of Aluminum Nitride

AlN is a nitride of aluminum, it is a III-V group semiconductor. Because of its hardness and corrosion resistance, as well as its high thermal stability, AlN is very attractive to many industrial applications and research works [LEVINSHTEIN, MICHAEL E. *et al.* 2001]. Besides, it has high temperature stability, high thermal conductivity and varying electrical properties, which make it attractive in many high temperature applications, besides, it is very inert to many chemical reactions [LEVINSHTEIN, MICHAEL E. *et al.* 2001]. Electrically, AlN is a wide band gap semiconductor with a band edge of 6.2eV above the valance band, which enables the application of AlN in many photonic applications [YU, H. Y. 2010].

More importantly, AlN is a piezoelectric material with high piezoelectricity. It is widely used as bio-sensors, pressure sensors [AKIYAMA *et al.* 2006; TIROLE *et al.* 1993] and Surface Acoustic Wave (SAW) sensors. The work presented here focuses on the application of AlN as distributed SAW sensors.

In this work, the substrate material is γ-TiAl, which is a very promising high temperature material in aerospace and automotive industries. The γ-TiAl is surface treated by depositing diamond on it to improve its wear resistance. Aluminum Nitride (AlN) is overlayed on the diamond surface as a multi-functional layer. It not only works as a corrosion and diffusion barrier, but also be used as a self-diagnostic sensor to monitor the health status of the structure, due to its excellent piezoelectric properties. The preliminary aim of this work is to setup a finite element model, which is used to investigate the propagation of SAW on the layered structure. The simulation results will give further references to the experimental work. Based on the piezoelectric properties of AlN, the whole system could be wireless.

A diamond layer is used as a buffer layer. Diamond has the highest speed of sound compared with other solids, and it is very sensitive to changes in the velocity of propagation of surface waves. With a combination of diamond and AlN, they are expected to achieve a high wave velocity.

5.2.3 Review of Surface Acoustic Waves (SAW)

Surface acoustic wave belongs to a group of elastic waves which is governed by elastic wave equations and boundary conditions which specifies a stress free surface. The existence of SAW in an isotropic material was first demonstrated by Lord Rayleigh in 1885 [LOVE 1923], therefore, SAW is also known as Rayleigh wave. Unlike other solid waves, SAW propagate on the surface of a solid and dies out within two or three wavelength in depth from the solid surface. The existence of SAW was theoretically predicted for a long time, the first experimental evidence obtained in observing SAW propagation was the SAW over earth surface [ROSE 1999]. Many reported works have discussed the propagation properties of SAW [CHADWICK and CURRIE 1977; OLINER 1978]. Figure 5.1 shows how the wave propagates on a structural surface. As illustrated, the particles vibrate along the solid surface and decays within two or three wavelength in the depth direction. The particle displacement is strictly confined to the sagittal plane as depicted in Figure 5.1. The particle displacement at any depth is describes by an ellipse and the shape of the ellipse changes with depth [OLINER 1978].
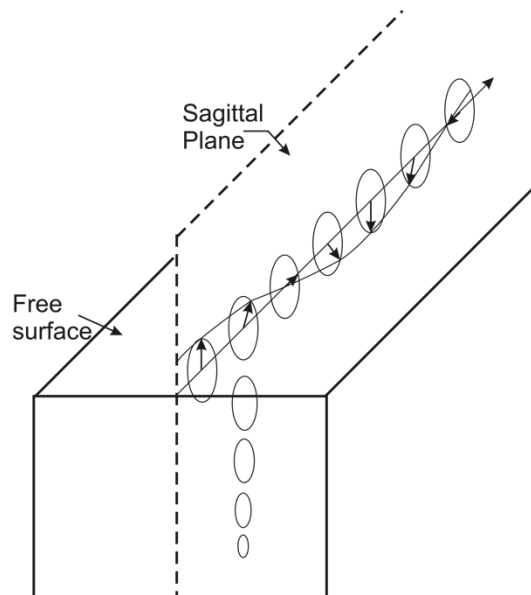
Figure 5.1 Surface acoustic waves and its particle displacement

Figure 5.2 simulates the particles displacement on the solid surface [Russell 2004]. The particles oscillate in an ellipse and its oscillation amplitude is the highest on the structural surface, and decays within the depth.
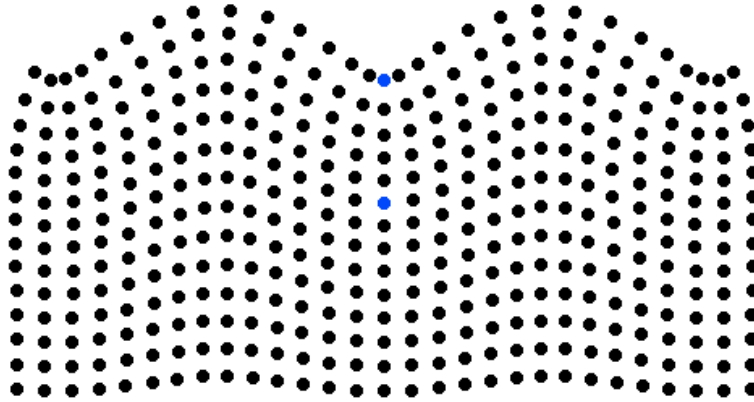
Figure 5.2 Particle displacement in solids (Courtesy of Dr. Dan Russell, 1999)

5.2.4 Review of Surface Acoustic Wave devices

SAW devices have been widely used in the last thirty years, recently it has been expanded to the fields of non-destructive testing [LONGO *et al.* 2010], chemistry [HO *et al.* 2003; STUBBS *et al.* 2003] and biology [ANDRÄ *et al.* 2008; TIGLI *et al.* 2010a]. In addition, it can be passive, wireless [CHANG, *et al.* 2007] which give it the opportunity to work in harsh environments like high temperature, high radiation. Under these conditions, conventional substrates such as silicon, Lithium niobate (LiNbO3), which cannot withstand a high temperature, is not suitable anymore. γ-TiAl, which belongs to the titanium alloy family, is a promising material in high temperature applications due to its light weight, high specific strength, good biological compatibility [RIVERA-DENIZARD *et al.* 2008] and excellent corrosion resistance. It has attracted great interests in aerospace, automobile, energy and chemical fields, which proved that γ-TiAl could be a substitute of the conventional substrates at high temperature. Recently, chemical vapor deposition of diamond on γ-TiAl to improve its wear resistance has been reported [SULIK *et al.* 2008]. Besides, diamond can improve the Rayleigh SAW velocity since it has the highest SAW velocity of all materials, when combining with piezoelectric materials, is an ideal choice for SAW sensors. The piezoelectric material here considered is from the group-III nitrides: Aluminum Nitride (AlN), which not only has good thermal, electrical and chemical stability, but also can function at a elevated temperature up to 1000°C. In addition, it can protect the diamond from oxidation in aforementioned temperatures [MCGEOCH *et al.* 1999]. The aim of the present work is to investigate the AlN/diamond/γ-TiAl based multiplayer SAW sensor which has the opportunity to work in high temperatures. Due to the time consuming and costly process of manufacturing,

before forming an experimental sample, a finite element analysis is applied to help exploring the Rayleigh SAW propagation properties.

In non-destructive testing and Structural Health Monitoring (SHM), many techniques have been developed to detect different kinds of structural failures [LONGO *et al.* 2010]. However, there are only few paper involving the use of SAW [DEBOUCQ *et al.* 2011; HO *et al.* 2003]. SAW is a kind of acoustic wave traveling along the surface of an elastic material, with most of its energy concentrating close to the surface. Therefore, it has high sensitivity to surface changes. In high temperature applications, one of the greatest challenges is to notice the failure of a mechanical component at an early stage to avoid damage of the whole system. These kinds of failures are generally caused by surface cracks, or high temperature induced chemical contaminations and oxidation [KHANNA 2002; YOUNG, D. 2008]. To solve these problems, coatings which act as corrosion resistance layers are applied. It was only after more than 80 years of the discovery of the SAW did its generation method was invented, which is the interdigitated comb-shaped electrodes deposited on a piezoelectric material [ROYER and DIEULESAINT 1980]. This method was documented in two patent files in 1963 by Mortley [MORTLEY 1963] and Rowen [ROWEN 1963], and was demonstrated experimentally by White and Voltmer [ROYER and DIEULESAINT 1980]. Surface acoustic waves are usually generated with the help of Interdigital Transducers (IDT). IDT are among the most commonly used periodic electrode structures [MAMISHEV *et al.* 2004]. It is a group of patterned electrodes which are deposited on the piezoelectric material surface to generate SAW. It is usually in the form of interlocking comb-shaped metallic coatings. Figure 5.3 shows three pairs of IDT to illustrate how the comb shaped pattern looks like.
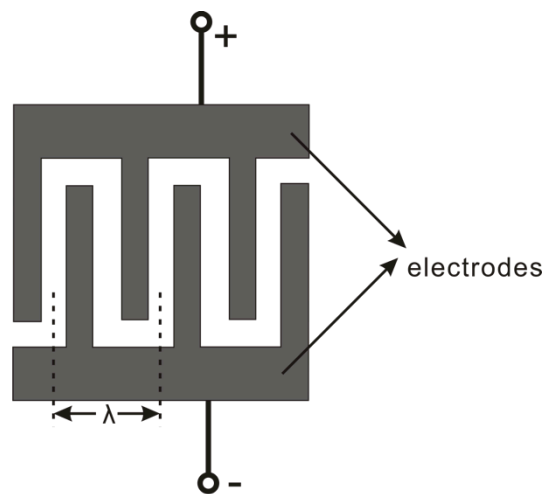
Figure 5.3 Comb shaped Interdigital transducer

It should be noticed that Figure 5.3 is only a demonstration of IDT pairs, in reality, there are hundreds to thousands of pairs to form a functionable SAW device. The IDT is patterned in a way such that the width between two fingers are one fourth of the SAW wavelength. In Figure 5.3 λ indicates the wavelength of the SAW. The upper half of the IDT is connected to the positive terminal of an electric field, and the low half is connected to the negative terminal.

In recent decades, the development of IDT was enabled and accompanied with the fast development of microelectronic technology [OLINER 1978; ROSEN *et al.* 1992b; RUPPEL and FJELDLY 2001; VELLA and STEGEMAN 1973]. Generally, the IDT is fabricated on the piezoelectric substrate surface by a lithography technology [LI, F. 2008; LIU 2008]. Before doing the lithography, a piezoelectric substrate is prepared by depositing a positive photo resist on the surface, this is usually done by a spin coating method. Afterwards a patterned mask is overlayed on the surface and the whole is exposed under UV light. The partial of photoresist which is not covered by the mask will react with the UV light, afterwards an inverse pattern is created. The resulted sample is taken for metallization, in this step, target material, for instance, gold, copper, or platinum is sputtered on the sample surface [LEVINSON, H. J. 1999; LEVINSON, H. J. 2004; MAC 2007]. Finally, the photo resist is removed and what left on the piezoelectric substrate is the patterned electrodes. Figure 5.4 clearly illustrates this process.
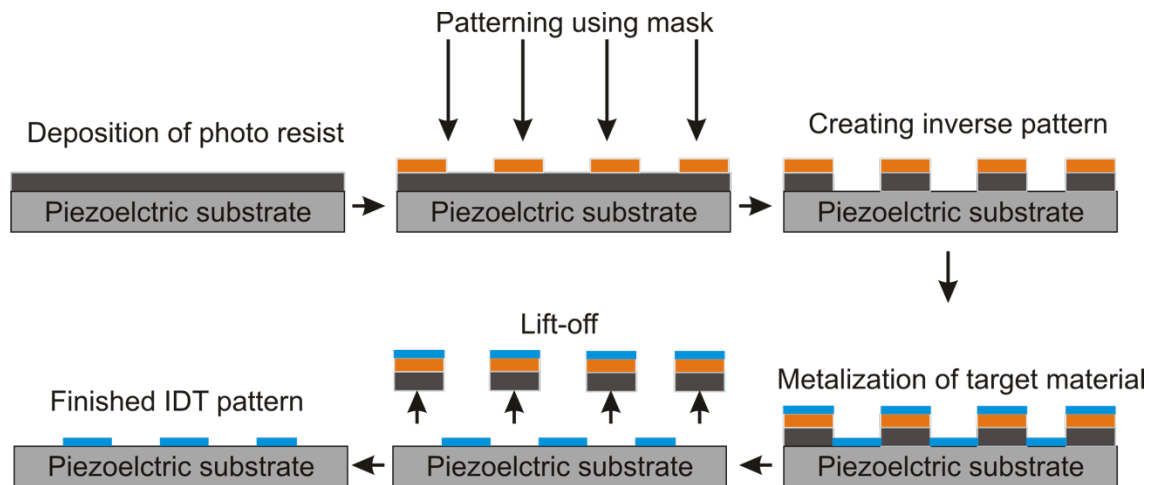
Figure 5.4 Lift-off technology

After being fabricated on the piezoelectric material surface, the IDT is ready to be used to generate SAW. As shown in Figure 5.5, this system contains two groups of IDT, the group on the left side is used as an SAW generator, and the another group resides the right side is used as an SAW receiver. When an electric field is applied on the generator, the IDT1 converts the electrical

energy into mechanical energy, the piezoelectric substrate is activated and SAW is generated, the generated SAW propagates on the solid surface, after reaching the receiver, the IDT2 converts mechanical energy into electrical energy, and the received electrical signal can be imaged or shown by an oscilloscope or a similar device.
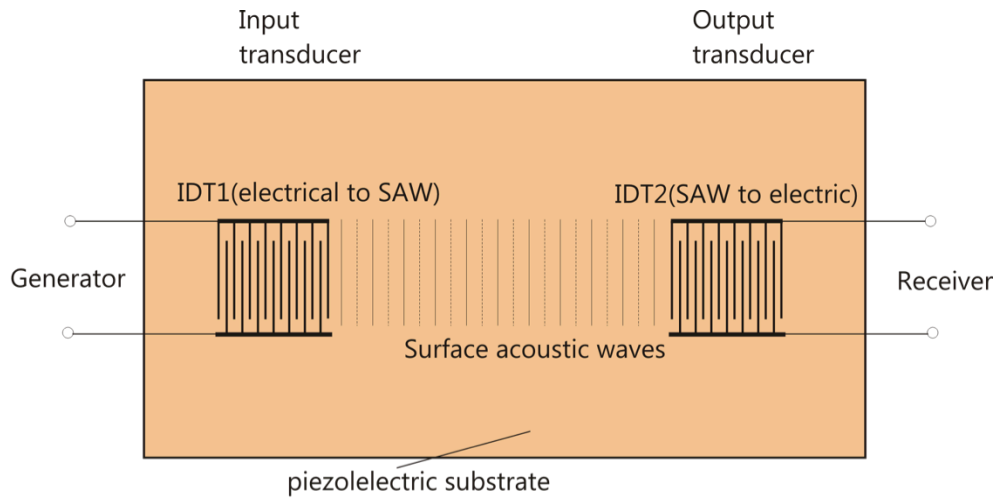
Figure 5.5 Working principle of IDT [OLINER 1978]

5.3 Surface acoustic wave equations

5.3.1 Elastic wave propagation in unbounded isotropic media

Before discussing the wave equation, the geometry model is introduced in Figure 5.6.
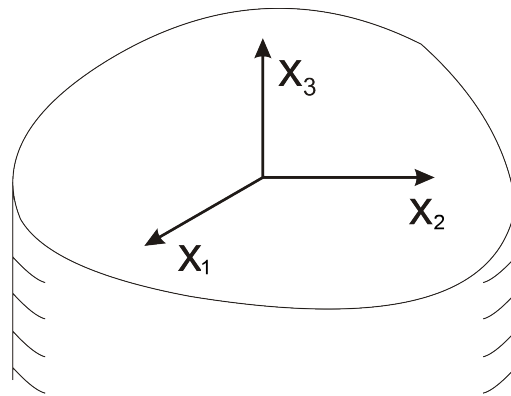
Figure 5.6 Cartesian coordinate system (x_1, x_2, x_3) for SAW propagation

Considering the surface wave propagates on an unbounded isotropic media shown in Figure 5.6, which represents the three-dimensional coordinate system for the surface wave solution, the solid surface resides at $x_3 = 0$. The surface wave propagates in the x_1 direction and decays in the

negative direction of x_3, above $x_3 = 0$ is the free space, therefore the $(x_1, 0, x_3)$ plane is defined as the sagittal plane. The propagation parameters have no dependence on the displacement amplitude of the x_2 coordinate [OLINER 1978].

Generally, a material structure has finite size, which will bring problems when solving the propagation of SAW. Therefore, the discussion starts from elastic waves in an infinite anisotropic medium, which will greatly simplify the wave propagation problem. First of all, considering again the relationship of stress and strain tensors [OLINER 1978],

$$T_{ij} = c_{ijkl} S_{kl} \tag{5-1}$$

where c_{ijkl} is a four-rank stiffness tensor with a total number of 81 components. However, due to the symmetry, it has the following relations,

$$c_{ijkl} = c_{jikl} = c_{ijlk} = c_{jilk} = c_{klij} \tag{5-2}$$

This symmetry reduces the number of tensor components to 21. In the case of an orthotropic material, the independent components reduce to 9, for a cubic symmetry, this reduces to 3, the simplest is for an isotropic material, which only has two independent components in the elastic tensor. The strain is defined as the deformation per unit length as,

$$S_{kl} = \frac{1}{2}(\frac{\partial u_l}{\partial x_k} + \frac{\partial u_k}{\partial x_l}) \tag{5-3}$$

By replacing (5-3) back into (5-1), the general form of Hooke's law is obtained as,

$$T_{ij} = c_{ijkl} \cdot S_{kl} = \frac{1}{2} c_{ijkl} \left(\frac{\partial u_l}{\partial x_k} + \frac{\partial u_k}{\partial x_l}\right) = \sum_{k=1}^{3} \sum_{l=1}^{3} \frac{1}{2} c_{ijkl} \left(\frac{\partial u_l}{\partial x_k} + \frac{\partial u_k}{\partial x_l}\right) \tag{5-4}$$

due to that $c_{ijkl} = c_{ijlk}$, finally,

$$T_{ij} = c_{ijkl} \frac{\partial u_l}{\partial x_k} = c_{ijkl} \frac{\partial u_k}{\partial x_l} \tag{5-5}$$

In the absence of an external force, the wave equations for an elastic, homogenous, anisotropic medium in full looks like,

$$\rho \frac{\partial^2 u_i}{\partial t^2} = \frac{\partial T_{ij}}{\partial x_j} = \frac{\partial}{\partial x_j}\left(c_{ijkl}\frac{\partial u_l}{\partial x_k}\right) = c_{ijkl}\frac{\partial^2 u_l}{\partial x_j \partial x_k} \tag{5-6}$$

where u_i is the displacement of an arbitrary point in the solid, it is measured along the three Cartesian axes x_i ($i = 1,2,3$). With coordinates x_k, it varies with time such that $u_i = u_i(x_k, t)$, ρ is the density of the medium. For an isotropic media, the elastic tensor c_{ijkl} has two independent components, thus

$$\begin{bmatrix} T_{11} \\ T_{22} \\ T_{33} \\ T_{23} \\ T_{31} \\ T_{12} \end{bmatrix} = \begin{bmatrix} c_{11} & c_{12} & c_{12} & 0 & 0 & 0 \\ c_{12} & c_{11} & c_{12} & 0 & 0 & 0 \\ c_{12} & c_{12} & c_{11} & 0 & 0 & 0 \\ 0 & 0 & 0 & c_{44} & 0 & 0 \\ 0 & 0 & 0 & 0 & c_{44} & 0 \\ 0 & 0 & 0 & 0 & 0 & c_{66} \end{bmatrix} \begin{bmatrix} S_{11} \\ S_{22} \\ S_{33} \\ S_{23} \\ S_{31} \\ S_{12} \end{bmatrix} \tag{5-7}$$

where $c_{44} = (c_{11} - c_{12})/2$. By taking (5-7) back into (5-6),

$$\rho \frac{\partial^2 u_1}{\partial t^2} = c_{11}\frac{\partial^2 u_1}{\partial x_1^2} + c_{44}\left(\frac{\partial^2 u_1}{\partial x_2^2} + \frac{\partial^2 u_1}{\partial x_3^2}\right) + (c_{12} + c_{44})\left(\frac{\partial^2 u_2}{\partial x_1 \partial x_2}\right.$$
$$\left. + \frac{\partial^2 u_3}{\partial x_1 \partial x_3}\right)$$

$$\rho \frac{\partial^2 u_2}{\partial t^2} = c_{11}\frac{\partial^2 u_2}{\partial x_2^2} + c_{44}\left(\frac{\partial^2 u_2}{\partial x_1^2} + \frac{\partial^2 u_2}{\partial x_3^2}\right) + (c_{12} + c_{44})\left(\frac{\partial^2 u_1}{\partial x_1 \partial x_2}\right. \tag{5-8}$$
$$\left. + \frac{\partial^2 u_3}{\partial x_2 \partial x_3}\right)$$

$$\rho \frac{\partial^2 u_3}{\partial t^2} = c_{11}\frac{\partial^2 u_3}{\partial x_3^2} + c_{44}\left(\frac{\partial^2 u_3}{\partial x_1^2} + \frac{\partial^2 u_3}{\partial x_2^2}\right) + (c_{12} + c_{44})\left(\frac{\partial^2 u_1}{\partial x_1 \partial x_3}\right.$$
$$\left. + \frac{\partial^2 u_2}{\partial x_1 \partial x_3}\right)$$

u_1, u_2 and u_3 are the three orthogonal displacements. The assumed plane wave solution for (5-6) with frequency ω in direction x_i is,

$$u_i = A_i \exp \, j[\Sigma(k_i x_i) - vt] \tag{5-9}$$

or

$$u_i = A_i \exp \left[j(k_1 x_1 + k_2 x_2 + k_3 x_3 - vt) \right] \tag{5-10}$$

where $j = \sqrt{-1}$, A_i is the amplitude of the displacement, λ is the wavelength, v is the phase velocity, $k_i (i = 1,2,3)$ is the wave vector in the x_i direction and is equal to $2\pi/\lambda$ or ω/v. (5-9) results in three waves: one quasi-longitudinal wave and two quasi-shear waves, they are named bulky waves in an unbounded medium. A wave vector parallel to the surface is defined as,

$$k_{\parallel} = k_1 \widehat{x_1} + k_2 \widehat{x_2} \tag{5-11}$$

so the plane wave solution can be rewritten as,

$$u_i = A_i \exp[jk_{\parallel}\beta x_3] \exp \left[jk_{\parallel}(\cos(\theta)\, x_1 + \sin(\theta)\, x_2 - vt) \right] \tag{5-12}$$

where θ is the angle between x_1 axis and $k_{\parallel}$. $\cos(\theta) = k_1/k_{\parallel}$, $\sin(\theta) = k_2/k_{\parallel}$, β is the decay constant in the x_3 direction and it is defined as $\beta = k_3/k_{\parallel}$. Due to equation (5-9), the differential operators in (5-8) can be interpreted as,

$$\frac{\partial}{\partial x_1} = jk_1 \qquad \frac{\partial}{\partial x_2} = jk_2 \qquad \frac{\partial}{\partial x_3} = jk_3 \qquad \frac{\partial}{\partial t} = -j\omega \tag{5-13}$$

substituting (5-12) and (5-13) back into (5-8) get,

$$M \cdot \begin{pmatrix} A_1 \\ A_2 \\ A_3 \end{pmatrix} = \begin{pmatrix} 0 \\ 0 \\ 0 \end{pmatrix} \tag{5-14}$$

where M is a 3×3 matrix in terms of θ, β and v, it is written as,

$$M = \begin{pmatrix} c_{11}\cos(\theta)^2 + c_{44}(\sin(\theta)^2 + \beta^2) - \rho v^2 & (c_{12} + c_{44})\cos(\theta)\sin(\theta) & (c_{12} + c_{44})\cos(\theta) \\ (c_{12} + c_{44})\cos(\theta)\sin(\theta) & c_{11}\sin(\theta)^2 + c_{44}(\cos(\theta)^2 + \beta^2) - \rho v^2 & (c_{12} + c_{44})\sin(\theta) \\ (c_{12} + c_{44})\cos(\theta)\beta & (c_{12} + c_{44})\sin(\theta)\beta & c_{11}\beta^2 + c_{44} - \rho v \end{pmatrix} \quad (5\text{-}15)$$

As the surface acoustic wave is considered, the most significant feature is that the solid particle displacement vanishes in the $x_3 \leq 0$ direction, which means β, the decay constant, must have a negative imaginary component. For a non trivial solution of (5-14), the determinant of M must be: $|M| = 0$. This leads to a 6th order equation of β with v and θ as parameters and results in six complex-conjugate roots [HATCH 2000]. For the three root which are lying in the upper half of the complex plane, they will lead to an exponentially increase of the displacement in the $x_3 \rightarrow -\infty$ direction, there three roots have to be abandoned as they do not fit the physical meaning of surface acoustic wave. Therefore the other three roots are selected. By linearly combining the three roots for each solution in (5-10), the following is obtained,

$$u_i = \sum_{r=1}^{3} A_{i,r} \exp[ik_\parallel \beta x_3] \exp[ik_\parallel(\cos(\theta) x_1 + \sin(\theta) x_2 - vt)] \quad (5\text{-}16)$$

in this equation, $A_{i,r}$ has to be found in combining with boundary conditions.

For a surface wave to propagate, the mechanical boundary conditions at the surface ($x_3 = 0$) must be traction free [TIERSTEN 1969], which means no external force acts upon it. Therefore,

$$T_{i3} = c_{i3kl} \frac{\partial u_l}{\partial u_k} = 0 \ (x_3 = 0) \quad (5\text{-}17)$$

This leads to

$$T_{13} = T_{23} = T_{33} = 0 \ (x_3 = 0) \quad (5\text{-}18)$$

therefore,

$$T_{13} = -ic_{44}(k_1 u_3 + k_3 u_1) = 0 \ (x_3 = 0)$$

$$T_{23} = -ic_{44}(k_2 u_3 + k_3 u_2) = 0 \ (x_3 = 0)$$

$$T_{33} = -ic_{12}(k_1 u_1 + k_2 u_2) - ic_{11}k_3 u_3 = 0 \ (x_3 = 0) \tag{5-19}$$

replacing (5-16) into (5-19) and finally the boundary conditions are constructed,

$$\sum_{r=1}^{3}\left(c_{44}\cos(\theta)\,A_{3,r} + c_{44}\beta_r A_{1,r}\right) = 0$$

$$\sum_{r=1}^{3}\left(c_{44}\sin(\theta)\,A_{3,r} + c_{44}\beta_r A_{2,r}\right) = 0 \tag{5-20}$$

$$\sum_{r=1}^{3}\left(c_{12}\cos(\theta)\,A_{1,r} + c_{12}\sin(\theta)\,A_{2,r} + c_{11}\beta_r A_{3,r}\right) = 0$$

Thus there are six equations: three wave equations and three boundary conditions, and the amplitude $A_{3,r}$ can be known by solving them.

5.3.2 Surface acoustic waves in piezoelectric media

In most cases, piezoelectric materials are used in SAW devices for wave generation and receiving with the help of IDT. Therefore, the piezoelectric effects should be considered in the wave equation, which make the wave equation a coupled one [OLINER 1978]. In a time varying fields, the electric field is produced by a static charge as well as a changing of magnetic field,

$$\begin{aligned}\mathbf{E} &= -\nabla\phi - \frac{\partial \mathbf{A}}{\partial t}\\[2mm]\mathbf{B} &= \nabla\times\mathbf{A}\end{aligned} \tag{5-21}$$

where $\mathbf{B}$ is the magnetic flux density, $\mathbf{A}$ is the magnetic vector potential, ϕ is the electric potential. Because the velocity of the acoustic waves is five orders smaller in magnitude than the electromagnetic waves, the electric field can be considered as quasi-static. Therefore, the curl of the electric field can be assumed vanishing, thus the Maxwell-Faraday equation is,

$$\nabla \times \mathbf{E} = \frac{\partial \mathbf{B}}{\partial t} = 0 \tag{5-22}$$

The electric field $\mathbf{E}$ can be expressed as the negative gradient of the scalar electric potential, which is a quasi-static approximation of the Maxwell equations,

$$\mathbf{E} = -\nabla\phi = -e_1^* \frac{\partial\phi}{\partial x_1} - e_2^* \frac{\partial\phi}{\partial x_2} - e_3^* \frac{\partial\phi}{\partial x_3} \tag{5-23}$$

where e_1^*, e_2^*, and e_3^* are unit vectors. The negative sign indicates that $\mathbf{E}$ is opposite to the direction of increasing potential. Therefore the coupled constitutive equations can be expressed in terms of the particle displacement as,

$$T_{ij} = c_{ijkl} \frac{\partial u_k}{\partial x_l} + e_{kij} \frac{\partial\varphi}{\partial x_k} \tag{5-24}$$

$$D_k = -\varepsilon_{ki} \frac{\partial\varphi}{\partial x_i} + e_{kij} \frac{\partial u_i}{\partial x_j} \tag{5-25}$$

where e_{kij} is a third-rank piezoelectric stress tensor, ε_{ij} is a second-rank permittivity tensor. It should be noticed that in (5-24) the elastic constant c_{ijkl} is measured at constant electric field, in (5-25) the second-rank tensor ε_{ij} is measured under constant strain. Substituting (5-24) back into (5-6) get [OLINER 1978],

$$c_{ijkl} \frac{\partial^2 u_i}{\partial x_j \partial x_k} + e_{kij} \frac{\partial^2 \phi}{\partial x_j \partial x_k} = \rho \frac{\partial^2 u_i}{\partial t^2} \tag{5-26}$$

For a charge free dielectric, $\nabla \cdot D = 0$, therefore [OLINER 1978],

$$e_{ikl} \frac{\partial^2 u_i}{\partial x_j \partial x_k} - \epsilon_{jk} \frac{\partial^2 \phi}{\partial x_j \partial x_k} = 0 \tag{5-27}$$

combined with the information from the last section, the four wave equations are written as,

$$\rho\frac{\partial^2 u_1}{\partial t^2} = c_{11}\frac{\partial^2 u_1}{\partial x_1^2} + c_{44}\left(\frac{\partial^2 u_1}{\partial x_2^2} + \frac{\partial^2 u_1}{\partial x_3^2}\right)$$
$$+ (c_{12} + c_{44})\left(\frac{\partial^2 u_2}{\partial x_1\partial x_2} + \frac{\partial^2 u_3}{\partial x_1\partial x_3}\right) + 2e_{14}\frac{\partial^2 \phi}{\partial x_2\partial x_3}$$

$$\rho\frac{\partial^2 u_2}{\partial t^2} = c_{11}\frac{\partial^2 u_2}{\partial x_2^2} + c_{44}\left(\frac{\partial^2 u_2}{\partial x_1^2} + \frac{\partial^2 u_2}{\partial x_3^2}\right)$$
$$+ (c_{12} + c_{44})\left(\frac{\partial^2 u_1}{\partial x_1\partial x_2} + \frac{\partial^2 u_3}{\partial x_2\partial x_3}\right) + 2e_{14}\frac{\partial^2 \phi}{\partial x_1\partial x_3}$$

(5-28)

$$\rho\frac{\partial^2 u_3}{\partial t^2} = c_{11}\frac{\partial^2 u_3}{\partial x_3^2} + c_{44}\left(\frac{\partial^2 u_3}{\partial x_1^2} + \frac{\partial^2 u_3}{\partial x_2^2}\right)$$
$$+ (c_{12} + c_{44})\left(\frac{\partial^2 u_1}{\partial x_1\partial x_3} + \frac{\partial^2 u_2}{\partial x_1\partial x_3}\right) + 2e_{14}\frac{\partial^2 \phi}{\partial x_2\partial x_1}$$

$$2e_{14}\frac{\partial^2 u_1}{\partial x_2\partial x_3} + 2e_{14}\frac{\partial^2 u_2}{\partial x_1\partial x_3} + 2e_{14}\frac{\partial^2 u_3}{\partial x_2\partial x_1} = 0$$

Similarly, a 4×4 matrix can be got from (5-28). The general solutions for u_i and ϕ are assumed to be a linear combination of the partial waves,

$$u_i = A_i \exp[k\beta x_3]\exp[jk(x_1 - vt)], i = (1,2,3) \tag{5-29}$$

$$\varphi = A_4 \exp[k\beta x_3]\exp[jk(x_1 - vt)] \tag{5-30}$$

By combing these four plane wave solutions and the stress free boundary condition, as well as the electrical boundary condition, the wave velocity can be solved. The solutions of these equations lead to determine the phase velocity and the electromechanical coupling coefficient K^2,

$$v = \lambda \cdot f \tag{5-31}$$

$$K^2 = 2 \cdot \frac{v_r - v_m}{v_r} \tag{5-32}$$

where λ is the wavelength, f is the SAW frequency, v_r and v_m is the phase velocity at open circuit and short circuit respectively [TIGLI et al. 2010b].

5.4 Modeling of SAW propagation on AlN/diamond/γ-TiAl

5.4.1 Mechanical boundary condition

Many works have investigated the SAW on two layered or three layered structures [BENETTI et al. 2004; EL HAKIKI et al. 2004; WU, S. et al. 2009]. They all assumed that the diamond layer was relatively thick, hence the effect of the real substrate on the wave propagation can be ignored. In this work, the diamond thickness is counted in. It is assumed that the SAW could reach to the γ-TiAl, therefore the sensor has a potential to sense unusual conditions between the layers, such as crack initiation, delamination, given the advantage that SAW devices could be made wireless.

A commercial FEM software package Comsol Multiphysics is used in the simulation. In the modeling, Interdigital Transducers (IDT) are applied on the structure surface as SAW generator and receiver [CHANG et al. 2007]. Due to a huge computation burden, to model a complete SAW device with FEM is almost impossible. Fortunately a SAW device can be treated as an infinitely extended periodic structure, since the length is of thousands wavelength, and the aperture is of hundreds wavelength [HOFER et al. 2006]. Based on this assumption, a simplified special boundary condition named Periodic Boundary Condition (PBC) is applied at the boundary. According to the floquet theory [KUCHMEN 1993], the general relation between the right and left boundary is,

$$P_R(x + p)e^{j\omega t} = P_L(x)e^{-(\alpha + j\tau)p}\, e^{j\omega t} \tag{5-33}$$

where P_R and P_L is the field distribution of the right and left boundary respectively. p is one half of the wavelength, ω is the angular frequency. α is the attenuation constant, and τ is the phase constant, its value is equal to the wavenumber. Generally, a time harmonic excitation is assumed, therefore the term $e^{j\omega t}$ is omitted in the future calculation, so the boundary condition is written as,

$$P_R = P_L e^{-\gamma x_1} \tag{5-34}$$

γ is the complex propagation constant, it is equal to $\alpha + j\tau$. In this case, the period (p) is $2\mu m$, which is half of the wavelength ($\lambda/2$). In this case, only the Rayleigh mode is considered, therefore the wave attenuation in the wave propagation direction could be ignored, which means α is zero. The mechanical boundary condition of the model surface is free of stress and the electrical boundary condition takes two special cases into consideration: the open circuit and the short circuit [OLINER 1978]. The bottom boundary of γ-TiAl is treated as absorbing boundary, thus the wave will not be reflected at the bottom. The schematic of the layered structure is depicted in Figure 5.7(a). Figure 5.7(b) shows the simplified model in finite element calculation.

As can be seen in Figure 5.7(b), an absorbing boundary condition named Perfectly Matched Layer (PML) resides at the bottom of the γ-TiAl, it is due to the very large thickness of the γ-TiAl substrate, thus its thickness can be assumed infinite compared with the SAW wave length [COMSOL 2008; JIN 2002; JOHNSON 2008]. The PML is an artificial absorbing layer that is designed to absorb waves, it is used to truncate computational burdens in numerical calculations. It works as, e.g. assuming a wave propagates in x direction, thus wherever in a wave equation, an

x derivative is replaced by $\dfrac{\partial}{\partial x} \rightarrow \dfrac{1}{1+\frac{i\alpha(x)}{\omega}}\dfrac{\partial}{\partial x}$, where α is some function of x. When α is positive,

the propagating wave will be attenuated.
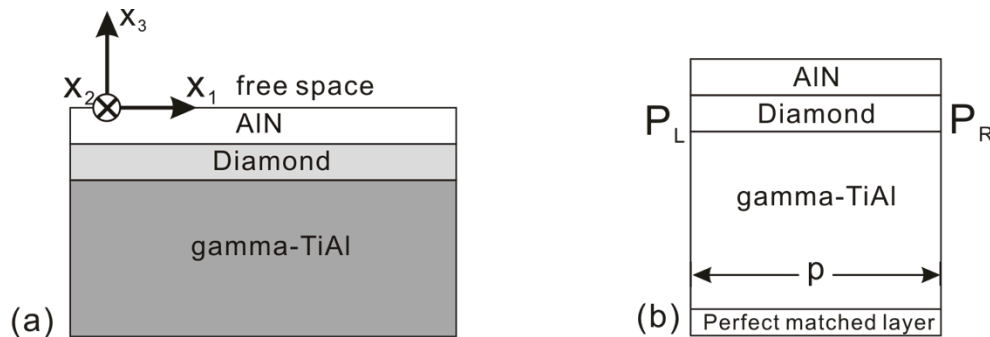
Figure 5.7 Schematic diagram of the SAW sensors (a) Coordinates of the structure (b) Periodic FEM model

5.4.2 Electrical boundary condition

To solve the SAW problems coupled with piezoelectricity, not only the mechanical boundary conditions are considered, there are also electrical boundary conditions to be considered. Generally, two electrical boundary conditions are of special interests: the open circuit boundary condition and short circuit boundary condition [OLINER 1978]. The open circuit boundary

condition means that the surface of the half space is electrically free, therefore there is no conducting layer at the surface [OLINER 1978]. It is presented mathematically as,

$$\varphi = \Phi(0) \cdot e^{-kx_3} \ \ (x_3 \geq 0) \tag{5-35}$$

at $x_3 = 0$, the normal component of electrical displacement is continuous. For the short circuit boundary condition, it means that the surface is covered with perfectly conducting layer (metalized) of a material which is thin enough that the mechanical boundary condition are unaffected, so that the electrical potential on the surface is zero [NOVGOROD and DVOESHERSTOV 2011; OLINER 1978]. It is described as,

$$\Phi = 0 \ \ (x_3 = 0) \tag{5-36}$$

5.5 Simulation results and discussion

Table 5.1 shows the material constants of diamond, AlN used in the calculation. The Young's modulus of γ-TiAl is 153GPa, possion's ratio is 0.237 and the density is $3800 kg/m^3$ [WELSCH *et al.* 1994].

Table 5.1 Elastic (c), piezoelectric (e), dielectric (ε) and density (ρ) of AlN and diamond used in calculation [BYKHOVSKI *et al.* 1997; GUALTIERI *et al.* 1994; LEVINSHTEIN, M. E. *et al.* 2001]

Material	Stiffness matrix (GPa)						Dielectric constant (Uniteless)		Piezoelectric coupling constant (C/cm^2)			Density (Kg/ m^3)
	c_{11}, c_{22}	c_{33}	c_{12}	c_{13}	c_{44}, c_{55}	c_{66}	$\varepsilon_{11}, \varepsilon_{22}$	ε_{33}	e_{15}, e_{24}	e_{31}, e_{32}	e_{33}	ρ
AlN	345	395	125	120	118	110	9.04	10.7	-0.48	-0.58	1.55	3260
diamond	1153.12		86.44		533.34		6.21					3512

Figure 5.8 shows the surface plot of a one-wavelength structure at 95.7MHz Figure 5.8(a), 194.3MHz(Figure 5.8(b)), 295.1MHz (Figure 5.8(c)) and 397.8MHz (Figure 5.8(d)) respectively. They corresponds to the first, second, third and fourth harmonics of the SAW. It can be noticed that the higher the harmonic, the weaker the ability of the SAW to reach the substrates. The particle displacement showed in Figure 5.8 is the total displacement, which is a combination of the displacement in x_1 and x_3 direction.
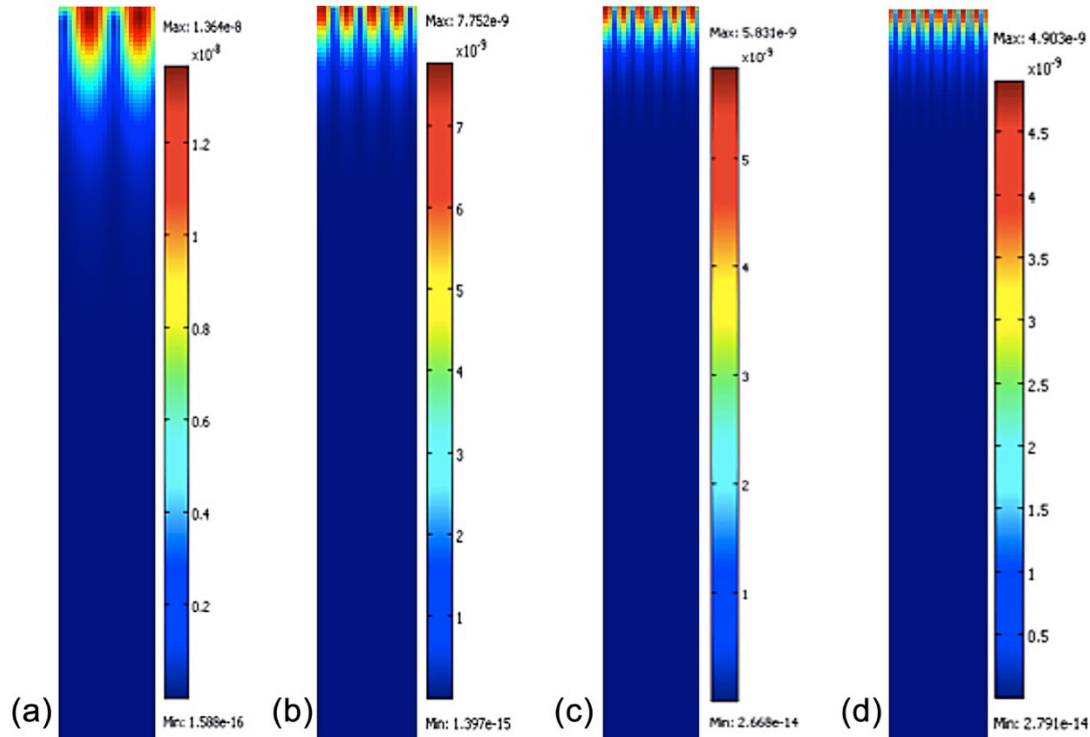
Figure 5.8 Surface plot of total displacement of standing SAW in (a) first harmonic (b) second harmonic (c) third harmonic and (d) fourth harmonic

The particle displacement in the x_1 and x_3 direction is illustrated with respect to the layers and substrate thickness in Figure 5.9 for a clear view. In this figure, the particle displacement is normalized with respect to its maximum value, and the structure thickness is normalized with respect to the wavelength. It could be seen that for the first harmonic, the particle displacement dies out at the structure thickness of approximately three times wavelength, this result agrees very well with the definition of SAW [OLINER 1978]. However, with the increase of harmonic order, the particle displacement dies out more and more closer to the structural surface. The u_1 displacement showed in Figure 5.9 (c) and (d) even starts to oscillate in the depth direction, in these two cases, the leaky wave appears [OLINER 1997]. The leaky wave attenuate the wave energy in the wave propagation direction, therefore it cannot propagate as far as the SAW.
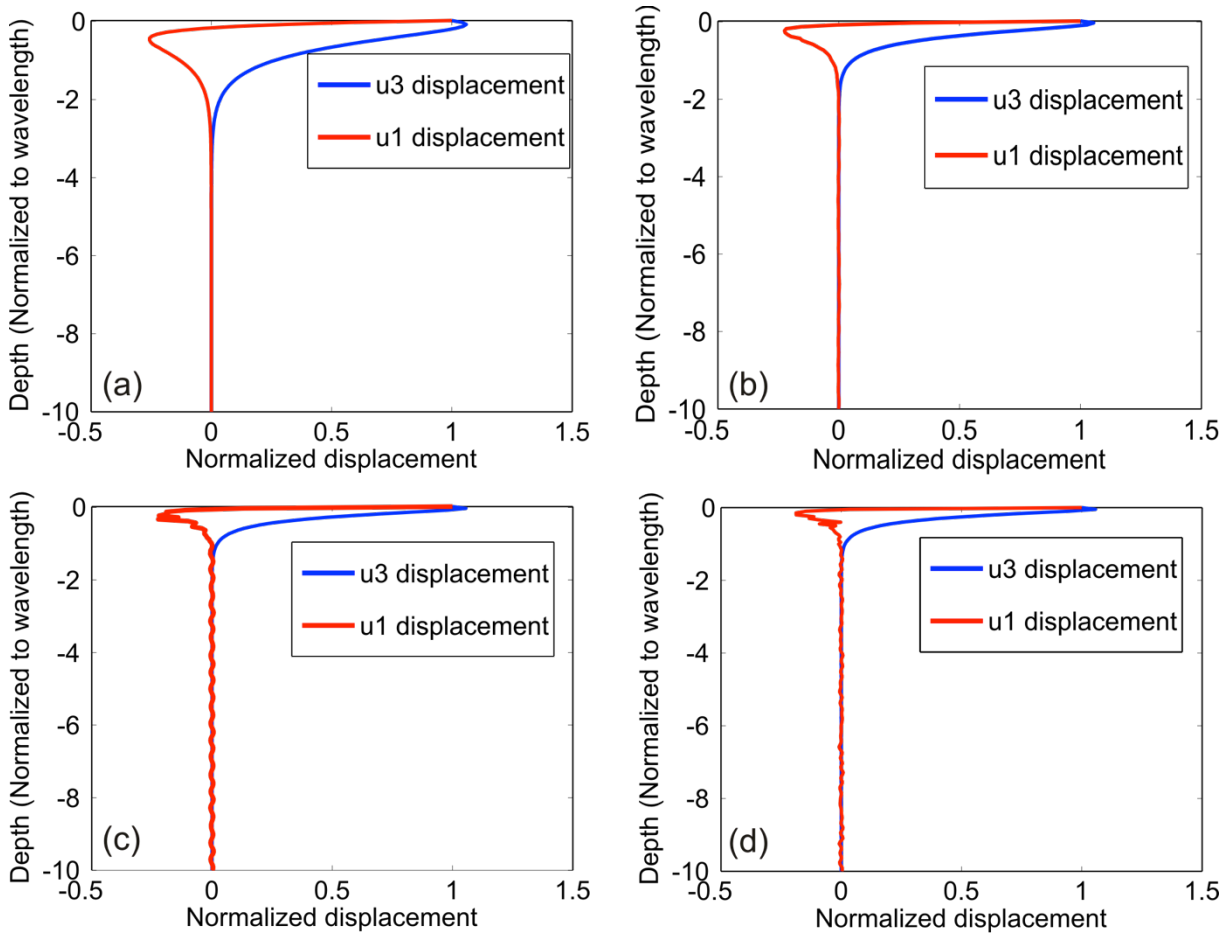
Figure 5.9 Particle displacement of SAW at (a) first harmonic (b) second harmonic (c) third harmonic (d) fourth harmonic

Figure 5.10 and Figure 5.11 shows the dispersion curves of phase velocity and Electromechanical Coupling Coefficient (EMCC) of the SAW in its four harmonics.
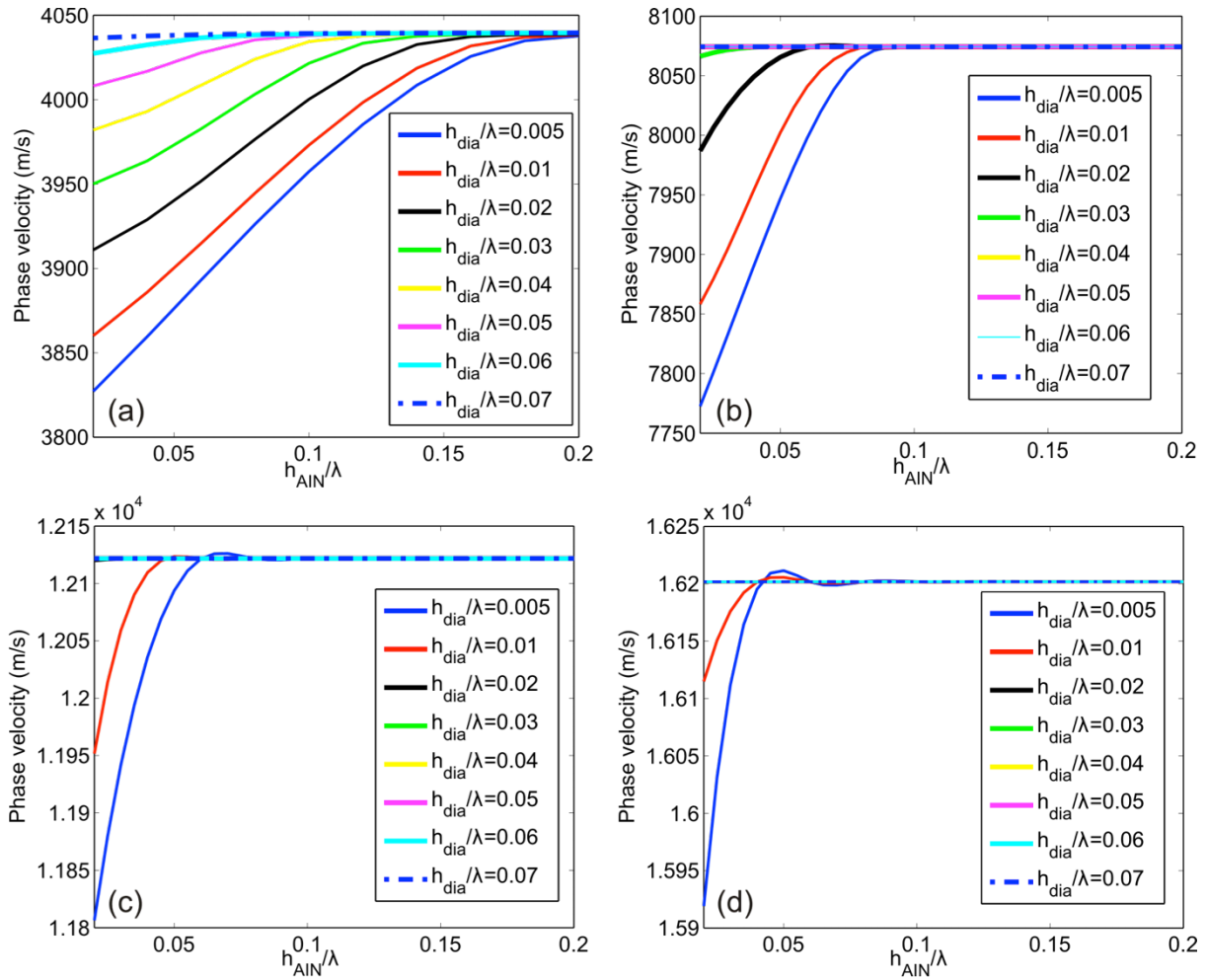
Figure 5.10 Phase velocity of SAW at (a) first harmonic (b) second harmonic (c) third harmonic (d) fourth harmonic

In the dispersion curves, the thickness of diamond layer and AlN layer is expressed with respect to the wavelength, where h with its subscript represents the according film thickness. Compared with the conventional dispersion curves which are based on a diamond substrate [BENSMAINE *et al.* 2008; HIKATA *et al.* 1995], the curves presented here are not monotonically increasing or monotonically decreasing anymore. If the diamond layer is treated as the substrate, the phase velocity of all harmonics will decrease with the increase of h_{AlN}/λ, this is due to diamond has the highest acoustic wave velocity of all materials [HRIBŠEK *et al.* 2010], therefore the smaller the h_{AlN}/λ, the closer the phase velocity becomes to the Rayleigh wave velocity of diamond. In the three layer structure, the existence of the diamond layer accelerates the phase velocity with the increase of its thickness. In Figure 5.10(a), the phase velocity approaches to the transverse velocity of γ-TiAl, which is $4034 m/s$, with the increase of h_{AlN}/λ to 0.2. $4034 m/s$ is the cut off velocity [CHANG, J. and XU 2005], above it the Rayleigh wave will couple with the bulk wave of

the substrate, and this will cause a leaky wave. Therefore the Rayleigh mode is the fundamental mode of the three layered structure. Similarly, the existence of the diamond layer accelerates the phase velocity with the increase of its thickness. From Figure 5.10 (b), (c) and (d) it can be seen that the phase velocity increases with the increase of the harmonic order, and it saturates very fast with the increase of the diamond layer thickness. Figure 5.10 proves that the thicker the diamond layer, the higher the phase velocity. However, as can be seen from Figure 5.11, the diamond layer decreases the electromechanical coupling coefficient. In Figure 5.11(a), the highest value of K^2 is 0.2%, it is at the point where $h_{diamond}/\lambda = 0$ and $h_{AlN}/\lambda = 0.14$. In the four harmonics, K^2 increases to a peak value with the increase of h_{AlN}/λ, afterwards it decreases with the increase of h_{AlN}/λ. It can be seen from Figure 5.10 and Figure 5.11 that with the increase of the harmonic order, the phase velocity increases, contrarily, the EMCC (k^2) decreases.
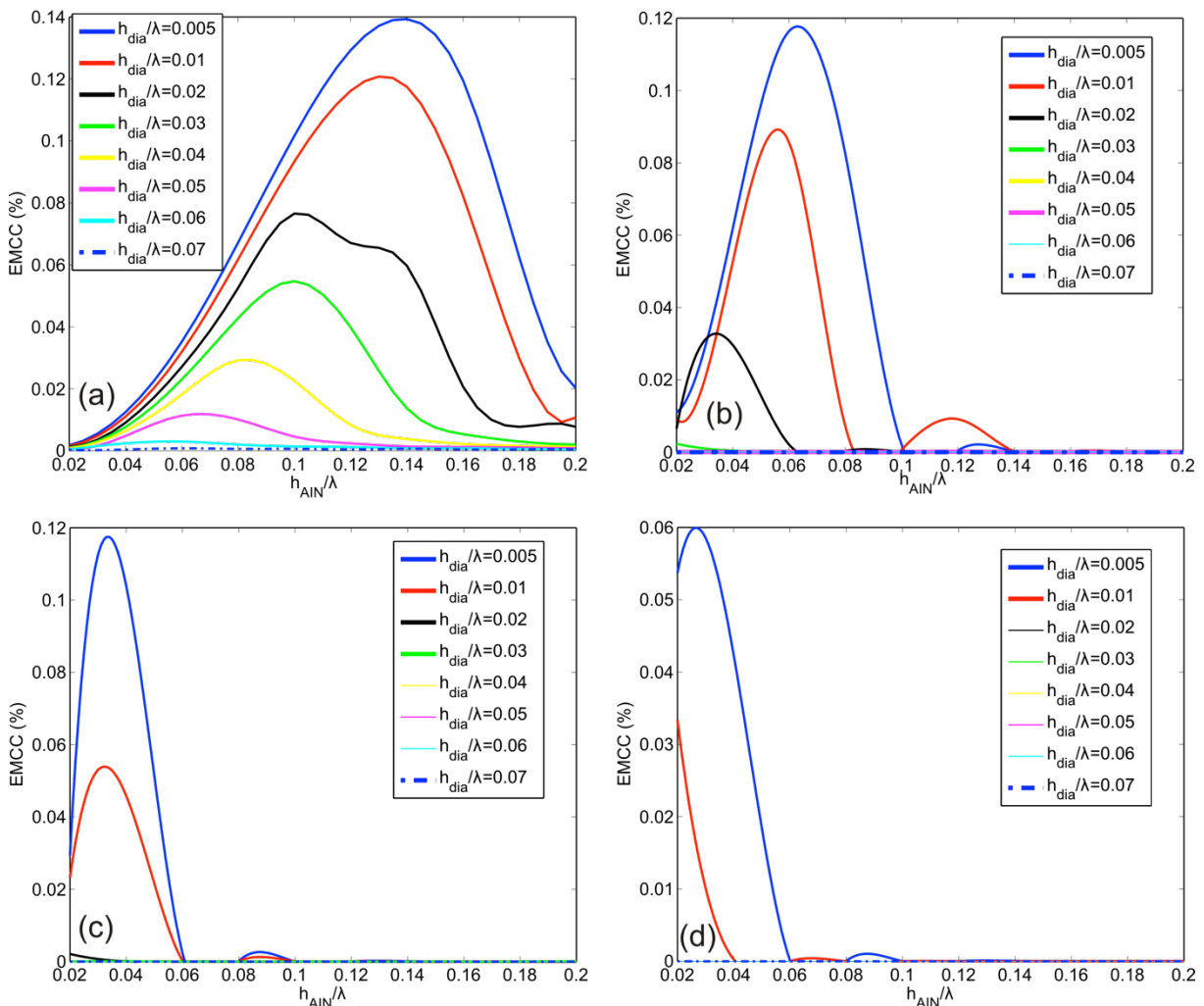
Figure 5.11 Electromechanical coupling coefficient of SAW at (a) first harmonic (b) second harmonic (c) third harmonic (d) fourth harmonic

To combine the effect of the diamond layer and AlN layer together, Figure 5.12 shows the 3D dispersion surface plot of the first harmonic. This figure gives a general view of the phase velocities and K^2 distribution with respect to h_{AlN}/λ and $h_{diamond}/\lambda$. From Figure 5.12(a), it can be observed that the phase velocity goes to a plateau with the increase of the layers thickness, and Figure 5.12(b) shows that the peak value of K^2 only appears at a certain point.
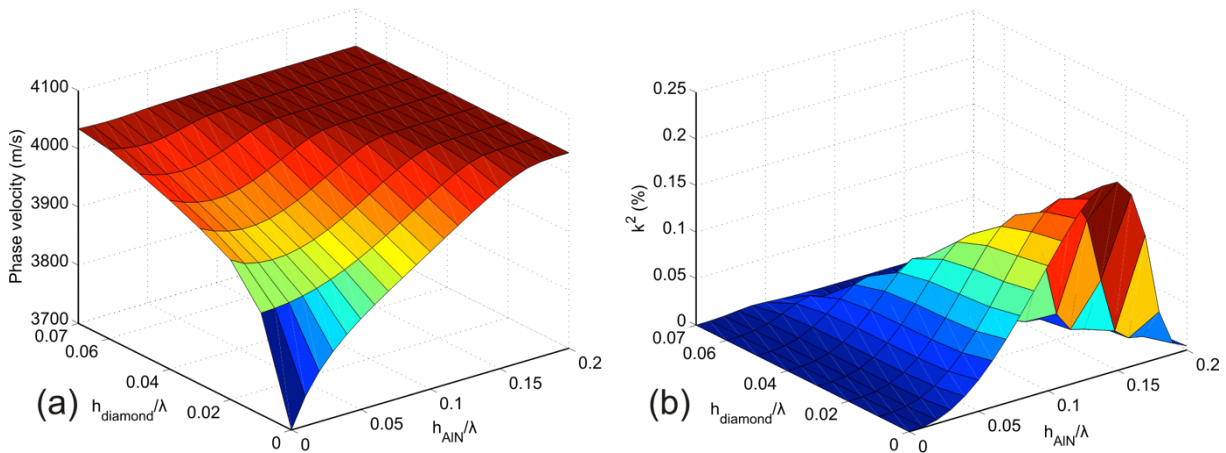
Figure 5.12 Three dimensional (a) phase velocity dispersion surface plots of AlN/diamond/γ-TiAl and (b) K^2 dispersion surface plot of AlN/diamond/γ-TiAl

5.6 Surface damage detection by SAW

To demonstrate the potential of SAW in surface defect detection function, indentation damages are simulated on the structure surface. The model is illustrated in Figure 5.13. Two pairs of IDT are applied on the structural surface, the left and right IDT functions as an actuator and sensor respectively. Absorbing boundary conditions PML are added on the left, right and bottom of the structure to avoid wave reflection at the boundaries.
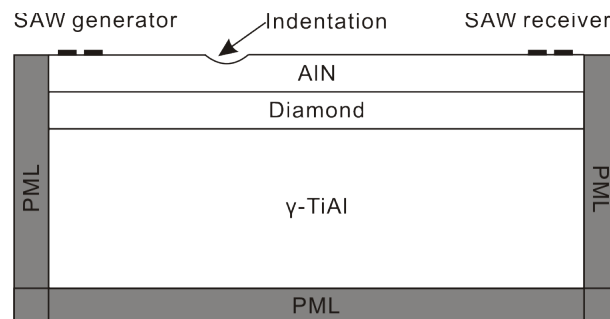
Figure 5.13. Schematic of damage detection

Two indentation scenarios are considered in the simulation. In the first one, the indentation radius is fixed and the indentation depth varies. In the second scenario, the indentation depth is fixed

and the indentation radius varies. Voltage is applied on the IDT actuator to generate an electric field, hence the AlN deforms due to its piezoelectricity, and converts the electrical energy into mechanical energy, by this method the SAW is generated and propagates on the surface. Afterwards, the IDT receiver converts the mechanical energy back into electrical energy and the voltage can be measured. Since the SAW is reflected and scattered by the surface defect during traveling, a diagnosis is performed based on calculating the admittance on the IDT receiver. The admittance is derived through integrating the current on the IDT surface and dividing it by the measured voltage, the results of different cases is showed in Figure 5.14.
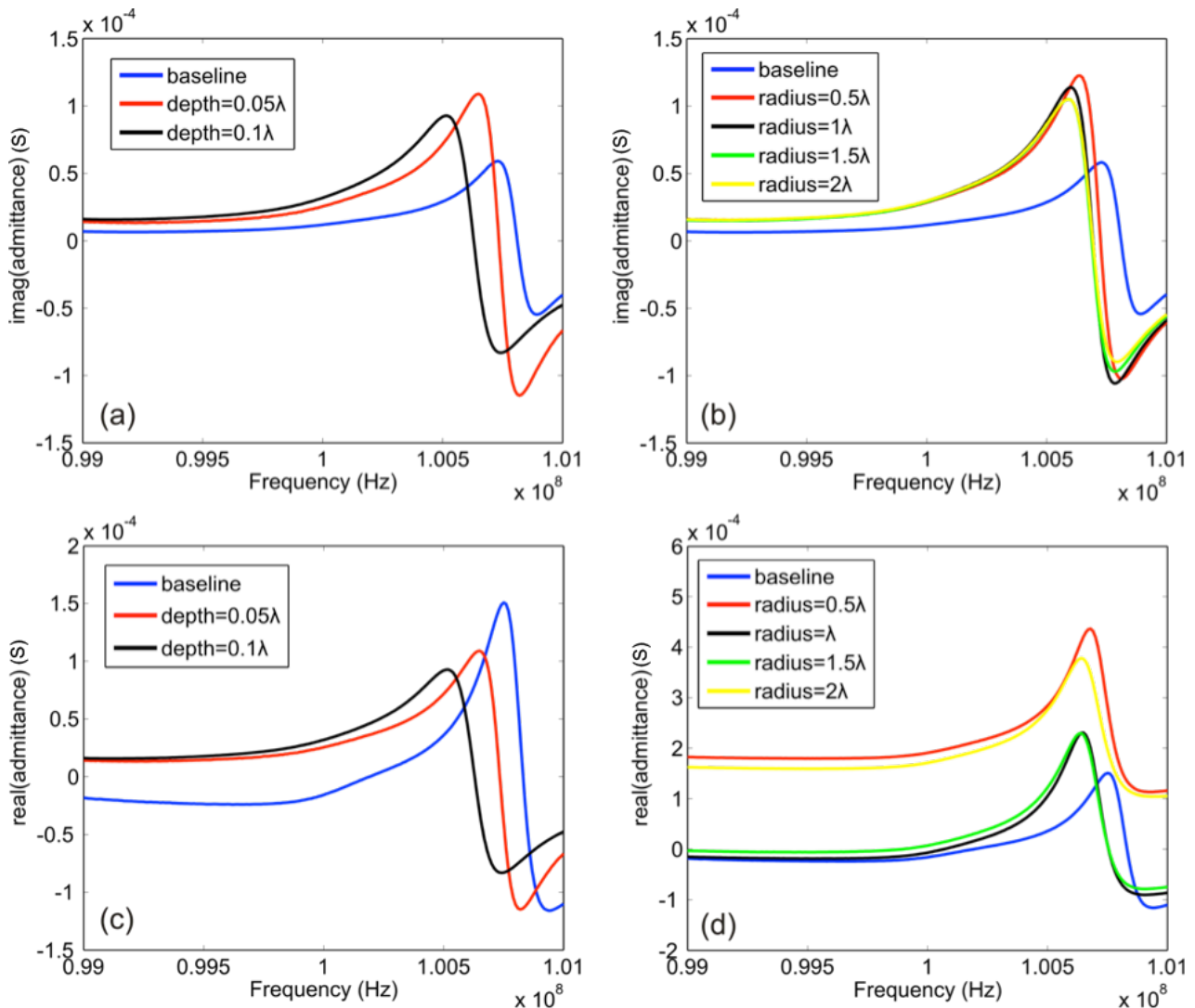
Figure 5.14. (a) Comparison of the imaginary part of admittance at the radius-fixed scenario (b) Comparison of the imaginary part of admittance at the depth-fixed scenario (c) Comparison of the real part of admittance at the radius-fixed scenario (b) Comparison of the real part of admittance at the depth-fixed scenario

As shown in Figure 5.14, the real and imaginary part of the admittance change with respect to different surface damage, by comparing them with the baseline, the health status of the structure can be obtained.
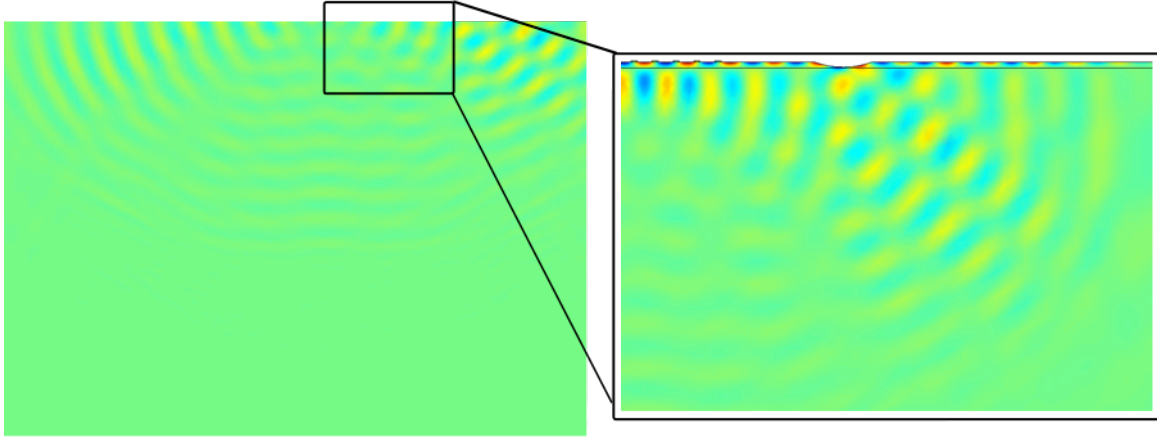
Figure 5.15 A time frame of wave propagation in the time domain

Figure 5.15 is a time frame of the SAW propagating on the structural surface, as could be seen the propagating SAW is reflected and refracted when passing through the surface damage. After passing through the damage, the wave energy is lost in the depth direction. Therefore by measuring the output of the IDT, the healthy status of the structure can be known.

5.7 Conclusion

This chapter considers a high temperature distributable multilayer SAW sensor based on AlN/diamond/γ-TiAl. The SAW wave equation was introduced and a numerical simulation was performed. Moreover, the dispersion curves of phase velocity and electromechanical coupling coefficient were calculated and analyzed. Afterwards, the surface defect detection is demonstrated. The diagnosis based on analyzing the admittance at the IDT receiver is performed.

Conventionally a SAW device based on diamond is analyzed as always assuming that the diamond layer is infinite, here it is treated as finite so the real substrate was taking into consideration. As an interlayer between the substrate and the piezoelectric layer, the diamond layer accelerates the phase velocity, meanwhile, it decreases the K^2 when it becomes thick. The result fills the gap in diamond-based SAW devices, particularly cases are the diamond layer cannot be assumed as infinite, and it proves that for a three layer structure like the AlN/diamond/γ-TiAl, the thickness of each functional layer cannot be chosen randomly, it must

be selected according to the dispersion curve, to get an optimal combination between phase velocity and EMCC.

The SAW sensors presented here have potential uses in high temperature applications, especially hot spots where special attention are required. The modeling results denote that a distributable piezoelectric material used SAW generation and receiving is a potential solution in high temperature SHM applications. The work in this chapter provides theoretical references for future designing of multilayer SAW sensors, as well as other related SAW devices.

6 Conclusion and outlook

6.1 Conclusion

Nowadays is an era that numerous amounts of new skyscrapers, bridges, aircrafts, high speed railways and automobiles never stop emerging in our daily lives, meanwhile, lots of aging civil structures and public transportation systems are still serving and functioning. To maintain and repair them is a great challenge and quite costly. Structural Health Monitoring is an effective solution to these problems and has been explored worldwide in the last twenty years. With the rapid rise of SHM technologies, smart sensors with multi-functionality are more and more favorable.

The work described in this dissertation explored a new group of piezoelectric composite materials as distributed transducers in SHM application - the piezoelectric paint and Aluminum Nitrides. The study of the distributed transducers started with production of high quality piezoelectric paint, and investigated its connectivity, micromechanical structures and surface morphology. In the following the piezoelectric paint was characterized to investigate its piezoelectric properties, mechanical properties, bandwidth, thermal properties and nonlinearity. In order to make the piezoelectric paint more competitive, an optimization was performed to improve the piezoelectric sensitivity of it. A typical application, sensors made of piezoelectric paint as modal sensors, was demonstrated. In addition, the application of piezoelectric paint as distributed transducers in SHM was explored. Due to the thermal limitation of piezoelectric paint, another piezoelectric material, AlN, was studied to be used as distributed transducers in high temperature SHM. In this

section, a three layer structure AlN/diamond/γ-TiAl was studied as SAW transducers. The theoretical SAW propagation equations were deduced and the numerical solution was obtained from SHM simulation, as well as dispersion curves. At the end, a surface defect was demonstrated to show the fault detection function of the distributed SAW sensor.

The studies presented in this work have shown that the piezoelectric paint and AlN are very promising smart materials in SHM fields. As there is no perfect sensor which can feed all application needs, the advantages and disadvantages of piezoelectric ceramic, piezoelectric paint, PVDF and AlN are compared and summarized in Table 6.1.

Table 6.1 Comparison and summarization of advantages (+) and disadvantages (-) of piezoelectric ceramic, piezoelectric paint, PVDF and AlN

Properties	Piezoelectric ceramic	Piezoelectric paint/composites	PVDF	Aluminum Nitride
Hardness	Hard (+)	Soft (+)	Soft (-)	Hard (+)
Brittleness	Brittle (-)	Resilient (+)	Resilient (+)	Brittle (-)
Flexibility	Stiff (-)	Flexible (+)	Flexible (+)	Stiff (-)
Flexible geometry	Difficult (-)	Easy (+)	Easy (+)	Difficult (-)
Conformability	Difficult (-)	Easy (+)	Easy (+)	Easy (+)
Adjustable properties according to applications	Difficult (-)	Easy (+)	Difficult (-)	Difficult (-)
Distribute ability	Difficult (-)	Easy (+)	Medium (+)	Easy (+)
Acoustic impedance	High (-)	Low (+)	Low (+)	High (-)
Coupling factor	High (+)	Low (-)	Low (-)	High (+)
Dielectric constant	High (+)	Medium (+)	Low (-)	High (+)
Thermo resistance	Medium (+)	Low (-)	Low (-)	High (+)
Charge constant	High (+)	Medium (+)	Low (-)	High (+)
Bandwidth	Narrow (-)	Wide (+)	Wide (+)	Narrow (-)

| Cost | Cheap (+) | Cheap (+) | Expensive (-) | Expensive (-) |

To draw a conclusion, this research work described in the dissertation has made the following contributions,

- A lab applicable cost-effective method for piezoelectric paint production was developed, by using this method, smooth, low cost, high quality and ready-to-use piezoelectric paint can be obtained, in addition, the paint thickness can be controlled by using this method.

- Surface morphology of the piezoelectric paint was investigated, the results helped to explain air voids formation and how to avoid them, and to understand the piezoelectric composites connectivity.

- Material properties including Young's modulus, sensitivity, piezoelectric charge constant d_{31} were characterized, in addition, the piezoelectricity of the paint was greatly improved by a refined method.

- Application of piezoelectric paint as spatially distributed modal sensors and vibration sensors were demonstrated. These demonstrations are typical applications of piezoelectric paint, which emphasize it is flexible, easy to be shaped, spatially distributable and competitive sensitivity.

- Application of AlN as spatially distributed transducers in high temperature SHM application was theoretically demonstrated. The SAW was solved numerically. AlN as sensor to detect a surface damage was demonstrated.

In addition, a variety of findings obtained from this research work are,

- Piezoelectric paint with improved piezoelectricity is very competitive compared with other piezoelectric transducers. The performance of it is comparable to the piezoelectric ceramic and strain gauges.

- By using the tape casting method to produce piezoelectric paint, the maximum weight percentage is 60%, higher than this would result in air avoids and finally lead to dielectric breakdown in poling.

- In thermal analysis, the weight property of the piezoelectric paint changes above 200°C, which means it can only be used in low temperature applications.

- Applying piezoelectric paint as modal sensors is applicable. However, due to geometric tolerance problems, in reality the result cannot be as good as the theoretical prediction.

- AlN is very applicable as SAW transducers in high temperature SHM applications. However, if a multilayered structure is considered, the thickness of each layer has to be taken into account for an optimized result.

6.2 Future work

For spatially distributed transducers, the future work can be classified as:

- Further development of piezoelectric paint
- Further application of piezoelectric paint
- Experimental realization of AlN based SAW transducers

For the further development of piezoelectric paint, the following work could be considered:

- Applying sprayed piezoelectric paint on multi-curved structural surfaces. At the moment some pioneer works have demonstrated sprayed piezoelectric paint, but the result is very rough and there is much room left for improvements [KOBAYASHI and JEN 2004; KOBAYASHI *et al.* 2006].

- Along with applying piezoelectric paint as sprayed sensors, corona polarization must be designed and performed. A cost-effective device to perform corona poling is expected.

- By adding other substances into piezoelectric paint, so that it could be not only spatially distributable, but also can protect a structural surface from corrosion.

- A piezoelectric sensor for end-users is expected.

For further application of piezoelectric paint as distributed sensors, possible applications could be,

- Ultrasonic transducers
- Acoustic emission sensors for pipe line

From the modal sensor sensitivity problems it could be concluded that if the sensor is to be used with specific shape, an effective shaping method must be built.

For the experimental realization of AlN based SAW transducers, a sample must be built to fabricate IDT on the AlN surface by lithography method. Afterwards, the surface failure detection function can be studied and compared with the simulation results.

References

ABDOLVAND, R., 2008, "*Thin-film piezoelectric-on-substrate resonators and narrowband filters*", Georgia Institute of Technology.

AKIYAMA, M., MOROFUJI, Y., KAMOHARA, T., NISHIKUBO, K., TSUBAI, M., FUKUDA, O. and UENO, N., 2006: "*Flexible piezoelectric pressure sensors using oriented aluminum nitride thin films prepared on polyethylene terephthalate films*", Journal of applied physics, Vol. 100, pp. 5.

ANDRÄ, J., BÖHLING, A., GRONEWOLD, T., SCHLECHT, U. and GUTSMANN, T., 2008: "*Surface Acoustic Wave biosensor as a tool to study the interaction of antimicrobial peptides with phospholipid and lipopolysaccharide model membranes*", Langmuir, Vol. 24, No. 16, pp. 6.

APC_INTERNATIONAL_LTD, 2002: *Piezoelectric Ceramics: Principles and Applications* APC International Ltd.

APPEL, F., DAVID, J., HEATON PAUL and OEHRING, M., 2011: *Gamma Titanium Aluminide Alloys Science and Technology*, Wiley, Weinheim.

ARNAU, A., 2008: *Piezoelectric Transducers and Applications*.

ASHBY, M. F., 2009: *Engineering Materials and Processes Desk Reference*, Butterworth-Heinemann, Oxford, UK.

BÄCKER, D., RICOEUR, A. and KUNA, M., 2011: "*Sensor Concept Based on Piezoelectric PVDF Films for the Structural Health Monitoring of Fatigue Crack Growth*", Structural Durability & Health Monitoring Vol. 7, No. 1, pp. 22.

BAHR, D. F., ROBACH, J. S., WRIGHT, J. S., FRANCIS, L. F. and GERBERICH, W. W., 1999: "*Mechanical deformation of PZT thin films for MEMS applications*", Materials Science and Engineering: A, Vol. 259, pp. 6.

BAILEY, T. and HUBBARD, J. E., 1985: "*Distributed piezoelectric-polymer active vibration control of a cantilever beam*", Journal of Guidance, Control, and Dynamics, Vol. 8, No. 5, pp. 7.

BALAGEAS, D., FRITZEN, C.-P. and GÜEMES, A., 2006: *Structural Health Monitoring*, Iste, Wiltshire

BALAS, M. J., 1978: "*Active control of flexible systems*", Journal of Optimization Theory and Applications, Vol. 25, No. 3, pp. 22.

BALLATO, A., 1996: "*Piezoelectricity: History and new thrust*", vol. 1, *IEEE Ultrasonic symposium*, San Antonio, Texas, USA, pp. 575-583.

BAO, J., 2003, "*Lamb wave generation and detection with piezoelectric wafer active sensors*", University of South Carolina, Columbia, South Carolina.

BENETTI, M., CANNATÀ, D., D'AMICO, A., PIETRANTONIO, F. D., MACAGNANO, A. and VERONA, E., 2004: "*SAW sensors on AlN/Diamond/Si structures*", 2004 IEEE Sensors Proceedings, Vol. 2, pp. 2.

BENSMAINE, S., BRIZOUAL, L. L., ELMAZRIA, O., FUNDENBERGER, J. J., BELMAHI, M. and BENYOUCEF, B., 2008: "*SAW devices based on ZnO inclined c-axis on diamond*", Diamond & Related Materials, Vol. 17, pp. 4.

BERGMAN, J. G., MCFEE, J. H. and CRANE, G. R., 1971: "*Pyroelectricity and optical second harmonic generation in polyvinylidene fluoride films*", Applied Physics Letters, Vol. 18, No. 5, pp. 203-205.

BHATTACHARYA, 1995: *Industrial Electronics and Control*, Tata McGraw-Hill Publishing Company Limited, New delhi.

BLEVINS, R. D., 1979: *Formulas for natural frequency and mode shape*, Van Nostrand Reinhold Co., New York.

BLOOMFIELD, P. E. and MARCUS, M. A., 1988: "*Production of ferroelectric polymer films*", in WANG, T. T., HERBERT, J. M. and GLASS, A. M. (Eds.), *The application of ferroelectric polymers*. Chapman and Hall, New York.

BOARD, N. T. S., 1988: "Aircraft accident report", in.

BOLLER, C., CHANG, F.-K. and FUJINO, Y., 2009: *Encyclopedia of Structural Health Monitoring*, Wiley, London.

BURKE, S. E. and HUBBARD, J. E., 1987: "*Active vibration control of a simply supported beam using a spatially distributed actuator*", Ieee control systems magazine, pp. 6.

BYKHOVSKI, A. D., GELMONT, B. L. and SHUR, M. S., 1997: "*Elastic strain relaxation and piezoeffect in GaN-AlN, GaN-AlGaN and GaN-InGaN superlattices*", Journal of applied physics, Vol. 81.

CADY, W. G., 1921: "*The piezoelectric resonator*", Physical Review A, Vol. 17, pp. 531-533.

CADY, W. G., 1923a: "Method of maintaining electric currents of constant frequency", in PATENT, U. S. (Ed.), USA.

CADY, W. G., 1923b: "Piezo-electric resonator", in PATENT, U. S. (Ed.), USA.

CARTZ, L., 1995: *Nondestructive Testing: Radiography, Ultrasonics, Liquid Penetrant, Magnetic Particle, Eddy Current* ASM International

CHADWICK, P. and CURRIE, P. K., 1977: "*Foundations of the theory of surface waves in anisotropic elastic materials*", in YIH, C.-S. (Ed.), *Advances in applied mechanics*. Academic press, London, pp. 77.

CHANG, J. and XU, J., 2005: "*The propagation of generalized rayleigh waves in a coated materials*", Acta mechanica sinica, Vol. 37, No. 2, pp. 7.

CHANG, K.-S., CHANG, C.-K., CHOU, S.-F. and CHEN, C.-Y., 2007: "*A surface acoustic wave sensor modified from a wireless transmitter for the monitoring of the growth of bacteria*", Sensors & Actuators: B, Vol. 125, pp. 7.

CHEN, K.-T., CHANG, C.-K., KUO, H.-L. and LEE, C.-K., 2011: "*Optically defined modal sensors Incorporating spiropyran-doped liquid crystals with piezoelectric sensors*", Sensors, Vol. 11, pp. 9.

CLARK, R. L. and BURKE, S. E., 1996: "*Practical limitations in achieving shaped modal sensors with induced strain materials*", Transactions of ASME, Vol. 118, pp. 8.

COLBERT, J. R. and DALE, W., 1968: "Piezoelectric ultrasonic transducer", in OFFICE, U. S. P. (Ed.), USA, pp. 3.

COLLET, M., WALTER, V. and DELOBELLE, P., 2003: "*Active damping of a micro-cantilever piezo-composite beam*", Journal of Sound and Vibration, Vol. 260, pp. 24.

COLLINS, S. A., 1990, "*Sensors for structural control applications using piezoelectric polymer film*", Massachusetts Institute of Technology.

COLLINS, S. A., D.W.MILLER and FLOTOW, A. H. V., 1994: "*Distributed sensors as spatial filters in active structural control*", Journal of Sound and Vibration, Vol. 173, No. 4, pp. 31.

COMSOL, 2008: "Comsol Multiphysics structural mechanical module user's guide", in.

CRAWLEY, E. F. and LUIS, J. D., 1985: "*Use of Piezo-Ceramics as Distributed Actuators in Large Space Structures*", vol., *Proceeding of AIAA/ASME/ASCE/AHS 26th structures, structural dynamics and materials Conference.*

CUI, C., BAUGHMAN, R. H., IQBAL, Z., KAZMAR, T. R. and DAHLSTROM, D. K., 1997: "Piezoelectric ceramic-polymer composite", in PATENT, U. (Ed.), USA.

CUI, C., BAUGHMAN, R. H., IQBAL, Z., KAZMAR, T. R. and DAHLSTROM, D. K., 1999: "Piezoelectric and related devices from ceramics dispersed in polymer", in PATENT, U. (Ed.), USA.

CURIE, P. and CURIE, J., 1882: "*Contractions et dilatations produites par des tensions électriques dans les cristaux hémièdres à faces inclinées*", Comptes rendus de l'Académie des Sciences, Vol. 93, pp. 1137–1140.

DEBOUCQ, J., DUQUENNOY, M., M, M. O., JENOT, F., CARLIER, J. and OURAK, M., 2011: "*Development of interdigital transducer sensors for non-destructive characterization of thin films using high frequency Rayleigh waves*", Review of Scientific Instruments, Vol. 82, No. 6, pp. 5.

DENNIS, J. W., 2007: "*Tape Casting Advanced Materials*".

DERAEMAEKER, A. and PREUMONT, A., 2005: "*Vibration based damage detection using large array sensors and spatial filters*", Mechanical systems and signal processing Vol. 20, pp. 16.

DIETZE, M. and ES-SOUNI, M., 2008: "*Structural and functional properties of screen-printed PZT-PVDF-TrEF composites*", Sensors and Actuators A: Physical, Vol. 143, No. 2, pp. 6.

DIMIDUK, D. M., 1999: "*Gamma titanium aluminide alloys—an assessment within the competition of aerospace structural materials*", Materials Science and Engineering A, Vol. 263, pp. 8.

DONOSO, A. and BELLIDO, J. C., 2009a: "*Systematic design of distributed piezoelectric modal sensors/actuators for rectangular plates by optimizing the polarization profile*", struct multidisc optim, Vol. 38, pp. 10.

DONOSO, A. and BELLIDO, J. C., 2009b: "*Tailoring distributed modal sensors for in-plane modal filtering*", Smart materials and structures, Vol. 18, pp. 4.

DUNN, M., 2003, "*Columbia's Problems Began on Left Wing*", The Baltimore Sun.

DUVAL, C., 1963: *Inorganic thermogravimetric analysis*, Chemical Physics and Chemistry, Amsterdam : North-Holland.

EGUSA, S. and IWASAWA, N., 1993: "*Piezoelectric paints: preparation and application as built-in vibration sensors of structural materials*", Journal of Materials Science, Vol. 28, pp. 6.

EGUSA, S. and IWASAWA, N., 1994: "*Preparation of piezoelectric paints and application as vibration modal sensors*", Journal of Intelligent Material Systems and Structures, Vol. 5, No. 1, pp. 140-144.

EGUSA, S. and IWASAWA, N., 1996: "*Application of piezoelectric paints to damage detection in structural materials*", Journal of Reinforced Plastics and Composites, Vol. 15, No. 8, pp. 806-817.

EGUSA, S. and IWASAWA, N., 1998: "*Piezoelectric paints as one approach to smart structural materials with heath-monitoring capabilities*", Smart materials and structures, Vol. 7, No. 4, pp. 8.

EL HAKIKI, M., ELMAZRIA, O., ASSOUAR, M. B., MORTET, V., TALBI, A. and SARRY, F., 2004: "*High SAW velocity and high electromechanical coupling coefficient with the new three layered structure: ZnO/AlN/diamond*", vol. 1, *IEEE Ultrasonics Symposium*, pp. 4.

ELMAZRIA, O., BENEDIC, F., HAKIKI, M. E., MOUBCHIR, H., ASSOUAR, M. B. and SILVA, F., 2006: "*Nanocrystalline diamond films for surface acoustic wave devices*", Diamond & Related Materials, Vol. 15, pp. 6.

FEENSTRA, J. and SODANO, H., 2008: "*Enhanced active piezoelectric 0-3 nanocomposites fabricated through electrospun nanowires*", Journal of applied physics, Vol. 103, pp. 5.

FRISWELL, M. I., 1999: "*Partial and segmented modal sensors for beam structures*", Journal of vibration and control, Vol. 5, pp. 19.

FRISWELL, M. I., 2001: "*On the design of modal actuators and sensors*", Journal of Sound and Vibration*,* Vol. 241, No. 3, pp. 12.

FRISWELL, M. I. and ADHIKARI, S., 2010: "*Structural health monitoring using shaped sensors*", Mechanical systems and signal processing*,* Vol. 24, pp. 13.

FRITZEN, C. P., 2005: "*Vibration-based Structural Health Monitoring – Concepts and Applications*", Key Engineering Materials*,* Vol. 293-294, pp. 18.

FURUKAWA, T., 1989: "*Piezoelectricity and pyroelectricity in polymers*", IEEE Transactions on Electrical Insulation Vol. 24, pp. 20.

FURUKAWA, T., FUJINO, K. and FUKADA, E., 1976: "*Electromechanical properties in the composites of epoxy resin and PZT ceramics*", Japanese journal of applied physics*,* Vol. 15, No. 11, pp. 11.

FURUKAWA, T. and SAKURAI, T., 1971: "*Piezoelectricity in polarized Poly(vinylidene Fluoride) films*", in T.WANG, T., HERBERT, J. M. and GLASS, A. M. (Eds.), *The application of ferroelectric polymers*. Chapman and Hall, New York.

GHODSSI, R. and LIN, P., 2011: *MEMS materials and processes handbook*, Springer, New York.

GILLMOR, C. S., 1971: *Coulomb and the Evolution of Physics and Engineering in Eighteenth - Century*, Princeton University Press.

GINIEWICZ, J., 1985, "*(Ph.Bi)(Ti,Fe)O3/Polymer Composite Materials for Hydrophone Applications*", Pennsylvania State University.

GIURGIUTIU, V., 2002: "*Lamb Wave Generation with Piezoelectric Wafer Active Sensors for Structural Health Monitoring*", vol., *SPIE's 10th Annual International Symposium on Smart Structures and Materials and 8th Annual International Symposium on NDE for Health Monitoring and Diagnosticspaper # 5056-17*, San Diego, CA.

GIURGIUTIU, V., 2003: "*Embedded Ultrasonics NDE with Piezoelectric Wafer Active Sensors*", Journal Instrumentation, Mesure*,* Vol. 3, No. 3-4, pp. 32.

GIURGIUTIU, V., 2008: *Structural health monitoring with Piezoelectric Wafer Active Sensors*, Elsevier Academic Press.

GIURGIUTIU, V. and ZAGRAI, A., 2005: "*Damage Detection in Thin Plates and Aerospace Structures with the Electro-Mechanical Impedance Method*", Structural Health Monitoring*,* Vol. 4, No. 2, pp. 20.

GOLDSTEIN, J., NEWBURY, D. E., JOY, D. C., LYMAN, C. E., ECHLIN, P., LIFSHIN, E., SAWYER, L. and MICHAEL, J. R., 2003: *Scanning Electron Microscopy and X-ray Microanalysis*, Springer.

GONZALO, J. A. and JIMENEZ, B., 2005: *Ferroelectricity: The fundementals collection*, Wiley-VCH Verlag GmbH & Co. KGaA, Weinheim.

GRAF, K. F., 1981: *A history of ultrasonics Physical Acoustics*, 15, New York: Academic.

GU, H. and WANG, M. L., 2009: "*A Monolithic Interdigitated PVDF Transducer for Lamb Wave Inspection*", Structural Health Monitoring*, Vol. 8, No. 2, pp. 12.

GU, H., ZHAO, Y. and WANG, M. L., 2005: "*A wireless smart PVDF sensor for structural health monitoring*", Structural control and health monitoring*, Vol. 12, pp. 27.

GU, Y., CLARK, R. L., FULLER, C. R. and ZANDER, A. C., 1994: "*Experiments on active control of plate vibration using piezoelectric actuators and polyvinylidene fluroride (PVDF) modal sensor*", Journal of Vibration and Acoustics*, Vol. 116, pp. 6.

GU, Y. W., LI, T., LI, Q. F., POOK, S. F. and GOH, C. W., 2008: "*Piezoelectric ceramics by powder processing*", SIMTech technical reports*, Vol. 9, No. 4, pp. 6.

GUALTIERI, J. G., KOSINSKI, J. A. and BALLATO, A., 1994: "*Piezoelectric materials for acoustic wave applications*", IEEE transaction on ultrasonics, ferroelectrics, and frequency control*, Vol. 41, No. 1, pp. 7.

GUO, H., XIAO, G., MRAD, N. and YAO, J., 2011: "*Fiber optic sensors for Structural Health Monitoring of air platforms*", Sensors*, Vol. 11, pp. 19.

GURURAJA, T. R., NEWNHAM, R. E., KLICKER, K. A., LYNN, S. Y., SCHUTZE, W. A., SHROUT, T. R. and BOWEN, L. J., 1980: "*Composite Piezoelectric Transducers*", vol., *IEEE Ultrasonic Symposium*.

GURURAJA, T. R., SCHULZE, W. A., CROSS, L. E. and NEWNHAM, R. E., 1985: "*Piezoelectric composite materials for ultrasonic transducer applications. Part II: evaluation of ultrasonic medical applications*", IEEE TRansactions on sonics and ultrasonics*, Vol. 32, No. 4, pp. 15.

GURURAJA, T. R., SCHULZE, W. A., CROSS, L. E., NEWNHAM, R. E., AULD, B. A. and WANG, Y. J., 1985: "*Piezoelectric composite materials for ultrasonic transducer applications. Part I: resonant modes of vibration of PZT rod-polymer composites*", IEEE TRansactions on sonics and ultrasonics*, Vol. 32, No. 4, pp. 18.

HALE, J. M., 2004: "*Piezoelectric paint: thick-film sensors for structural monitoring of shock and vibration*", vol. 3, *ASME 7th Biennial Conference on Engineering Systems Design and Analysis*, Manchester, England.

HALE, J. M. and TUCK, J., 1999: "*A novel thick-film strain transducer using piezoelectric paint*", vol. 213, *Proceedings of the Institution of Mechanical Engineers Part C*, pp. 22.

HAN, K., SAFARI, A. and RIMAN, R. E., 1991: "*Colloidal Processing for Improved Piezoelectric Properties of Flexible 0-3 Ceramic-Polymer Composites*", Journal of the American Ceramic Society Vol. 74, No. 7, pp. 4.

HAN, K. H., RIMAN, R. E. and SAFARI, A., 1990a: "*Chemically Precipitated (Pb0.5,Bi0.5)(Ti0.5, Fe0.5)O3 Ceramic Powder for 0-3 Ceramic/Polymer Composites*", Ceramic Transactions, Vol. 8, pp. 8.

HAN, K. H., RIMAN, R. E. and SAFARI, A., 1990b: "*Dielectric and Piezoelectric Properties of Flexible 0-3 Piezoclectric Composites Prepared with Coprecipitated (Pb0.5, Bi0.5)(Ti0.5, Fe1-x, Mnx)O3 Ceramic Powders*", vol., *International Symposium on Application of Ferroelectrics*, Urbana, IL.

HANAGUD, S., OBAL, M. W. and MEYYAPPA, M., 1985: "*Electronic damping techniques and active vibration control*", vol., *Proceeding of AIAA/ASME/ASCE/AHS 26th structures, structural dynamics and materials*.

HANNER, K. A., SAFARI, A., NEWNHAM, R. E. and RUNT, J., 1989: "*Thin-film 0–3 polymer piezoelectric ceramic composites-piezoelectric paints*", Ferroelectrics Vol. 100, pp. 255–260.

HARDING, T. S. and JONES, J. W., 1999: "*Behavior of Gamma TiAl Subjected to Impact Damage and Elevated Temperature Fatigue*", Scripta Materialia, Vol. 42, No. 2, pp. 6.

HARUTA, A. and HALLAHAN, K., 2003: "*Cultural issues in airline crisis communications: A Japan-US comparative study*", Asian Journal of Communication, Vol. 13, No. 2, pp. 29.

HATCH, S., 2000, "*Surface Acoustic Waves on Piezoelectric Media Applications to Acoustic Charge Transport*", University of Western Australia.

HEYWANG, W., LUBITZ, K. and WERSING, W., 2008: *Piezoelectricity: Evolution and Future of a Technology*, Springer, Berlin.

HIKATA, S. S., NAKAHATA, H., K.HIGAKI, .FUJII, S., KITABAYASHI, H., TANABE, K. and SEKI, Y., 1995: "*SAW device application of diamond*", vol., *18th IEEE/CPMT International Electronic Manufacturing Technology Symposium*, Japan, pp. 4.

HO, C. K., LINDGREN, E. R., RAWLINSON, K. S., MCGRATH, L. K. and WRIGHT, J. L., 2003: "*Development of a Surface Acoustic Wave Sensor for In-Situ Monitoring of Volatile Organic Compounds*", Sensors*, Vol. 3, No. 7, pp. 12.

HOFER, M., N.FINGER, KOVACS, G., SCHÖBERL, J., ZAGLMAYR, S., LANGER, U. and LERCH, R., 2006: "*Finite-element simulation of wave propagation in periodic piezoelectric SAW structures*", IEEE Trans Ultrason Ferroelectr Freq Control.*, Vol. 53, No. 6, pp. 11.

HOWATT, G. N., 1952: "Method of Producing High-Dielectric High-Insulation Ceramic Plates", in PATENT, U. S. (Ed.).

HOWATT, G. N., BRECLTENRIDGE, R. G. and BROWNLOW, J. M., 1947: "*Fabrication of Thin Ceramic Sheets for Capacitors*", Journal of the American Ceramic Society*, Vol. 30, No. 8, pp. 6.

HRIBŠEK, M. F., RISTIC, S. S. and RADOJKOVIC, B. M., 2010: "*Diamond in Surface Acoustic Wave Sensors*", ACTA PHYSICA POLONICA A*, Vol. 117, No. 5, pp. 5.

HSU, T.-R., 2008: *MEMS & Microsystems: Design, Manufacture, and Nanoscale Engineering*, John Wiley & Sons, Inc., New Jersey.

HUBBARD, J. E. and MILLER, S. E., 1987: "*Observability of a Bernoulli-Euler beam using PVF2 as a distributed sensor*", vol., *Proceeding of the 6th VPI&SU/AIAA Symposium*, Blacksburg.

HUBTECHINSIDER, 2009: "*The Advantages and Disadvantages of Fiber Optics*": available at: http://hubtechinsider.wordpress.com/2009/06/04/the-advantages-and-disadvantages-of-fiber-optics/ (accessed).

INAUDI, D., 2007: "*Fiber Optic Sensors for Structural Monitoring*", vol., *Proceedings of the OPTIMESS2007 Workshop*, Leuven, Belgium, pp. 10.

INMAN, D. J., 2001: *Engineering vibration*, Prentice Hall.

JAYASUNDERE, N., SMITH, B. V. and DUNN, J. R., 1994: "*Piezoelectric constant for binary piezoelectric 0-3 connectivity composites and the effect of mixed connectivity*", Journal of applied physics*, Vol. 76, pp. 7.

JIAN, K. and FRISWELL, M. I., 2007: "*Distributed modal sensors for retangular plate structures*", Journal of Intelligent Material Systems and Structures*, Vol. 18, pp. 9.

JIN, J., 2002: *The finite element method in electromagnetics*, Wiley, New York.

JOHNSON, S. G., 2008: "Notes on Perfectly Matched Layers (PMLs)", in.

Martin, W. N., GHOSHALL, A., LEBBBYZ, G., SUNDARESANL, M. J., SCHU1Z, M. J. and PRATAP, A. P., 2001: "*Artifical nerves for structural condition monitoring*", vol., *Third Workshop on Structural Health Monitoring,*, Stanford, CA.

KAWAI, H., 1969: "*The Piezoelectricity of Polyvinylidene Fluoride*", Japanese journal of applied physics*, Vol. 8, pp. 975-976.

KHANNA, A. S., 2002: *Introduction to High Temperature Oxidation and Corrosion*, Materials Park, USA.

KLEIN, K. A., SAFARI, A., NEWNHAM, R. E. and RUNT, J., 1986: "*Composite piezoelectric paints*", vol., *IEEE 6th Int. Symp on Applied Ferroelectrics*, Pennsylvania, pp. 285-287.

KOBAYASHI, M. and JEN, C.-K., 2004: "*Piezoelectric thick bismuth titanate/lead zirconate titanate composite film transducers for smart NDE of metals*", Smart Materials and Structure*, Vol. 13, pp. 6.

KOBAYASHI, M., JEN, C.-K., BRUSSIERE, J. F. and WU, K.-T., 2009: "*High-temperature integrated and flexible ultrasonic transducers for nondestructive testing*", NDT & E International*, Vol. 42, pp. 5.

KOBAYASHI, M., JEN, C.-K., HUI, R., YICK, S. and WU, K.-T., 2006: "*Fabrication and Characterization of Thick Film Piezoelectric Ultrasonic Transducers*", vol., *2006 IEEE Ultrasonics Symposium*.

KOBAYASHI, M., JEN, C.-K., MOISAN, J. F., NRAD, N. and NGUYEN, S. B., 2007: "*Integrated ultrasonic transducers made by the sol-gel spray technique for structural health monitoring*", Smart Materials and Structure*, Vol. 16, pp. 6.

KUCHMEN, P., 1993: *Floquet Theory for Partial Differential Equations: Operator Theory*, Birkhäuser Verlag, Basel.

LAMARA, T., BELMAHI, M., ELMAZRIA, O., BRIZOUAL, L. L., BOUGDIRA, J., RÉMY, M. and ALNOT, P., 2004: "*Freestanding CVD diamond elaborated by pulsed-microwave-plasma for ZnO/diamond SAW devices*", Diamond & Related Materials*, Vol. 13, No. 4-8, pp. 4.

LAU, K.-T., 2003: "*Fibre-optic sensors and smart composites for concrete applications*", Magazine of Concrete Research*, Vol. 55, No. 1, pp. 16.

LAU, S. T., LI, K. and CHAN, H. L. W., 2004: "*PT/P(VDF-TrFE) Nanocomposites for Ultrasonic Transducer Applications*", Ferroelectrics*, Vol. 304, pp. 4.

LAU, S. T., ZHOU, Q. F., KWOK, K. W., CHAN, H. L. W. and C.L.CHOY, 1999: "*PZT/P(VDF-TrFE) Nanocomposites for Ultrasonic Hydrophone Application*", vol., *10th International Symposium on Electrets*.

LEE, C.-K., 1992: *Piezoelectric laminates: theory and experiments for distributed sensors and actuators*, Kluwer academic publishers, Netherland.

LEE, C.-K. and MOON, F. C., 1989: "*Modal sensors/actuators*", Transactions of the ASME, Vol. 68, pp. 8.

LEVINSHTEIN, M. E., RUMYANTSEV, S. L. and SHUR, M. S., 2001: *Properties of advanced semiconductor materials*, Wiley.

LEVINSHTEIN, M. E., RUMYANTSEV, S. L. and SHUR, M. S., 2001: *Properties of Advanced Semiconductor Materials: GaN, AlN, InN, BN, SiC, SiGe*, John Wiley & Sons, New York.

LEVINSON, H. J., 1999: *Lithography Process Control*, SPIE, Washington.

LEVINSON, H. J., 2004: *Principles Of Lithography*, SPIE, Washington.

LEVINSON, L. M. and DEKKER, M., 1988: *Electronic Ceramics*, New York.

LI, F., 2008, "*The Acoustic Wave Sensor and Soft Lithography Technologies for Cell Biological Studies*", University of Pittsburgh.

LI, S. and WU, Z., 2007: "*Development of Distributed Long-gage Fiber Optic Sensing System for Structural Health Monitoring*", Structural Health Monitoring, Vol. 6, No. 2, pp. 12.

LI, W.-C. and HARRIS, D., 2005: "*Where Safety Culture Meets National Culture: The How and Why of the China Airlines CI-611 Accident*", in *Human Factors and Aerospace Safety*. Ashgate Publishing Limited.

LI, X., 2009, "*Electroelastic properties of piezoelectric paint for ultrasonic guided wave sensing and damage detection*", Leigh University.

LI, X., SHIH, W. Y., AKSAY, I. A. and SHIH, W.-H., 1999: "*Electromechanical Behavior of PZT–Brass Unimorphs*", Journal of the American Ceramic Society, Vol. 82, No. 7, pp. 8.

LI, X. and ZHANG, Y., 2008: "*Analytical study of piezoelectric paint sensor for acoustic emission-based fracture monitoring*", Fatigue & Fracture of Engineering Materials & Structures, Vol. 31, No. 8, pp. 684-694.

LIPPMANN, G., 1881: "*Principe de la conservation de l'électricité" (in French).*", Annales de chimie et de physique*, Vol. 24, pp. 145.

LIU, C.-H. H., 2008: "*High-frequency surface acoustic wave (SAW) devices fabricated by contact-transferred and mask-embedded lithography*", vol., *3rd IEEE International Conference on Nano/Micro Engineered and Molecular Systems*, pp. 4.

LONGO, R., VANLANDUIT, S., VANHERZEELE, J. and GUILLAUME, P., 2010: "*A method for crack sizing using laser doppler vibrometer measurements of surface acoustic waves*", Ultrasonics*, Vol. 50, No. 1, pp. 5.

LOVE, E. H., 1923: "*Some electrostatic distributions in two dimensions*", vol. 22, *Proc. London Mathematical Soc.*, pp. 31.

LOVINGER, A. J., 1983: "*Ferroelectric Polymers*", Science*, Vol. 10, No. 4602, pp. 1115-1121.

MAASKAN, R., ALAVIE, T., MEASURES, R. M., TADROS, G., RIZKALLA, S. H. and GUHA-THAKURTAD, A., 1997: "*Fiber-optic Bragg Grating Sensors for Bridge Monitoring*", Cement and Concrete Composites*, Vol. 19, pp. 13.

MAC, C., 2007: *Fundamental Principles of Optical Lithography: The Science of Microfabrication*, Wiley.

MAMISHEV, A. V., SUNDARA-RAJAN, K., YANG, F., DU, Y. and ZAHN, M., 2004: "*Interdigital Sensors and Transducers*", Proceeding of the IEEE*, Vol. 92, No. 5, pp. 38.

MARTIN, P. M., GOOD, M. S., JOHNSTON, J. W., POSAKONY, G. J., BOND, L. J. and CRAWFORD, S. L., 2000: "*Piezoelectric films for 100-MHz ultrasonictransducers*", Thin solid films*, Vol. 379, No. 1-2, pp. 6.

MARTIN, T., HUDD, J., WELLS, P., TUNNICLIFFE, D. and DAS-GUPTA, D., 2001: "*The Use of Low Profile Piezoelectric Sensors for Impact and Acoustic Emission (AE) Detection in CFRC Structures*", Journal of Intelligent Material Systems and Structures*, Vol. 12, pp. 8.

MASON, W. P., 1950: *Piezoelectric crystals and their application to ultrasonics*, Van Nostrand, New York.

MCGEOCH, S. P., PLACIDO, F., GOU, Z., WORT, C. J. H. and SAVAGE, J. A., 1999: "*Coatings for the protection of diamond in high-temperature environments*", Diamond and Related Materials*, Vol. 8, No. 2-5, pp. 4.

MEASURES, R. M., 2001: *Structural Monitoring With Fiber Optic Technology*, Academic Press, San Diego, California.

MICHAELS, J. E. and MICHAELS, T. E., 2004: "*Ultrasonic signal processing for structural health monitoring*", Review of Quantitative Nondestructive Evaluation*,* Vol. 23, pp. 1476.

MISTLER, R. E. and TWINAME, E. R., 2000: *Tape Casting: Theory and Practice*, Wiley.

MORGANCERAMICS, 2009: "*Piezoelectric ceramic limitations*": available at: http://www.morganelectroceramics.com/resources/piezo-ceramic-tutorials/limitations/ (accessed).

MORTET, V., ELMAZRIA, O., NESLADEK, M., D'HAEN, J., VANHOYLAND, G., ELHAKIKI, M., TAJANI, A., BUSTARRET, E., GHEERAERT, E., D'OLIESLAEGERA, M. and ALNOT, P., 2003: "*Study of aluminium nitride/freestanding diamond surface acoustic waves filters*", Diamond and Related Materials*,* Vol. 12, No. 3-7, pp. 5.

MORTET, V., WILLIAMS, O. A. and HAENEN, K., 2008: "*Diamond: a material for acoustic devices*", Physica status solidi*,* Vol. 205, No. 5, pp. 12.

MORTLEY, W. S., 1963: "Improvements in or relating to wave-energy delay cells ", in PATENT, B. (Ed.), England.

MURAYAMA, N., NAKANURA, N., OBARA, H. and SEGAWA, M., 1976: "*The strong piezoelectric in Polyvinylidene Fluoride (PVDF)*", Ultrasonic*,* Vol. 14, No. 9, pp. 15.

NAKAMURA, K. and WADA, Y., 1971: "*Piezoelectricity, pyroelectricity, and the electrostriction constant of ply(viny1idene fluoride)*", Journal of Polymer Science Part A*,* Vol. 9, pp. 161-173.

NEBEL, C. E. and RISTEIN, W., 2003: *Thin film diamond: I*, Elsevier, Amsterdam.

NEBEL, C. E. and RISTEIN, W., 2004: *Thin film diamond: II*, Elsevier, Amsterdam.

NEWNHAM, R. E., 1986: "*Composite electroceramics*", Annal review of Material Science*,* Vol. 16, pp. 20.

NEWNHAM, R. E., SKINNER, D. P. and CROSS, L. E., 1978: "*Connectivity and piezoelectric-pyroelectric composites*", Materials Research Bulletin*,* Vol. 13, pp. 10.

NI, Y. Q., LI, B., LAM, K. H., ZHU, D. P., WANG, Y., LYNCH, J. P. and LAW, K. H., 2011: "*In-construction vibration monitoring of a supertall structure using a long-range wireless sensing system*", International Journal of Smart Structures & Systems*,* Vol. 7, No. 2, pp. 20.

NI, Y. Q., XIA, Y., LIAO, W.-Y. and ZHANG, P., 2008: "*Development of a Structural Health Monitoring System for Guangzhou New TV Tower*", Advances in Science and Technology, Vol. 56, No. 6, pp. 6.

NI, Y. Q. and ZHOU, H. F., 2010: "*Guangzhou New TV Tower: Integrated Structural Health Monitoring and Vibration Control*", vol., *Structures Congress 2010*.

NOLIACCERAMIC, "Nolica ceramics datasheet", in.

NORMUNG, D. I. F., 2003: "Plastics - Determination of tensile properties - Part 3: Text conditions for films and sheets", in.

NOVGOROD, N. and DVOESHERSTOV, M. Y., 2011: "*Surface acoustic wave, electric boundary conditions, velocity control, sensors*", vol., *2011 International Conference on Multimedia Technology (ICMT)*, Hangzhou, pp. 3.

OLINER, A. A., 1997: "*Leaky waves: basic properties and applications*", vol., *Asia Pacific Microwave Conference*, pp. 4.

OLINER, A. A., 1978: *Topics in applied physics*, 24, Springer-Verlag, Berlin.

OOIJEVAAR, T. H., WARNET, L. L., LOENDERSLOOT, R., AKKERMAN, R. and BOER, A. D., 2012: "*Vibration based damage identification in a composite T-beam utilising low cost integrated actuators and sensors*", vol. I, *Sixth European Workshop on Structural Health Monitoring*, Dresden, Germany, pp. 8.

PARK, S., YUN, C.-B. and INMAN, D. J., 2008: "*Structural health monitoring using electro-mechanical impedance sensors*", Fatigue Fracture Engineering and Material Structure, Vol. 31, pp. 11.

PAYO, I. and HALE, J. M., 2010: "*Dynamic characterization of piezoelectric paint sensors under biaxial strain*", Sensor and actuators A: Physical, Vol. 163, No. 1, pp. 150-158.

PAYO, I. and HALE, J. M., 2011a: "*Sensitivity analysis of piezoelectric paint sensors made up of PZT ceramic powder and water-based acrylic polymer*", Sensor and actuators A: Physical, Vol. 168, No. 13, pp. 77.

PAYO, I. and HALE, J. M., 2011b: "*Sensitivity analysis of piezoelectric paint sensors made up of PZT ceramic powder and water-based arcylic polymer*", Sensor and actuators A: Physical, Vol. 168, No. 1, pp. 77-89.

PEAIRS, D. M., 2006, "*High Frequency Modeling and Experimental Analysis for Implementation of Impedance-based Structural Health Monitoring*", Virginia Polytechnic Institute and State University, Blacksburg.

PHILIP, J., HESS, P., FEYGELSON, T., BUTLER, J. E., CHATTOPADHYAY, S., CHEN, K. H. and CHEN, L. C., 2003: "*Elastic, mechanical, and thermal properties of nanocrystalline diamond films*", Journal of applied physics*, Vol. 93, No. 4, pp. 8.

PIERCE, G. W., 1923: *Piezoelectric Crystal Resonators and Crystal Oscillators Applied to the Precision Calibration of Wavemeters, by George W. Pierce*, the American academy of arts and sciences.

PIEZOTEST, 2004: "Precision PiezoMeter Systems: A flexible, precision range of equipment for testing piezoelectric materials", in *PiezoMeter System Overview*.

PLANO-GMBH, "REM/TEM Zubehör", in.

PLUMP, J., HUBBARD, J. E. and BAILEY, T., 1987: "*Nonlinear control of a distributed system: Simulation and experimental results*", Journal of Dynamic Systems, Measurement, and Control*, Vol. 109, No. 2, pp. 7.

PREUMONT, A., FRANCOIS, A., MAN, P. D., LOIX, N. and HENRIOULLE, K., 2004: "*Distributed sensors with piezoelectric films in design of spatial filters for structural control*", Journal of Sound and Vibration*, Vol. 282, pp. 12.

PREUMONT, A., FRANCOIS, A., MAN, P. D. and PIEFORT, V., 2002: "*Spatial filters in structural control*", Journal of Sound and Vibration*, Vol. 265, pp. 19.

PRIYA, S. and INMAN, D. J., 2009: *Energy Harvesting Technologies*, Springer, New York.

RIVERA-DENIZARD, O., NAVAS, V., SUNDARAM, P. A. and DIFFOOT-CARLO, N., 2008: "*Biocompatibility studies of human fetal osteoblast cells cultured on gamma titanium aluminide*", Journal of Materials Science: Materials in Medicine*, Vol. 19, No. 1, pp. 6.

ROSE, J. L., 1999: *Ultrasonic waves in solid media*, Cambridge university press, Cambridge, UK.

ROSEN, C. Z., HIREMATH, B. V. and NEWNHAM, R., 1992a: *Key papers in physics: Piezoelectricity*, American Institute of Physics, New York.

ROSEN, C. Z., HIREMATH, B. V. and NEWNHAM, R. E., 1992b: *Piezoelectricy*, America Institute of Physics, New York.

ROWE, D. H., 1984: "Fiber optic sensors", in PATENT, U. S. (Ed.). GTE produces corporation, USA, pp. 4.

ROWEN, J. H., 1963: "Tapped ultrasonic delay line and uses therefore", in PATENT, U. S. (Ed.), USA.

ROYER, D. and DIEULESAINT, E., 1980: *Elastic Waves in Solids I: Free and Guided Propagation*, John Wiley & Sons Ltd.

RUPPEL, C. and FJELDLY, T., 2001: *Advances in Surface Acoustic Wave Technology, Systems and Applications: Voume 2*, 2, World Scientific Publishing, Singarpore.

RUSSELL, D., 2004: "*Longitudinal and Transverse Wave Motion*": available at: http://www.acs.psu.edu/drussell/Demos/waves/wavemotion.html (accessed).

RYTTER, A., 1993, "*Vibration Based Inspection of Civil Engineering Structures*", Aalborg University, Denmark.

SA-GONG, G., SAFARI, A., JANG, S. J. and NEWNHAM, R. E., 1986: "*Poling flexible piezoelectric composites*", Ferroelectric letters*, Vol. 5, pp. 12.

SACHSE, W. and HSU, N., 1988: "*Ultrasonic transducers*", in BEVER, M. B. (Ed.), *Encylopedia of Materials Science and Engineering* New York, pp. 5192-5198.

SAFARI, A. and AKDOGAN, E. K., 2008: *Piezoelectric and Acoustic Materials for Transducer Applications*.

SAKAMOTO, W. K., SOUZAB, E. D. and DAS-GUPTA, D. K., 2001: "*Electroactive properties of flexible piezoelectric composites*", Materials research Vol. 4, No. 3, pp. 4.

SCHADOWITZ, A., 1988: *The electromagnetic fields*, General publishing company, Ltd., Toronto, Canada.

SESSLER, G. M., 1981: "*Piezoelectricity in Polyvinylidene Fluoride*", Journal of Acoustic Society of America*, Vol. 70, No. 13, pp. 1596.

SHARPE, W. N., 2008: *Springer Handbook of Experimental Solid Mechanics*, Springer, New York.

SILVA, C. W. D., 2007: *Vibration fundamentals and practice*, Taylor & Francis Group, Florida.

SINGH, M. D. and JOSHI, J. G., 2006: *Mechatronics*, PHI.

SITTI, M., CAMPOLO, D., YAN, J. and FEARING, R. S., 2001: "*Development of PZT and PZN-PT Based Unimorph Actuators for Micromechanical Flapping Mechanisms*", vol., *2001 IEEE International Conference on Robotics 8 Automation*, Seoul, Korea, pp. 8.

SIZOV, G. Y., SAYED-AHMED, A., YEH, C.-C. and DEMERDASH, N. A. O., 2008: "*Analysis and Diagnostics of Adjacent and Nonadjacent Broken-Rotor-Bar Faults in Squirrel-Cage*

Induction Machines", IEEE Transactions on Industrial Electronics*,* Vol. 56, No. 11, pp. 15.

SPECHT, C. G., WILLIAMS, O. A., JACKMAN, R. B. and SCHOEPFER, R., 2004: "*Ordered growth of neurons on diamond*", Biomaterials*,* Vol. 26, No. 7, pp. 8.

STUBBS, D. D., LEE, S. H., HUNT, W. D. and 6231., A. C., 2003: "*Investigation of cocaine plumes using surface acoustic wave immunoassay sensors*", Analytical Chemistry*,* Vol. 75, pp. 5.

SULIK, S. B. A., OHSHIMA, M., TETSUI, T. and HASEZAKI, K., 2008: "*Preparation of CVD diamond coatings on gamma titanium aluminide using MPECVD with various interlayers* ", Vacuum*,* Vol. 82, No. 7, pp. 1325.

SUNG, C.-C., VARADAN, V. and BAO, X.-Q., 1990: "*Active control of torsional vibration using piezoceramic sensors and actuators*", vol., *Proceeding AIAA/ASME/ASCE/AHS/ASC 31st structures, structural dynamics, and materials conference*

SUNNYTEC, 2010: available at: http://www.sunnytec.com.cn/ (accessed).

SUNNYTEC, 2012: "*Typical values of piezoelectric ceramic materials*": available at: http://www.sunnytec-piezo.com/en/productview.asp?id=170 (accessed).

SUSSNER, H. and DRANSFELD, K., 1979: "*Piezoelectric effect in Polyvinylidene Fluoride and its applications*", Colloid Polymer Science*,* Vol. 257, No. 6, pp. 12.

TAMURA, M., YAMAGUCHI, T., OYABA, T. and YOSHIMI, T., 1975: "*Electroacoustic transducers with piezoelectric high polymer films*", Journal of the Audio Engineering Society*,* Vol. 23, No. 1, pp. 6.

TANAKA, N. and SANADA, T., 2007: "*Modal control of a rectangular plate using smart sensors and smart actuators*", Smart materials and structures*,* Vol. 16, pp. 11.

TASHIRO, K., TADOKORO, H. and KOBAYASHI, M., 1981: "*Structure and piezoelectricity of poly(vinylidene fluoride)*", Ferroelectrics*,* Vol. 32, pp. 9.

THAKRAL, S. and MANHAS, P., 2011: "*Fiber optic sensors technology & their applications*", International Journal on Electronics & Communication Technology*,* Vol. 2, No. 2, pp. 3.

THOMAS, D., WELTER, J. and GIURGIUTIU, V., 2004: "*Corrosion Damage Detection with Piezoelectric Wafer Active Sensors*", vol., *SPIE's 11th Annual International Symposium on Smart Structures and Materials and 9th Annual International Symposium on NDE for Health Monitoring and Diagnostics,*, San Diego, CA.

TICHÝ, J., ERHART, J., KITTINGER, E. and PRÍVRATSKÁ, J., 2010: *Fundamentals of Piezoelectric Sensorics*, Springer.

TIERSTEN, H. F., 1969: *Linear piezoelectric plate vibrations*, Plenum, New York.

TIGLI, O., BIVONA, L., BERG, P. and ZAGHLOUL, M., 2010a: "*Fabrication and Characterization of a Surface-Acoustic-Wave Biosensor in CMOS Technology for Cancer Biomarker Detection*", IEEE Transactions on Biomedical Circuits and Systems, Vol. 4, No. 1, pp. 12.

TIGLI, O., BIVONA, L., BERG, P. and ZAGHLOUL, M., 2010b: "*Fabrication and Characterization of a Surface Acoustic Wave Biosensor in CMOS technology for Cancer Biomarker Detection*", IEEE Transactions on Biomedical Circuits and Systems, Vol. 4, No. 1, pp. 12.

TING, Y., HARIYANTO, G., HOU, B. K., RICKY, S., AMELIA, S. and WANG, C.-K., 2009: "*Investigation of Energy Harvest and Storage by Using Curve-shape Piezoelectric Unimorph*", vol., *IEEE International Symposium on Industrial Electronics*, Seoul Olympic Parktel, Seoul, Korea, pp. 6.

TIROLE, N., CHOUJAA, A., HAUDEN, D., MARTIN, G., BLIND, P., FROELICHER, M., BLIND, P., FROELICHER, M., POMMIER, J. C. and CACHARD, A., 1993: "*Lamb waves pressure sensor using an AlN/Si structure*", Ultrasonic symposium.

TOLE, N. M. and OSTENSEN, H., 2005: *Basic Physics of Ultrasonographic Imaging*, WHO Press, Geneva.

TRAINER, M., 2003: "*Kelvin and piezoelectricity*", European Journal of Physics, Vol. 24, No. 5, pp. 535-542.

TZOU, H. S., 1989: "*Integrated distributed sensing and active vibration suppression of flexible manupulators using distributed piezoelectrics*", Journal of Rototic System, Vol. 6, No. 6, pp. 23.

TZOU, H. S. and ANDERSON, G. L., 1992: *Intelligent Structural Systems (Solid Mechanics and Its Applications)*, Springer, Gainesville, FL, USA.

TZOU, H. S. and GADRE, M., 1988: "*Theoretical analysis of a multi-layered thin shell coupled with piezoelectric shell actuators for distributed vibration controls*", Journal of Sound and Vibration, Vol. 132, No. 3, pp. 18.

TZOU, H. S. and TSENG, C. I., 1990: "*Distributed piezoelectric sensor/actuator design for dynamic measurement/control of distributed parameter systems: A piezoelectric finite element approach*", Journal of Sound and Vibration, Vol. 138, No. 1, pp. 18.

UDD, E., MICHAL, R. J., WATANABE, S. F., THERIAULT, J. P. and CAHILL, R. F., 1988: "Fiber optic sensor", in PATENT, U. S. (Ed.). McDonnell Douglas Corporation, USA, pp. 18.

VASQUES, C. M. A. and RODRIGUES, J. D., 2008: "*Modal sensing of beams via spatially shaped distributed piezoelectric transducers*", Mecanica Experimental, Vol. 15, pp. 4.

VELLA, P. J. and STEGEMAN, G. I. A., 1973: *Parametric Coupling of Bulk Acoustic Waves at Surface Interdigital Transducer*, Defense Technical Information Center, Toronto.

VOIGT, W., 1890: "*General theory of the piezo- and pyroelectric properties of crystals*", Abhandlungen Göttingen, Vol. 36, No. 1, pp. 1-99.

VOIGT, W., 1910: *Lehrbuch der Kristallphysik*, Teubner, Leipzig.

VURPILLOT, S., INAUDI, D. and DUCRET, J.-M., 1996: "*Bridge monitoring by fiber optic deformation sensors: design, emplacement and results*", vol., *SPIE, Smart Structures and Materials*, San Diego, USA.

WADA, Y. and HAYAKAWA, R., 1976: "*Piezoelectricity and pyroelectricity of polymers*", Japanese Journal of Applied Physics, Vol. 15, No. 11, pp. 17.

WALLER, D. and SAFARI, A., 1988: "*Corona poling of PZT ceramics and flexible piezoelectric composites*", Ferroelectrics, Vol. 87, pp. 7.

WANG, J. and ZENG, S., 2011: "*Dynamics of Piezoelectric Smart Beams Using a Three-Parameter Elastic Foundation Model*", Journal of Intelligent Material Systems and Structures, Vol. 22, pp. 14.

WANG, Q. and QUEK, S. T., 2004: "*Repair of delaminated beams via piezoelectric patches*", Smart Materials and Structures, Vol. 13, pp. 8.

WEAVER, W., TIMOSHENKO, S. P. and YOUNG, D. H., 1990: *Vibration problems in engineering*, Wiley New york.

WEBSTER, J. G., 1999: *The Measurement, Instrumentation, and Sensors Handbook*, Springer-Verlag, New York.

WELSCH, G., BOYER, R. F. and COLLINGS, E. W., 1994: *Materials Properties Handbook: Titanium Alloys*, ASM International.

WU, K.-T., JEN, C.-K., KOBAYASHI, M. and BLOUIN, A., 2011: "*Integrated Piezoelectric Ultrasonic Receivers for Laser Ultrasound in Non-destructive Testing of Metals*", Journal of Nondestructive Evaluation*, Vol. 30, pp. 8.

WU, K.-T. and KOBAYASHI, M., 2009: "*Integrated High-Temperature Piezoelectric Plate Acoustic Wave Transducers Using Mode Conversion*", IEEE Transactions on UltrasonicsFerroelectrics, and Frequency Control*, Vol. 56, No. 6, pp. 7.

WU, S., RO, R. and LIN, Z. X., 2009: "*Rayleigh surface acoustic wave modes of (100) ZnO films on (111) diamond*", Applied Physics Letters*, Vol. 94, No. 3, pp. 3.

YADAV, V. S., SAHU, D. K., SINGH, Y. and D.C.DHUBKARYA, 2010: "*The Effect of Frequency and Temperature on Dielectric Properties of Pure Poly Vinylidene Fluoride (PVDF) Thin Films*", vol., *International MultiConference of Engineers and Computer Scientists*, Hongkong.

YAMADA, T., UEDA, T. and KITAYAMA, T., 1982: "*Piezoelectricity of a highcontent lead zirconate titanate/polymer composite*", Journal of applied physics*, Vol. 53, pp. 6.

YANG, C. and FRITZEN, C.-P., 2011: "*Characterization of piezoelectric paint and its refinement for structural health monitoring applicatios*", vol., *3rd International conference on smart materials and nanotechnology in Engineering*, Shen Zhen, China.

YANG, C. and FRITZEN, C.-P., 2012: "*Piezoelectric paint: characterization for further applications*", Smart materials and structures*, Vol. 21, pp. 8.

YANG, C., TORRES-ARREDONDO, M. A. and FRITZEN, C.-P., 2011: "*Acoustic Emission Simulation for Online Impact Detection*", vol., *Comsol conference 2011* Stuttgart, pp. 8.

YOUNG, D., 2008: *High Temperature Oxidation and Corrosion of Metals*, Elsevier Science, Oxford, UK.

YOUNG, D. J., 2008: *High temperature oxidation and corrosion of metals*, 1, Elsevier, Cambridge.

YU, H. Y., 2010, "*Aluminum Nitride nano wires for electronic and photonic applications*", The Hong Kong polytechni university.

YU, L. and GIURGIUTIU, V., 2012: "*Piezoelectric Wafer Active Sensors in Lamb Wave-Based Structural Health Monitoring*", JOM*, Vol. 64, No. 7, pp. 9.

ZAGRAI, A. and GIURGIUTIU, V., 2002: "*Health Monitoring of Aging Aerospace Structures using the Electro-Mechanical Impedance Method*", vol., *SPIE's 9th Annual International*

Symposium on Smart Structures and Materials and 7th Annual International Symposium on NDE for Health Monitoring and Diagnostics, San Diego, CA.

ZHANG, Y., 2006a: "*In situ fatigue crack detection using piezoelectric paint sensor*", Journal of Intelligent Material Systems and Structures*,* Vol. 17, No. 10, pp. 9.

ZHANG, Y., 2006b: "*In situ fatigue crack detection using piezoelectric paint sensor*", Journal of Intelligent Material Systems and Structures*,* Vol. 17, No. 10, pp. 843-852.